AB INITIO MOLECULAR ORBITAL THEORETICAL STUDIES OF THE MOLECULAR COMPLEXES OF BORON TRIFLUORIDE AND OXYGEN ELECTRON DONOR LIGANDS

ERIC MODAU

SUPERVISOR: Prof. L.M. NXUMALO

CO-SUPERVISOR: Ms G.C. SELEPE

A Thesis Submitted to the Faculty of Science;

Vista University Soweto Campus, JHB

For the degree of Masters of Science

Johannesburg, October 2001

DECLARATION

I declare that the thesis is my own, unaided work. It is being submitted for the Masters of science degree in the Department of Chemistry at the Soweto Campus of Vista University. It has not been submitted before for any degree or examination in any other University.

ERIC MODAU

...16..... **DAY OF**...December....**2001**

Abstract

The optimized geometrical structures, the interaction energies, the basis set superposition errors (BSSEs) and the infrared spectra of the monomers, homodimers and the molecular complexes formed between BF_3 and a number of bases have been determined by means of ab initio theoretical calculations using the Gaussian-98W (Widows version) computer program package. Three levels of theory have been used. These are the Restricted Hartree-Fock (RHF) level, the second-order Möller-Plesset (MP2) perturbation theory and the Density Functional Theory (DFT). The basis set used was the 6-31G(d, p) split-valence polarized basis set in order to identify the most reliable computational method in the prediction of their molecular properties.

Full geometry optimizations using the BERNY optimization procedure, were carried out at the tight level of convergence using the tight (TIGHT) convergence criterion.

The vibrational spectra of the monomers, dimers and molecular complexes were also obtained using the same three levels of theory and same basis set. The interaction energies of each binary species have been computed and corrected for the basis set superposition error (BSSE) by using the full counterpoise methods.

The monomers, dimers and molecular complexes, which were investigated for their molecular properties, are as follows:

Monomers: BF_3, CO, CO_2, H_2O, N_2O, O_2, O_3 and SO_2

Dimers: $(BF_3)_2$, $(CO)_2$, $(CO_2)_2$, $(H_2O)_2$, $(N_2O)_2$ and $(SO_2)_2$

Molecular Complexes: $BF_3.CO$, $BF_3.CO_2$, $BF_3.H_2O$, $BF_3.N_2O$, $BF_3.O_2$, $BF_3.O_3$ and $BF_3.SO_2$

Ab initio molecular orbital calculations have been employed in these studies as very useful tools in the prediction of molecular parameters, interaction energies, and the interpretation of the infrared spectra.

The good correlation that exist between the theoretical and the experimental results obtained from the literature, emphasises the strength of using the matrix isolation technique together with ab initio molecular orbital (MO) calculations for studying molecular interactions. The structures, interaction energies and infrared spectra of both dimeric isomers and molecular complexes mentioned in this work have been predicted by means of ab initio MO calculations at the HF, MP2 and DFT levels of theory with the standard 6-31G(d, p) split-valence polarized basis set. The computed infrared spectra obtained in this way have been analysed and used as guides in the assignment and interpretation of the matrix isolation infrared spectra obtained from the literature, where available.

All the complexes studied in this work feature the dominant B...O electron donor-acceptor intermolecular interaction. For both the dimeric isomers and the molecular complexes mentioned above, the calculated dimerization and interaction energies, after being corrected for basis set superposition errors by employing the full counterpoise method, present strong evidence that the interactions are weak ones. All the wavenumber shifts for both the homo-dimers and hetero-dimers showed small perturbation at all the three levels of theory.

By correlating the calculated wavenumbers of the complex together with those of the parent monomers, it has been established that the degree of the magnitudes of the in-plane bending mode and the antisymmetric stretching modes wavenumber shifts of the electron acceptor moiety in the complex can be employed as guides for determining the strength of the binding energy as well as the nature of the intermolecular interaction. The small wavenumber shifts expressed in terms of the in-plane bending and antisymmetric stretching modes signify very weak intermolecular interactions accompanied by a large intermolecular interaction distances and a low interaction energies, after the latter have been corrected for basis set superposition errors (BSSE). For the future works the MP2 method should be used since it is more reliable than the DFT approach in the prediction of the experimental results, and It is virtually always an improvement on the Hatree-Fock method.

Acknowledgement

I would like to thank Prof. L.M. Nxumalo for all the support he was giving to me, the encouragement and the time he was spending with me. For his continuous presence in times where help was needed most, so I say thanks to him, may God, the Father bless him and his family. I would like to thank Prof. D. Levendis from the school of chemistry at Wits University for the time he spent with us and teaching us on how to run some computer programmes.

Finally, I would like to thank the National Research Foundation and Vista University for the ongoing support they were giving to me, both financially and psychologically and, lastly, not forgetting to thank my co-worker Miss D. Nkosi and the rest of the members of the staff in the Department of Chemistry at the Soweto campus of Vista University

LIST OF PUBLICATION ARISING FROM THIS WORK

1. Ab initio MO predictions of the structures, energies and the infrared spectra of the $BF_3.H_2O$, $BF_3.O_2$ and $BF_3.O_3$ complexes. University of Pretoria, Pretoria, Republic of South Africa, 2001

2. E. Modau, and L.M. Nxumalo, Infrared Spectroscopic and ab initio Molecular Orbital Studies of the Carbon Monoxide Dimers, S. Afr. J. Chem, in Preparation.

3. E.Modau and L.M. Nxumalo, ab initio Molecular Orbital Theoretical Studies of the Vibrational Spectra of the $BF_3.H_2O$ Molecular Complex, Theor. Acc. in Preparation.

TABLE OF CONTENTS Page

CHAPTER THREE

CHAPTER FOUR

CHAPTER FIVE

LIST OF TABLES

Table **page**

CHAPTER FOUR

Table **page**

CHAPTER FIVE

Table **page**

Table **page**

Table **page**

Table **page**

Table **page**

CHAPTER SIX

Table **page**

Table **page**

Table **page**

Table **page**

Table **page**

CHAPTER SEVEN

Table **page**

LIST OF FIGURES

CHAPTER SIX

FIGURE page

CHAPTER ONE

1. AIM AND MOTIVATION FOR THIS WORK

In the past, chemistry has been traditionally an experimental science. This implied that no molecules or complexes could be investigated until they were synthesized or found in nature. However, with the advent of computers, chemistry no longer depended upon the availability of the laboratory for the investigation of molecular properties but on the availability of a more powerful computers, which can be employed to perform similar investigations.

In this work the properties of the 1:1 complexes of boron trifluoride with some oxygen electron donors were investigated by using ab initio molecular orbital theoretical calculations. The properties of interest are the geometrical structures, interaction energies and the vibrational spectra of the complexes formed between BF_3 and the oxygen electron donor ligands. The calculations were carried out using the GAUSSIAN-98W suite of programs at the Hartree-Fock (HF), the second-order MØller-Plesset (MP2) and the Density Functional Theory (DFT) levels of theory using the 6-31G(d, p) split-valence polarized basis set. In addition, the properties of the homo-dimers of both the boron trifluoride and the oxygen donor ligands were investigated. The computationally predicted results were then compared with the experimentally generated infrared data, where available, and were used as an aid in the assignment of the absorption bands as well as in the interpretation of the experimental infrared spectra retrieved from the literature.

The results obtained in this work were expected to throw some light on the nature and strength of the molecular interactions (hydrogen bonding, electron donor-acceptor, or van der Waals type). This work also serves to identify which amongst the three methods of computation (HF, MP2 and DFT) is the most suitable for the prediction of the molecular properties of the complex under investigation. This work also serves the purpose of selecting the best method which has to be adopted for the prediction of the molecular properties in the future calculations of the molecular systems.

The aim of this project is therefore to attempt to select which of the three astablished levels of theory describing all the various types of molecular interactions formed between any given pair of the interacting monomeric species.

1.1 Molecular interactions

Atoms combine to make all substances in the world around us, but they do so in a very orderly fashion. Most substances that are encountered in day-to-day life are made up of small units of matter called molecules. A molecule is a combination of two or more atoms held together in a specific shape by attractive forces. A molecule that contains two atoms is called a diatomic molecule, one that contains three is called a triatomic molecule and so on. Molecules interact either reactively, resulting in the formation and breaking of covalent bonds, or non-reactively in the formation of a molecular complex. The former is clearly a covalent bond interaction. The latter which is termed a weak, non-covalent, non chemical, physical or van der Waal interactions leads to the formation of molecular complexes that are called hydrogen-bonded or electron donor- acceptor (EDA) or van der Waals complexes. All these three types of interactions are discussed in the next section.

1.1.1 Electron donor-acceptor (EDA) complexes

This type of complex was discussed by Benasi and Hildebrand [1] in 1949 by the observation of new absorption bands in the ultraviolet (uv) spectrum of the complex. In EDA complexes there is a donor and an acceptor molecule. The donor molecule may donate an unshared pair (an n donor) or a pair of electrons in a pi orbital of a double bond or aromatic system (a pi donor). One test for the presence of an EDA complex is the electronic spectrum (called a charge-transfer spectrum) that is not the same as the sum of the two individual molecular spectra. Due to the fact that the first excited state of a complex is relatively close in energy to the ground state there is usually a peak in the visible or near-uv region and EDA complexes are often colored. Many EDA complexes are unstable and exist only in solutions in equilibrium with their

components but others are stable solids. In most EDA complexes the donor and acceptor molecules are present in an integral ratio 1:1 [2], but complexes with non-integral ratios are also known.

1.1.2 Hydrogen bonding

Hydrogen bonding occurs when a covalently bound hydrogen atom forms a second bond to another atom. The hydrogen bond is usually represented as A--H-B, where A is an atom with electronegavity greater than that of hydrogen (e.g. C,N,Cl and etc), and B can be any s or pi electron donor site (e.g. a Lewis base).

A hydrogen bond is the attractive force that arises between the proton donor covalent pair A-H, with a significant bond dipole, and the non-covalently bound nearest-neighbour electronegative proton-acceptor atom B. It is in part the Coulombic interaction of the dipole with the excess electron density at the proton-acceptor atom that forms the hydrogen bond interaction. This strength of the hydrogen bond formed is believed to be best described with the acidity of the hydrogen atom and basicity of the atom B although electrostatic interactions are also important. Unless the acidity of hydrogen and the basicity of the acceptor atoms are sufficient, any hydrogen bonds formed are usually too weak to be of significance.

Although the hydrogen bond is much weaker than the normal chemical bond, its strength varies considerably with A---B and B. It has long been known that with very electronegative donor and acceptor atoms, the hydrogen resembles a covalent bond, whereas, with weakly electronegative atoms, it is primarily electrostatic. Hydrogen bonds can either be intramolecular or intermolecular. For intramolecular hydrogen bonding to occur, A and B of A-H---B must be in a favourable spatial configuration in the same molecule or the interaction, which is taking place with the molecule itself. When the hydrogen bond A-H--B is formed:

- The molecules concerned come much closer together than the sum of the van der Waals radii of the nearest atoms that would otherwise allow.
- The lengths of the A-H bonds are some what increased (bond length).
- The band width mode of the A-H stretching is increased (intensity).

- The linearity of the A-H---B segment is increased, as the hydrogen bond strength is increased (the bond angle becomes closer to 180.0 degree).

From the above discussion it can be concluded that the electron donor-acceptor interaction and hydrogen bonding are H-donor and E-donor, even though there is a slight difference in terms of their strengths.

1.1.3 van der Waals complexes

van der Waals complexes are weakly bound assemblies of atoms or molecules, having large amplitude vibrational motions, which are held together by dispersion, induction, charge transfer or hydrogen interactions [3]. Experimentally, the advent of supersonic free expansion technigue enables a wide variety of different complexes to be probed using molecular spectroscopy [4,5]. Theoretically, many advances have been made in analyzing the intermolecular potential, including Stone`s distributed multipole analysis (DMA)[6]. Furthermore, in complexes governed by electrostatic interactions the geometries of the van der Waals complexes can be predicted by the Buckingham-Fowler hard-sphere model [7,8,9]. Legon and Millen [10,11] have devised a set of rules facilitating the prediction of molecular geometry for small molecular systems and the distribution on complexation is neglected. The binding energies of van der Waals complexes are typically not greater than 20 kJ mol^{-1}, being approximately the thermal energy of molecules at room temperature. Another result of van der Waals interactions are that there is very little redistribution of electronic charge. As a result the individual molecules retain their separate character. van der Waals forces are responsible for complex formation in inert and non-polar molecules at low temperatures. The stability of van der Waals complexes depends on the balance between the exchange repulsion which decrease exponentially with the intermolecular distance, r, and the attractive forces due to the electrostatic induction and dispersion interaction, which decrease as r^{-n} at large distances [12].

CHAPTER TWO

2.1 ab initio Molecular Orbital Theory

The term ``ab initio`` implies a rigorous, non-parametrized molecular orbital treatment derived from first principles. This is not completely true. There are a number of simplifying assumptions in ab initio theory, but the calculations are more complete, and therefore more expensive than that of the Semi emperical method. It is possible to obtain chemical accuracy via ab initio calculations, but only small systems can be treated this accurately at present. In practice most calculations are performed at lower levels of theory than would be considered definitive, and the shortcomings are taken into account.

Ab initio theory makes use of the Born-Oppenheimer approximation i.e that the nuclei remain fixed on the time scale of electron movement and that the electronic wave function is unaffected by nuclear motion. This is a very good approximation is nearly all cases. Only for extremely flat potential surfaces, as for instance in some Jahn-Teller systems, may significant coupling exist between the vibrational and electronic wave functions.

Ab initio calculations are almost always of either the variation or perturbation type, though there are others. The two methods can also be used in combination. In calculations of molecular energies and geometries, variation calculations are more common than perturbation calculations.

2.1.1 Basis sets

The term basis set mean an internally standard set of coefficients and exponents. Most of the wave functions to be considered are constructed in some form from molecular orbitals (MOs). In practical applications of the theory, a further restriction is imposed, requiring that the individual molecular orbitals be expressed as linear combination of a finite set of N prescribed one-electron functions known as basis functions.

In a simple quantitative version of molecular orbital theory, atomic orbitals constituent atoms are used as basis functions. Such treatment is often described as a linear combination of atomic orbitals (LCAO) theory. There are two types of basis functions which are generally used. These are Gaussian-Type Functions (GTFs) and Slater-Type Functions (STFs).

Gaussian-Type Functions used in molecular calculations are usually expressed as

$$\chi^{g}_{ijk}=N_g x^i y^j z^k \exp(-\varepsilon_{ijk} r^2) \quad \ldots\ldots (2.1)$$

Where i, j and k are positive integers

The normalized Slater-Type Functions in a spherical co-ordinate are defined as

$$\chi^{s}_{nl}=N_{sr}{}^{n-l} \exp(-\varepsilon_{nl} r)\, Y_{lm}(\theta, \phi) \quad \ldots\ldots (2.2)$$

Where n, l and m are principal, azimuthal and magnetic quantum numbers respectively, εnl an exponential prefactor of orbital exponents, and Ylm (θ, ϕ) a spherical harmonic linear combination of STFs are used in approximating atomic orbitals (AOs).

In equation (2.1) and (2.2) the independent variables (r, θ, ϕ) or (x, y, z) refer to the displacement of an electron from a chosen point of reference (for example, nuclear position) and N_s and N_g are appropriate normalization factors. Gaussian-Lobe Functions (GLFs) are special cases of equation (2.1) with i=j=k, that is, only the $\exp(-\varepsilon r^2)$ is used and several such lobes are placed at appropriate positions to appropriate the angular characteristics of the spherical harmonic.

The minimal basis sets are used to describe the minimum number of basis functions required for each atom in a molecule, e.g. STO-3G, which is three primitive Gaussians per basis function, and it approximates STFs with GTFs.

In the minimal basis set only the exact number of functions needed for each electron in the atoms is used. An extension of minimal basis set is to double

the number of functions representing the valence region. In a split-valence basis set, hydrogen and two s-type functions and the first-and second-row atoms represent helium atoms by two complete set of valence s and p functions. The type of split-valence basis set used in this project is the 6-31G(d, p) basis set, comprising inner shell function expanded in terms of six primitive Gaussian functions.

Basis sets with full diffuse functions are useful for systems containing electrons which are far from the nucleus, e.g. molecules with lone pair electrons and ions. These types of functions contain larger s and p orbital functions, thus allowing the orbitals to occupy larger regions of space. The 6-31+G basis set adds diffuse functions to the heavy atoms, whilst the 6-31++G basis adds diffuse functions to the heavy atoms and the hydrogen atoms as well.

2.1.2 Self-Consistent-Field Methods (SCFM)

Quantum mechanics studies using ab initio methods depend on what properties are to be determined in a given series of calculations. Presently, for large molecules or large basis set studies on even relatively small molecules quantum mechanical calculations are at stage where electron repulsion integrals must be evaluated and processed. Consequently SCF-MO studies (for closed-shell system with only a single Slater determinant or open-shell system with a fixed linear combination of a small number of Slater determinants) still constitute the largest class.

At the SCF level the electron-electron repulsion is actually overestimated. The theory does not allow the electron to avoid each other but assumes that their instantaneous positions are independent of one another. However, the error is reasonable consistent so that its effect can be made to cancel by the use of proper comparisons. The SCF methods are known as Single-determinant or Hartree-Fock (HF).

Self-consistent field calculations can be used successfully as long as the number and the type of electron pair does not change from one side of the equation to another. This is because the amount by which the electron repulsion is overestimated is approximately constant for each type of electron

pair. This consideration leads to the use of isodemic equations for evaluation of results of SCF calculations. One of the major problems in using the SCF-MO method is how to treat both open and close-shell molecules consistently. The application of SCF procedures to open-shell molecules has also become relatively commonly used. The SCF wavefunction is a Slater determinant, or a fixed linear combination of Slater determinants that exhibits the proper spatial and spin symmetry for the open-shell configuration and the desired state.

2.1.2.1 Hartree-Fock Method (HF)

A half-electron calculation for an open-shell system is simply a Restricted Hartee-Fock (RHF) [13] calculation in which the singly occupied orbitals contain not one electron that would have a spin but rather two half electrons of opposite spin. A small correction (the half-electron correction) is applied to compensate for the pairing energy of two half electrons. The half-electron has the advantage that it is on the same energy scale as RHF calculation for closed-shell molecules; this means for instance, that the relative energy for singlet and triplet state can be compared directly if the singlet is calculated with RHF and the triplet with the half-electron method. The disadvantages of the half-electron approach are that no information about spin densities is available and that the method is not well suited for optimization using analytical calculation forces, thus half-electron optimization may be very slowly.

An alternative method of calculating open-shell system is the Unrestricted Hartree-Fock (UHF) [14] formalism, which is most often used for open-shell calculations with the GAUSSIAN series of ab initio programs. The Unrestricted Hartree-Fock (UHF) method (also referred to as different orbital for different spin (DODS)) is more flexible than RHF because the paired alpha and beta orbitals [15], which correspond to doubly occupied molecular orbitals in the RHF formalism, need not be identical. This is both the strength and weakness of the method. On the other hand, it allows for spin polarization, the process by which an unpaired electron perturbs formally paired spins, and, therefore, it gives realistic estimates of spin densities. On the other hand, this extra flexibility gives a more negative electronic energy than would be obtained with spin-restricted theory. It is, therefore, not possible to compare the energies of open and closed-shell systems directly.

The UHF wavefunction is not limited to one pure electronic state, but can also be mixed in with states of higher spin. Spin contamination is not a problem in half-electron calculations or for the open-shell restricted Hartree-Fock (ROHF) procedure. In these the doubly occupied orbitals are restricted so as to be identical for alpha and beta spins, thus no admixture of higher-spin states is possible. Open-shell restricted Hartree-Fock calculations are possible with ab initio programs.

2.1.2.2 Electron Correlation Methods

The exact wavenumber described by a single determinant is the major weakness of single determinant molecular orbital (MO) theory since the electronic motion is completely neglected. This leads to the Hartree-Fock energies being significantly higher than the exact value. Correlation effects span through the energies, structural parameters and vibrational frequencies. There are various ways to incorporate correlation effects, e.g. through either configuration interaction (CI) method, Møller and Plesset[34] (MP) perturbation theory or Density Functional theory (DFT).

2.1.3. Møller-Plesset Second-Order Perturbation Theory (MP2)

Møller and Plesset[34] were the first to develop a perturbation theory (PT) in which the Hartree-Fock (HF) wavefunction and energy are taken to zero-order solution to the exact wavefuction and energy. The difference between the exact Hamiltonian and the HF Hamiltonian is considered as a small perturbation which correct the average-field approximation of HF theory in such a way that the correlated movement of the electron is explicity considered.

The perturbation theory of Møller and Plesset,[34] closely related to many-perturbation theory, is an alternative approach to the correction problem within a given basis sets. Its aim is still to find the lowest eigenvalue and corresponding eigenvector of the full Hamiltonian matrix. However, the approach is not to truncate the matrix as in limited CI, rather to treat it as the sum of two parts, the second being the perturbation on the first.

The next step in many calculations is to apply some sort of correction for electron correlation to the SCF energy. The GAUSSIAN programs traditionaly use the Rayleigh-Schrødinger [16] many body perturbation theory (RSMBPT) as applied to molecular systems by Møller and Plesset and implemented at the second (MP2), third (MP3) or fourth (MP4), as based on perturbation theory and, like many methods, for calculating the correlation-energy and always rely on a good description of the virtual orbital in the original SCF wavefunction. However, MP2 is relatively economic to evaluate and gives a reasonable proportion of the correlation energy. Higher order terms become more and more expensive. MP3 is commonly used but does not seem to give much improvement over MP2. MP4, with some terms removed to speed things up, is often used. MP4 gives reasonable results but it is much more expensive than MP2; so the levels of theory selected for this project is MP2.

2.1.4 Density Functional Method (DFT)

Density functional theory (DFT) has emerged in recent years as a promising alternative to conventional ab initio method in computational chemistry. The DFT methods are similar to ab initio methods in many ways. The popularity of DFT is largely due to its computational simplicity as compared with the Hartree-Fock (HF) based ab initio quantum mechanical methods, especially with the corrected levels of ab initio methods. Kohn and Sham [17] proposed the present form of DFT computation in 1965. DFT computations are of accuracy that is approaching what quantum chemists call ``chemical accuracy``. DFT methods are attractive because they include the effects of electron correlation.

2.1.3.1 Brunacker 3rd Order Lee-Young-Parisser functional

There are also several hybrids functionals, which define the exchange function as a linear combination of Hartree-Fock (HF), local and gradient exchange term. This exchange function is then combined with a local and gradient corrected correlation functional. One choice is Becke's three parameter of exchange [18] (B3) and the correlation functional is the Lee-Young-Parr (LYP) [19] functional. Exchange and correlation functionals are grouped in different categories, LYP functional, grouped under gradient-

corrected functional and B3 functional, mixing some HF exchange, are examples of hybrid function (also known as adiabatic connection method). Then, the exchange functional (B3) is combined with the gradient-corrected correlation functional (LYP) to give a Brunacker 3rd Order Lee-Young-Parisser functional (B3LYP).

2.2 Equilibrium Geometries and Vibrational Properties

One of the most important and the most successful application of ab initio calculations to polyatomic molecules has been the confirmation and the prediction of molecular geometries. The Born-Oppenheimer approximation and the variation principle allow for the determination of the minimum point-by-point mapping through successive calculations of the total energy.

Although this procedure must ultimately lead, for bound systems, to a minimum corresponding to the equilibrium geometry, it becomes increasingly more complicated as the number of atoms increase. This is due to the existence of 3N-6 degrees of freedom (3N-5 for a linear molecule), where N is the number of atoms. However, symmetry consideration and a reasonable guess of the equilibrium geometry reduce the complexity to some degree. Pople and co-workers [20] have been successful in the determination of geometries of a large number of molecules using such a point-by-point procedure.

It has become apparent over the past several years that a more efficient procedure for determining the characteristics of a potential energy surface is through the calculation of derivatives of the total energy directly from the molecular wavefunction. Pople and Krishnan [20] have developed a method by which this can be accomplished through a computation of three types of force integrals, thus the Hell-Feynman density and integral forces.

In addition to the first derivative or gradient, which is used primarily to determine the equilibrium geometry, higher derivatives can be calculated using this gradient method. Additional points must be calculated but the number is still fewer than that required in a point-by-point procedure. The option increments geometry for mapping out the surface has been investigated [21,22]. The gradient method has recently been applied using Møller-Plesset Perturbation theory [23], Open-shell SCF [24] and MCSCF [25] procedures.

CHAPTER THREE

3.1 Practical aspects of ab initio SCF MO calculations

The minimum possible input for a MO calculation consist of the molecular charge and multiplicity and some definition of the molecular structure, i.e., the types of atoms involve and their geometrical positions. The structure is conveniently defined by means of a Z-matrix, which is a method of defining the molecule atom by atom in terms of bond lengths, bond angles and dihedral angles. The GAUSSIAN-98W MO computer program employed in this work is capable of automatically optimizing the molecular geometry within the specified symmetry constraints.

Geometry optimization may be performed in three different ways with the GAUSSIAN-98W program. The first of these methods, commonly known as the Berny optimization [25], is usually the fastest and is selected automatically by GAUSSIAN-98W program if no other mode of optimization is specified. Berny optimization uses analytical atomic forces and guessed force-constant matrix, which is continuously updated during the optimization, to predict the atomic positions of the minimum energy structure. This type of optimization is very fast and effective for acyclic molecules, but may either be very slow or fail completely for molecules with cyclic structures. This problem can, however, often be overcome by the use of an appropriate strategy, such as the use of the dummy atoms, in writing the Z-matrix.

The second type of optimization available in the GAUSSIAN-98W program is the Murtaugh-Sargent algorithm [26]. This method, which does not rely on a guessed-force constant matrix, is slower but more reliable than Berny optimization. It too, uses analytically evaluated atomic forces to predict the minimum-energy structure.

The third type of optimization available in GAUSSIAN-98W program is the Fletcher-Powell method [27]. The program selects this method automatically for those calculations for which no analytical forces are available. The Fletcher-Powell procedure can be used with any type of energy calculation, but is extremely slow in comparison with the method that uses analytical forces. This method also gives reliable optimizations.

In this project all calculations were performed using the Berny optimization method, which is the default option to predict a local minimum structure for HF, MP2, DFT and CI procedures. The 'TIGHT' keyword was used to determine convergence. For a systems with very small force constants (low frequency vibrational modes), "VERTIGHT`` option may be very necessary to ensure adequate and reliably of frequencies computed in a subsequent step.

Having reached the minimum-energy structure, the GAUSSIAN-98W program calculates both the vibrational frequencies and the infrared and Raman intensities by using the FREQ keyword. Vibrational frequencies are computed by determining the second derivative of the energy with respect to the nuclear Cartesian coordinates and then transforming them to mass-weighted coordinates. This transformation is only valid at a stationary point.

3.2 Basis Set Superposition Error (BSSE)

This error (BSSE) occurs when a finite basis set is used since the electronic description of either sub-unit in a complex is improved when the basis set for the supermolecule makes use of the orbital associated with the other monomer unit. The inclusion of the functions from one monomer with those of other results in lowering of the interaction energy. This lowering in energy is known as the BSSE. An approximation method for taking account of this is the counterpoise correction [28] in which the energy of each monomer unit is calculated using a full basis set [29]. There have been many studies criticising the counterpoise correction (CPC) [30,31], and alternative suggestions have been made. However, the CPC still produces acceptable, accurate results [32,33].

Many variation of the counterpoise correction scheme have been reported. One reason why there should be so many are that the counterpoise correction is only an estimate. It is the most reasonable estimate. However, it provides neither an upper nor a lower bound of the extent of BSSE.

3.3 Infrared band assignments and nomeclature

3.3.1 The plotting program ORTEP

The oak ridge thermal ellopsoidal program (ORTEP) [34] was used for the facilitation of the assignments of the calculated infrared wavenumbers to particular modes of vibration. The first method involves adding the Cartesian coordinate of the calculated eigenvectors, for each mode, to the principal Cartesian coordinates, thereby obtaining the coordinates of the positions attained by atoms at the turning points of each normal modes of vibration. The pictorial plots obtained using the ORTEP program were then used as an aid in the description of the normal mode of vibration [35]. Using the standard orientation of the optimized structure, the ORTEP program was then used to draw the structure of the monomers, dimers and molecular complex [36, 37].

3.3.2 Execution of the computer program

All the theoretical calculations involving the equilibrium geometries, infrared wavenumbers and band intensities of the monomers, dimers and molecular complexes were performed using the Window version of the GAUSSIAN-98W computer program package [38,39] at the HF, MP2, and DFT level of theory [40,41], using the polarized 6-31G(d, p) split-valence basis set [42,43]. Geometry optimizations were carried out using the energy gradient procedure, commonly known as the Berny optimization method [43].

CHAPTER FOUR

Theoretical predictions of the geometries, energies and vibrational spectra of the monomers BF_3, CO, CO_2, H_2O, N_2O, O_2, O_3 and SO_2

4.1 The boron trifluoride monomer

In the past years a great amount of theoretical and experimental information about boron trifluoride, boron tribromide and aluminium trichloride trapped in cryogenic matrices has become available [44-48]. We are not going to focus more on the monomer; however, we are going to use them in the next two chapters since they have enjoyed a lot of investigation in the past years. Our main focus will be the geometrical parameters, wavenumbers and the band intensities of the boron trifluoride monomer.

4.1.1 The equilibrium geometries

The equilibrium geometry of the boron trifluoride monomer was optimized at the TIGHT level, using the Berny optimization procedure and the use of the FREQ option to establish the equilibrium structure for the monomer. It is observed from Table 4.1 that the HF method predicts shorter bond lengths as compared to other methods of computation. This simply imply that for both the MP2 and DFT methods the predicted bond lengths are overestimated by small amounts when compared with the experimental results. The $F\hat{B}F$ bond angle is not changed as compared with the experimental gas phase value.

4.1.2 The vibrational wavenumbers and the band intensities

The molecular energies determined at the HF, MP2 and DFT levels of computation using the 6-31G(d, p) split-valence polarized basis set are collected in Table 4.2. These energies are going to be used in the next two chapters for calculating the interaction energies and the BSSEs. The computed wavenumbers of BF_3 and the other monomers are listed in Table 4.3, along with experimental wavenumbers. Tables 4.4 and 4.5 show the

calculated/experimental wavenumber ratios of the $^{11}BF_3$ and $^{10}BF_3$ isotopomers, respectively. This tables show that the ab initio calculations at the HF level of the type reported here typically overestimate the experimental wavenumbers by ca. 7% whereas the MP2 and DFT methods better fit the experimentally determined values. It is probable that, for these molecules are hevelly complex, at the HF level of theory, the absence of electron correlation limits the accuracy with which the experimental wavenumbers may be expected to be reproduced.

Table 4.6 shows the calculated and the experimental gas-phase intensities of BF_3 [49] .The calculated/experimental intensity ratio are shown in Table 4.7. As was found for the wavenumbers, the agreement between theory and experiment is better for the BF_3 [49] monomer at both MP2 and DFTlevels of theory. At the HF approach using the 6-31G(d, p) basis set we expect to reproduce the IR band intensities to within a factor of two of the experimental observed ones [50-53]. For the BF_3 monomer this is indeed the case, with the out-of-phase bending intensity being overestimated, and the intensities of the doubly degenerate modes being predicted to be too low compaead with experimentally mearured ones.

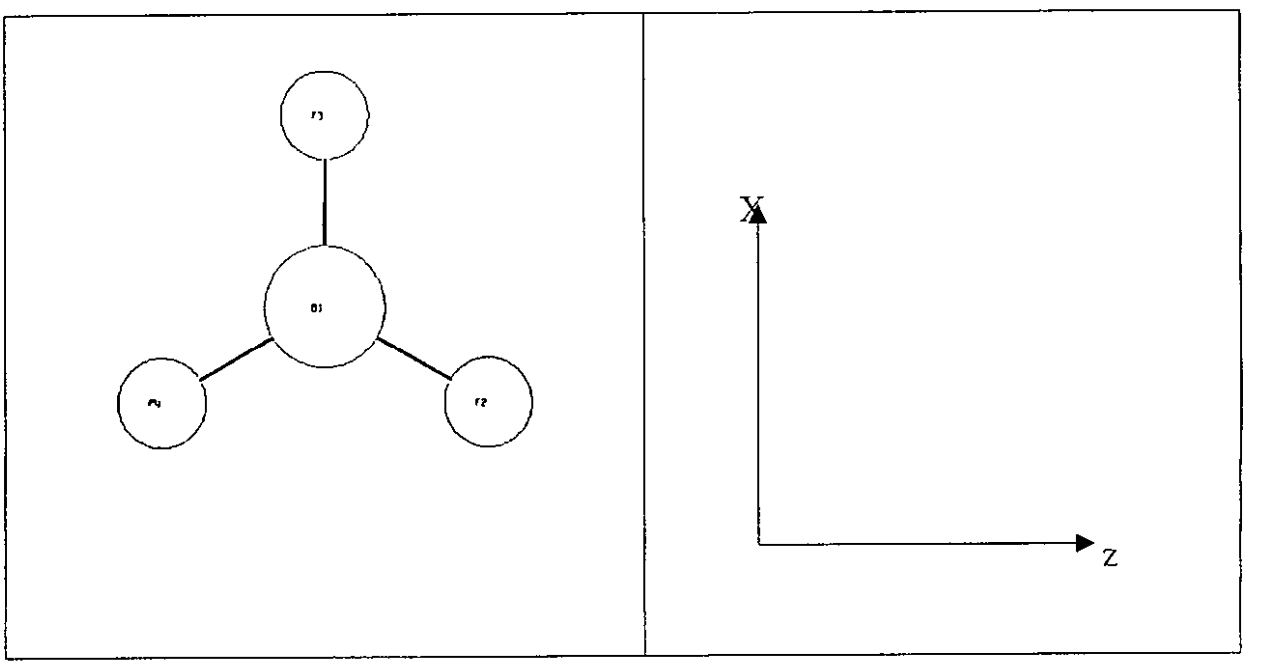

Figure 4.1 The structure of boron trifluoride monomer and the numbering of atoms together with the orientation of the axis.

4.2 The diatomic monomers (CO and O_2)

A number of van der Waals complexes containing BF_3 have been studied to date [53-60]. In every case the boron atom acts as the binding site and it is natural to interpret the bonding in terms of the Lewis acidity of BF_3. The current study was initiated in order to investigate the nature of the van der Waals bonding or electron donor-acceptor interaction with BF_3 when the bonding partners are CO and O_2. These complexes are fertile grounds for ab initio calculations because the self-consistent-field (SCF) calculations appear reliable enough for the prediction of some of the properties of interest such as geometries and frequencies [61]. Carbon monoxide is one of the most stable first row diatomic molecules and has accordingly been extensively investigated both experimentally [53-58] and theoretically [50,51,53-63].

4.2.1 The equilibrium geometries

It is observed from Table 4.1 that the HF level of theory predicts shorter bonds lengths when compared with the other two methods. This trend can also be observed in the dioxygen monomer. The molecular energies of the diatomic monomers are also collected in Table 4.2. The geometrical paramers are overestimated at both MP2 and DFT levels of theory when compared with the experimental ones.

4.2.2. The vibrational wavenumbers

The predicted vibrational wavenumbers of the CO and O_2 monomers, calculated at the three levels of computation, are listed in Table 4.3. All the computed vibrational wavenumbers of the oxygen are lower than the experimental values with the exception of the HF level of computation. This trend is also observed for the carbon monoxide monomer and this implies that for both monomers the HF method typically overestimates the experimental values.

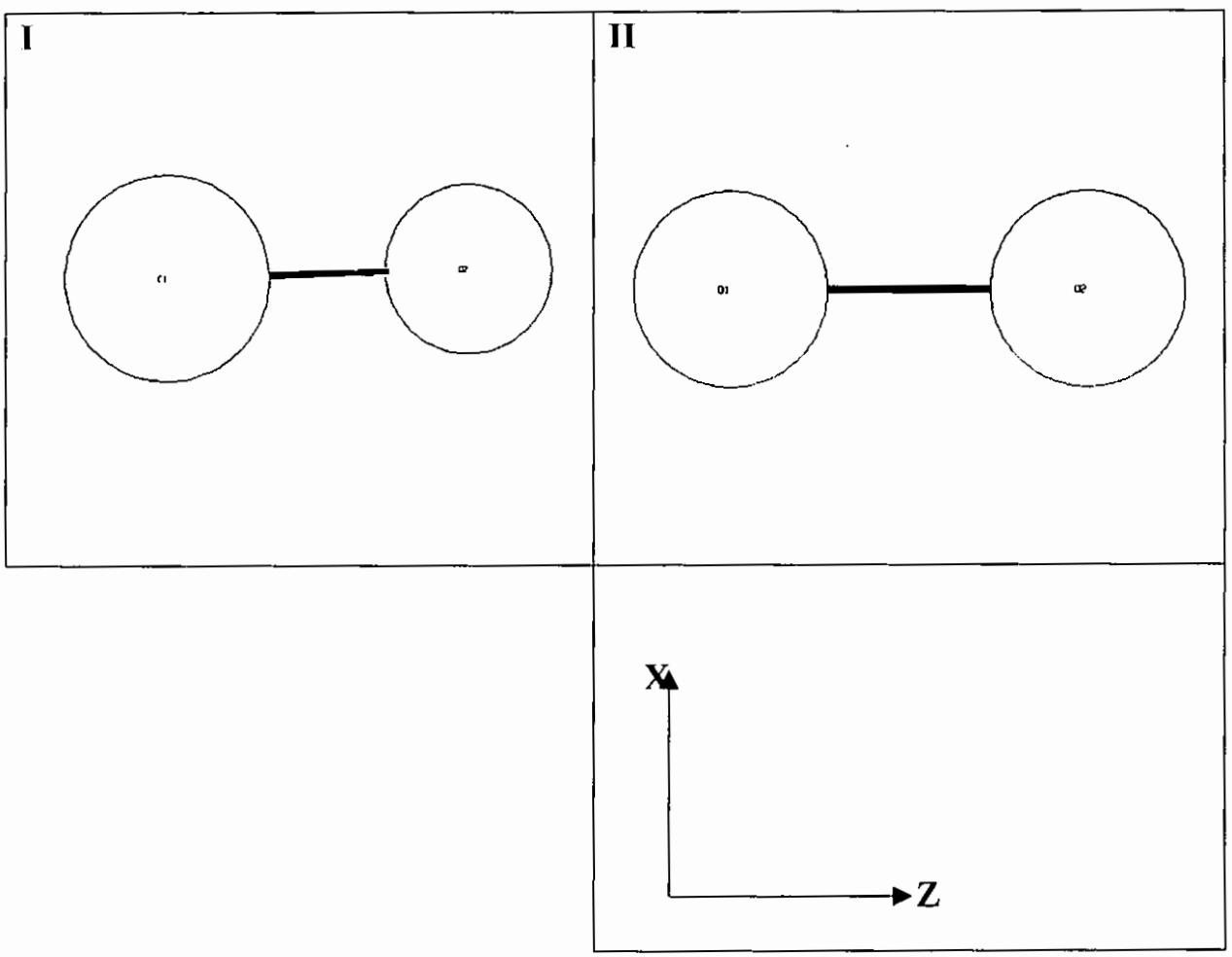

Figure 4.2 The structures, orientation of axis and the numbering of atoms of the diatomic monomers (**I**) CO and (**II**) O_2.

4.3.1 The triatomic monomers CO_2, H_2O, O_3, N_2O and SO_2

In the last few years a great amount of experimental and theoretical information on molecular interactions has become available [64-69]. Among molecular complexes the weakly bound systems, especially those in which the component interact through either a hydrogen bond or van der Waals or electron donor-acceptor interactions, have attracted special interest, mainly because of the prevalence of such bonds in nature.

4.3.1. The optimized geometrical parameters

The optimized geometrical parameters of the CO_2, H_2O, N_2O, O_3 and SO_2 monomers, calculated at the three levels of computation using the 6-31G(d, p) split-valence polarized basis set are also presented in Table 4.1, together with the experimental geometrical parameters. The ab initio results show that the equilibrium bond distances are shorter than the experimental values at the HF level of computation. Differences between the calculated and the experimental values are quite small, the largest deviation being in the bond length of the N_2O monomer. The HF method also predicts larger bond angles as compared with both the MP2 and DFT methods. At the HF level of computation the bond angle in the water monomer is slightly larger than the experimental values which was not expected. The bond angle in the corresponding sulphur dioxide monomer is underestimated by 1.1 deg from the experimental value while the MP2 and DFT methods are overestimate the value.

The equilibrium structures, the numbering of atoms and the relative orientation of the monomers are shown in Fig 4.3. The molecular energies of the triatomic monomers are also listed in Table 4.2.

4.3.2 The vibrational wavenumbers and the band intensities

The calculated and experimental wavenumbers for the triatomic monomers are collected in Table 4.3. All the wavenumbers calculated at the three levels of computation are consistently larger than the experimental values

with the exception of the ν_3 mode of the sulphur dioxide monomer. The calculated/experimental ratios of the triatomic monomers observed in nitrogen matrices are presented in Table 4.8. This table indicates that the HF method overestimates the experimental wavenumbers by ca. 13% on average while both the MP2 and DFT levels of computation predict the correct values for the carbon dioxide monomer. This trend is also observed for the other monomers at the HF method, while at the MP2 and DFT approaches the changes are minimal.

The predicted intensities are less useful than the wavenumbers for comparison purposes, since the experimental intensities are very difficult to measure. Moreover, the precision with which intensities may be calculated is intrinsically lower typically within a factor of two of the experimental value [70]. All the predicted infrared modes of the H_2O, O_3 and SO_2 triatomic monomers are expected to be observed.

In the Raman spectrum, only one strong band would be expected to be observed. In the case of the N_2O monomer it should be noted that there is a mixing of ν(NN) and ν(NO) vibrations giving rise to ν_1 and ν_2 modes, respectively. All calculated infrared active fundamental intensities are overestimated with the exception of the ν_1 and ν_2 modes at both the MP2 and DFT levels of theory.

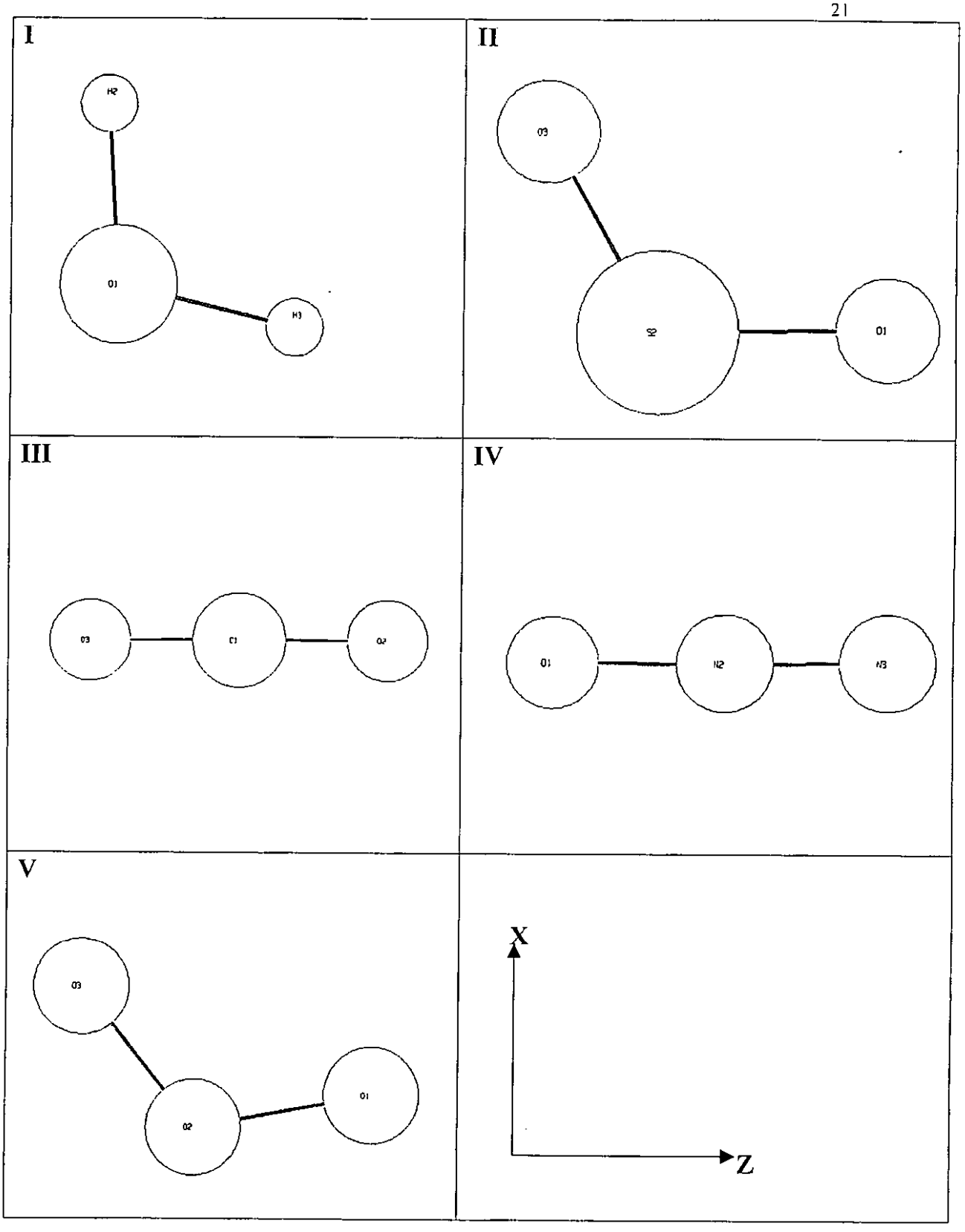

Figure 4.3 The structures of the (**I**) H_2O and (**II**) SO_2, (**III**) CO_2, (**IV**) N_2O and O_3 monomers together with the numbering of the atoms and orientation of the axis.

Table 4.1 The optimized geometrical parameters of BF_3, CO, CO_2, N_2O, H_2O, O_2, O_3, and SO_2 monomers using the 6-31G(d, p) split-valence polarized basis set.

			Level of theory			
Species	Point group	Parameters	HF	MP2	DFT	[a]Experimental
BF_3	$D_{\infty h}$	r(BF)/pm	130.1	132.2	131.8	131.3
		$F\hat{B}F$ /deg	120.0	120.0	120.0	120.0
CO	$C_{\infty v}$	r(CO)/pm	111.4	115.1	113.8	112.8
CO_2	$C_{\infty v}$	r(CO)/pm	114.3	118.0	116.9	116.0
		$O\hat{C}O$ /deg	180.0	180.0	180.0	180.0
H_2O	C_{2v}	r(OH)/pm	94.0	96.1	96.5	95.8
		$H\hat{O}H$ /deg	105.8	103.8	103.7	104.5
N_2O	$C_{\infty v}$	r(ON)/pm	117.8	119.3	119.2	118.4
		r(NN)/pm	109.2	117.2	113.4	112.8
		$N\hat{N}O$ /deg	180.0	180.0	180.0	180.0
O_2	$D_{\infty h}$	r(OO)/pm	116.8	124.7	121.4	120.8
O_3	C_{2v}	r(OO)/pm	121.4	130.0	126.4	125.3
		$O\hat{O}O$ /deg	117.9	116.3	117.9	118.2
SO_2	C_{2v}	r(SO)/pm	141.4	147.8	146.4	143.1
		$O\hat{S}O$ /deg	118.2	119.8	119.1	119.3

[a]Ref: 71

Table 4.2. Energies of the monomers calculated at the HF, MP2 and DFT levels of theory using the 6-31G(d, p) split-valence polarized basis set

Monomers	E(HF)/a.u	E(MP2)/a.u	E(DFT)/a.u
BF_3	-324.553222	-323.193822	-323.553221
CO	-112.737877	-113.021215	-113.309454
CO_2	-187.634176	-188.118363	-188.580940
H_2O	-76.022840	-76.219786	-76.419736
N_2O	-183.680122	-184.213684	-184.660270
O_2	-149.617908	-149.949732	-150.320042
O_3	-223.695277	-224.869545	-225.426484
SO_2	-547.169006	-547.682446	-548.587464

Table 4. 3 The calculated and the experimental wavenumbers of the BF_3, CO, CO_2, N_2O, H_2O, O_2, O_3, and SO_2 monomers.

Species	Symmetry species	Mode	Approximate description	Level of theory HF/cm^{-1}	MP2/cm^{-1}	DFT	[a]Expt/cm^{-1}
BF_3	a'_1	ν_1	$\nu_s(BF_3)$	943	889	889	888
	a'_2	ν_2	$\tau(BF_3)$	738	699	685	691
	e'	ν_3	$\nu_a(BF_3)$	1575	1497	1448	1449
		ν_4	$\delta_a(BF_3)$	508	481	479	480
CO	Σ_g	ν_1	(CO)	2439	2119	2209	2018
CO_2	Σ^+_g	ν_1	$\nu_s(CO_2)$	1519	1337	1338	1334
	$\prod$	ν_2	$\delta(CO_2)$	746	642	633	667
	Σ^-_u	ν_3	$\nu_a(CO_2)$	2585	2455	2448	2349
H_2O	a_1	ν_1	$\nu_s(H_2O)$	4102	3892	3786	3650
	a_2	ν_2	$\delta(H_2O)$	1753	1682	1666	1588
	b_1	ν_3	$\nu_a(H_2O)$	4249	4030	3912	3742
N_2O	Σ^+	ν_1	ν(NN)	2633	2247	2371	2224
	Σ^+	ν_2	ν(NO)	1393	1289	1344	1585
	$\prod$	ν_3	$\delta(N_2O)$	689	575	604	589
O_2	Σ_g^+	ν_1	ν(OO)	1998	1409	1660	1689
O_3	a_1	ν_1	ν_s(OO)	1256	1173	1266	1103
		ν_2	δ(OO)	1753	727	735	701
	b_1	ν_3	ν_a(OO)	849	2381	1240	1042
SO_2	a_1	ν_1	ν_s(SO)	1359	1077	1139	1151
		ν_2	δ(SO)	592	486	502	518
	b_1	ν_3	ν_a(SO)	1569	1305	1336	1362

[a]Ref: 71

Table 4.4 The calculated/experimental wavenumber ratios of the $^{11}BF_3$ monomer of D_{3h} symmetry calculated at the HF, MP2 and DFT levels of theory using the 6-31G(d, p) split-valence polarized basis set

Symmetry species	Mode	Approximate description	[a]wavenumber ratio HF	MP2	DFT
a'_1	ν_1	$\nu_s(BF_3)$	1.06	1.00	1.00
a''_2	ν_2	$\tau(BF_3)$	1.07	1.01	0.99
e'	ν_3	$\nu_a(BF_3)$	1.09	1.03	1.00
	ν_4	$\delta_a(BF_3)$	1.06	1.00	1.00
		Mean Average	1.07	1.01	1.00

Table 4.5 The calculated/experimental wavenumber ratios of the $^{10}BF_3$ monomer of D_{3h} symmetry calculated at the HF, MP2 and DFT levels of theory using the 6-31G(d, p) split-valence polarized basis set.

Symmetry species	mode	Approximate description	[a]wavenumber ratio HF	MP2	DFT
a'_1	ν_1	$\nu_s(BF_3)$	1.06	1.00	1.00
a''_2	ν_2	$\tau(BF_3)$	1.07	1.01	0.99
e'	ν_3	$\nu_a(BF_3)$	1.09	1.03	1.00
	ν_4	$\delta_a(BF_3)$	1.06	1.00	1.00
		Average mean	1.07	1.01	1.00

[a]Ratio= $\tilde{\upsilon}_{calc} / \tilde{\upsilon}_{exp}$

Table 4.6 Calculated infrared band intensities of the BF_3, CO, CO_2, N_2O, H_2O, O_2, O_3, and SO_2 monomers.

Species	Symmetry species	Vibrational mode	Approximate description	Level of theory HF	MP2	DFT	[a]Expt/km mol^{-1}
BF_3	a'_1	ν_1	$\nu_s(BF_3)$	—[b]	—[b]	—[b]	—[b]
	a''_2	ν_2	$\tau(BF_3)$	149	101	56	69
	e'	ν_3	$\nu_a(BF_3)$	485	409	382	1449
		ν_4	$\delta_a(BF_3)$	16	13	11	480
CO	Σ_g	ν_1	(CO)	138	26	70	70
CO_2	Σ_g	ν_1	$\nu_s(CO_2)$	0	0	0.3	9
	Π_u	ν_2	$\delta(CO_2)$	69	26	30	503
	Σ_u	ν_3	$\nu_a(CO_2)$	985	453	576	989
H_2O	a_1	ν_1	$\nu_s(H_2O)$	94	4	2	2
	a_1	ν_2	$\delta(H_2O)$	73	78	70	54
	b_3	ν_3	$\nu_a(H_2O)$	15	34	20	45
N_2O	Σ_g	ν_1	ν(NN)	490	263	310	346
	Σ_g	ν_2	ν(NO)	165	8	49	55
	Π	ν_3	δ(N2O)	20	5	9	7
O_2	Σ_g^+	ν_1	ν(OO)	—[b]	—[b]	—[b]	—[b]
O_3	a_1	ν_1	ν_a(OO)	849	2	0.2	1103
		ν_2	δ(OO)	9	8	8	701
	b_2	ν_3	ν_s(OO)	0.1	1489	166	1042
SO_2	a_1	ν_1	ν_s(SO)	64	13	28	1101
		ν_2	δ(SO)	62	32	34	497
	b_1	ν_3	ν_a(SO)	322	79	165	1318

[a]Ref: 71, [b] infrared inactive band

Table 4.7 The calculated/experimental intensity ratios of the boron trifluoride monomer of D_{3h} symmetry calculated at the HF, MP2 and DFT levels of theory using 6-31G(d, p) basis set.

Symmetry species	Mode	Approximate description	Levels of theory HF	MP2	DFT
a'_1	ν_1	$\nu_s(BF_3)$	___[a]	___[a]	___[a]
a''_2	ν_2	$\tau(BF_3)$	2.16	1.43	0.81
e'	ν_3	$\nu_a(BF_3)$	0.33	0.26	0.26
	ν_4	$\delta_a(BF_3)$	0.03	0.28	0.02

[a] infrared inactive band

Table 4.8 Calculated/experimental wavenumber ratios of the CO_2, N_2O, H_2O, O_3, and SO_2 monomers.

Species	Symmetry species	Mode	Approximate description	[a]Level of theory HF	MP2	DFT
CO_2	Σ_g	ν_1	$\nu_s(CO_2)$	1.14	1.00	1.00
	Π_u	ν_2	$\delta(CO_2)$	1.12	0.96	0.95
	Σ_u	ν_3	$\nu_a(CO_2)$	1.10	1.05	1.05
		Average mean		1.12	1.00	1.00
H_2O	a_1	ν_1	$\nu_s(H_2O)$	1.12	1.06	1.04
	a_1	ν_2	$\delta(H_2O)$	1.10	1.05	1.04
	b_3	ν_3	$\nu_a(H_2O)$	1.13	1.07	1.05
		Average mean		1.12	1.06	1.04
N_2O	Σ_g	ν_1	$\nu(NN)$	1.18	1.01	1.07
	Σ_g	ν_2	$\nu(NO)$	1.08	1.01	1.05
	Π	ν_3	$\delta(N_2O)$	1.17	0.98	1.03

Table 4.8 continue

Species	Symmetry species	Mode	Approximate description	[a]Level of theory HF	MP2	DFT
		Average mean		1.14	1.00	1.05
O_3	a_1	ν_1	ν_a(OO)	1.14	1.06	1.15
		ν_2	δ(OO)	1.21	1.04	1.05
	b_2	ν_3	ν_s(OO)	1.68	1.05	1.19
		Average mean		1.34	1.05	1.13
SO_2	a_1	ν_1	ν_s(SO)	1.18	0.94	0.98
		ν_2	δ(SO)	1.14	0.93	0.97
	b_1	ν_3	ν_a(SO)	1.15	0.96	0.98
		Average mean		1.16	0.95	0.98

[a]Ratio=$\tilde{\upsilon}_{calc} / \tilde{\upsilon}_{exp}$

CHAPTER FIVE

Theoretical predictions of the geometries, energies and vibrational spectra of the homo-dimers.

5.1 The boron trifluoride dimer

The boron trifluoride dimer has been subjected to several matrix isolation and theoretical studies by a number of authors [55,57,72,73,76] and the presence of the dimer was detected by means of infrared spectroscopy. The suggested configuration for the dimer was a bridged cyclic dimeric species of D_{2h} symmetry similar to that of the B_2H_6 [74], Al_2Cl_6 and Al_2Br_6 [75] dimers. In the latest study by Nxumalo *et. al* [130] the authors based their investigations on a bridged cyclic dimeric structure of C_{2h} configuration calculated at the HF level using the 6-31G* basis set. The findings of Nxumalo and his co-workers [130] confirm that this dimer is more stable than the D_{2h} dimer and this was also supported by matrix isolation results [76]. In ab initio results obtained, the mainly focussed would be based on the investigations of the bridged cyclic dimeric structure of C_{2h} configuration using the 6-31G(d, p) basis set. The three levels of theory were employed to determine the BSSEs, the vibrational wavenumbers and band intensities of the ^{10}B and ^{11}B isotopic species.

5.1.1 The optimized geometrical parameters of the boron trifluoride dimer.

Fig 5.1 illustrates the structure of the boron trifluoride dimer of the C_{2h} symmetry with the orientation of the axis and the numbering of atoms for identification purposes. The structure was drawn from the standard orientation of the optimized structure using an Oak Ridge Thermal Ellipsoidal Program (ORTEP). Table 5.1.1 presents the values of the geometrical parameters of the boron trifluoride dimer of C_{2h} symmetry. The boron trifluoride monomer bond lengths calculated at the HF, MP2 and DFT levels of theory are equal to 130.1, 132.2 and 131.8 pm, respectively. Table 5.1.1 shows that the BF bond length of the boron trifluoride subunits in the

dimer is slightly changed from the monomer value at all three levels of theory. The intermolecular bond length, $r(B_1...B_2)$ is equal to 337.6, 230.4 and 323.9 pm at the HF, MP2 and DFT levels of theory, respectively. The bonded BF bond length, i.e., $r(B_1F_3)$ and $r(B_2F_4)$, at the HF and DFT levels show an increase relative to the monomer value while the terminal non-bonded BF bond lengths, for example, $r(B_1F_5)$=$r(B_1F_6)$, undergo slight decreases at both levels of computation. The MP2 level shows inconsistency relative to the two methods, i.e. an increase to 146.9 pm as well as increases to 132.5 pm for the bond BF bond length and the terminal non-bonded BF bond lengths, respectively. The boron trifluoride monomer bond angle calculated at all levels equal to 120.0. Table 5.1.1 shows that the BF bond angle of the boron trifluoride subunits in the dimer are completely unchanged from the monomer value at the DFT and HF methods and at the MP2 approach it is substantially changed. These minor changes accompanying the dimerization of boron trifluoride are indicative of the presence of some weak donor-acceptor interactions.

5.1.2 The dimerization energy

The dimerization energies of the boron trifluoride dimer of C_{2h} symmetry before and after correction for BSSEs by the full counterpoise method [77] are listed in Table 5.1.2. As illustrated in this table, the boron trifluoride dimer of the C_{2h} symmetry is strongly bonded, although it must be stressed that the interactions found in all the methods are strong. The difference between the uncorrected dimerization energies of either of the methods is not that large, and the BSSEs account for about two thirds of the interaction energies calculated at both the HF and DFT levels of theory.

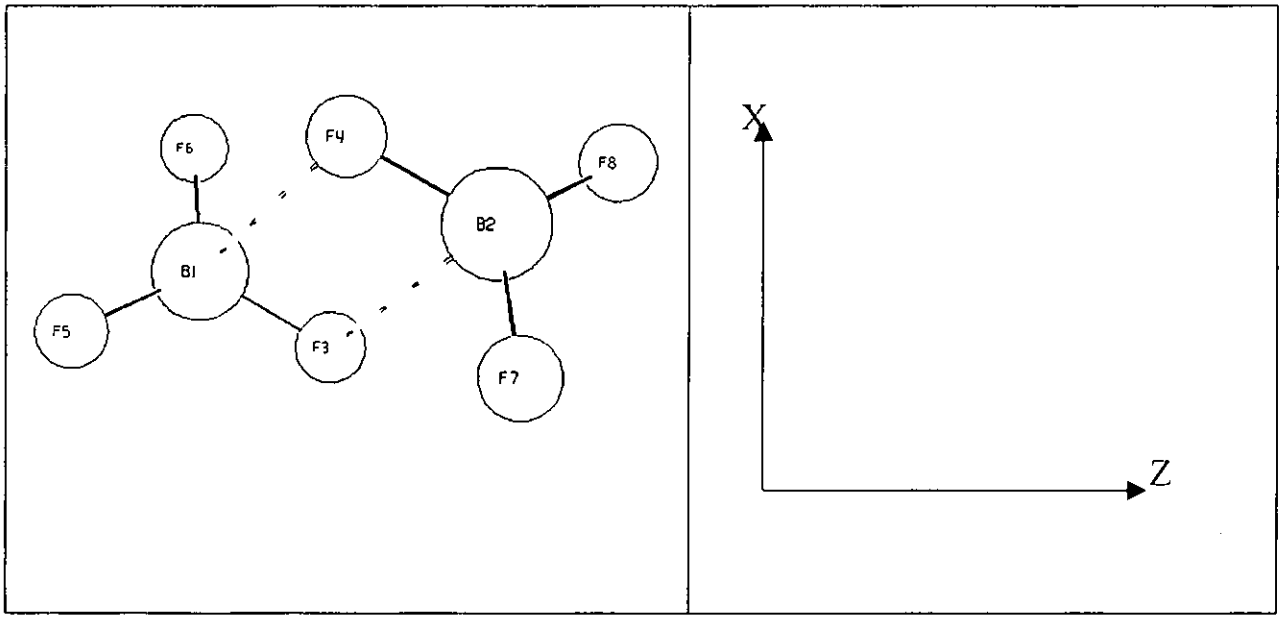

Figure 5.1 The structure of the boron trifluoride dimer of C_{2h} symmetry together with the numbering of atoms and the orientation of the axis.

Table 5.1.1 The optimized geometrical parameters of the $(BF_3)_2$ dimer calculated at the HF, MP2 and DFT levels of theory using the 6-31G(d, p) split-valence polarized basis set

		Level of theory		
Species	Parameters	HF	MP2	DFT
$(BF_3)_2$	$r(B_1...B_2)$/pm	337.6	230.4	323.9
	$r(B_1F_3) = (B_2F_4)$/pm	131.0	146.9	132.9
	$r(B_1...F_4) = r(B_2...F_3)$/pm	277.4	169.3	266.8
	$r(B_1F_5) = (B_1F_6)$/pm	129.8	132.5	131.5
	$r(B_2F_7) = (B_2F_8)$/pm	129.8	132.5	131.5
	$B_2...\hat{B}_1F_3 = B_1...\hat{B}_2F_4$ /deg	52.2	47.2	53.3
	$B_2...\hat{B}_1F_5 = B_1...\hat{B}_2F_8$ /deg	108.2	117.9	108.0
	$F_3\hat{B}_1F_5 = F_4\hat{B}_2F_8$ /deg	119.6	114.0	119.6
	$B_2...\hat{B}_1F_6 = B_1...\hat{B}_2F_6$ /deg	108.2	117.9	108.0
	$F_3\hat{B}_1F_6 = F_4\hat{B}_2F_7$ /deg	119.6	114.0	119.6
	$F_5\hat{B}_1F_6 = F_7\hat{B}_2F_8$ /deg	120.8	122.2	120.0

Table 5.1.2 The dimerization energies and the basis set superposition errors of the $(^{11}BF_3)_2$ dimer calculated at the HF, MP2, and DFT levels of theory using the 6-31G(d, p) split-valence polarized basis set.

			Level of theory		
Species	Point group	Energy/kJ mol^{-1}	HF	MP2	DFT
$(BF_3)_2$	C_{2h}	ΔE (uncorrected)	-12.42	-4.89	-8.43
		[b]BSSE	8.22	2.92	2.18
		ΔE (corrected)	-4.20	-1.97	-6.25

[b]basis set superposition error

5.1.3 The vibrational wavenumbers and band intensities

The HF, MP2 and DFT harmonic vibrational analyses for the boron trifluoride dimer, together with the approximate description of the normal modes, are given in Table 5.1.3. The vibrations belonging to a_g and b_g symmetry species are infrared inactive, those belonging to a_u and b_u species are infrared active. Table 5.1.3 and 5.1.4 show $5a_u$ and $2b_g$ modes shift the b_g up. Table 5.1.3 list ν_{10} (HF level) as being IR Inactive. The $(^{10}BF_3)_2$ and $(^{11}BF_3)_2$ isotopic variants of the boron trifluoride dimer have a C_{2h} symmetry, and their normal modes transform as

$$F_{vib}=6a_g+4a_u+3b_g+5b_u$$

Based on the relative abundances of the ^{10}B and ^{11}B isotopes, the concentration of the $(^{10}BF_3)_2$ and $(^{11}BF_3)_2$ species in any natural matrix isolation sample were predicted to be in the ratio 16:1 [55]. Therefore, in order to fully interpret the matrix isolation spectrum of such a sample, it is necessary to predict the positions and intensities of the bands of the two isotopomers. The vibrational wavenumbers and intensites for the boron trifluoride monomers are shown in Table 4.3 and Table 4.4, respectively (see chapter 4, page 24 and 25) together with the approximate descriptions of normal modes and the experimental gas phase results for the $^{10}BF_3$ species only.

Table 5.1.3 Calculated wavenumber together, with the intensities of the $^{11}BF_3$ dimer of C_{2h} symmetry structure calculated at the HF, MP2 and DFT levels of theory using the 6-31G(d, p) split-valence polarized basis set and the experimental wavenumbers.

Symmetry Species	mode	approximate description	HF $\tilde{\upsilon}/cm^{-1}$	[a]A/km mol^{-1}	MP2 $\tilde{\upsilon}/cm^{-1}$	[a]A/km mol^{-1}	DFT $\tilde{\upsilon}/cm^{-1}$	[a]A/km mol^{-1}	[d]Experimental $\tilde{\upsilon}/cm^{-1}$
a_g	ν_1	ν(BF)(I.P.)	1542	____[b]	1262	____[b]	1449	____[b]	____[c]
	ν_2	ν_s(BF)(I.P.)	936	____[b]	753	____[b]	881	____[b]	____[c]
	ν_3	T(BF)(I.P.)	732	____[b]	625	____[b]	669	____[b]	____[c]
	ν_4	$\delta(BF_2)$(I.P.)	509	____[b]	534	____[b]	481	____[b]	____[c]
	ν_5	ring deformation	154	____[b]	280	____[b]	153	____[b]	____[c]
	ν_6	ring stretch	49	____[b]	214i	____[b]	54	____[b]	____[c]
a_u	ν_7	$\nu_a(BF_2)$(O.P.)	1599	928	1522	744	1514	724	1458
	ν_8	$\delta_a(BF_3)$(O.P.)	510	29	508	16	477	19	459
	ν_9	$t_w(BF_3)$(O.P.)(I.M)	42	0.01	186	0.4	41	0.01	____[c]
	ν_{10}	ring pucker	16	____[b]	62	[b]	10	[b]	____[c]
b_g	ν_{11}	$\nu_a(BF_2)$(I.P)	1582	____[b]	1483	____[b]	1455	____[b]	____[c]
	ν_{12}	$\delta(BF_3)$(I.P.)	500	____[b]	395	____[b]	470	____[b]	____[c]
	ν_{13}	$t_w(BF_2)$(I.P)(I.M)	43	____[b]	303	____[b]	42	____[b]	____[c]
b_u	ν_{14}	ν(BF)(O.P.)	1546	976	1163	801	1455	792	1443
	ν_{15}	$\nu_s(BF_3)$(O.P.)	939	0.6	882	254	885	0.8	820
	ν_{16}	$T(BF_3)$(O.P.)(I.M)	719	355	632	500	662	247	652
	ν_{17}	$\delta(BF_3)$(O.P.)	506	33	455	13	477	19	459
	ν_{18}	ring stretch (O.P)(I.M)	35	1	316	24	51	2	____[c]

[a]A~ band intensity, [b]infrared inactive, [c]band not observed in this region, IP~in-phase, OP~ out-of-Phase and IM~ intermolecular mode

d Ref: 130

Table 5.1.4 Calculated wavenumber together, with the intensities and the experimental wavenumbers of the $^{10}BF_3$ dimer of the C_{2h} symmetry structure calculated at the HF, MP2 and DFT levels of theory using the 6-31G(d, p) split-valence polarized basis set.

Symmetry Species	mode	approximate description	HF $\tilde{\upsilon}/cm^{-1}$	HF A[a]/km mol^{-1}	MP2 $\tilde{\upsilon}/cm^{-1}$	MP2 A[a]/km mol^{-1}	DFT $\tilde{\upsilon}/cm^{-1}$	DFT A[a]/km mol^{-1}	[d] Experimental $\tilde{\upsilon}/cm^{-1}$
a_g	ν_1	ν(BF)(I.P.)	1599	——[b]	1308	——[b]	1503	——[b]	——[c]
	ν_2	ν_s(BF)(I.P.)	936	——[b]	757	——[b]	882	——[b]	——[c]
	ν_3	T(BF)(I.P.)	791	——[b]	631	——[b]	697	——[b]	——[c]
	ν_4	$\delta(BF_2)$(I.P.)	511	——[b]	540	——[b]	483	——[b]	——[c]
	ν_5	ring deformation	154	——[b]	281	——[b]	154	——[b]	——[c]
	ν_6	ring stretch	50	——[b]	220i	——[b]	55	——[b]	——[c]
a_u	ν_7	$\nu_a(BF_2)$(O.P.)	1658	1007	1579	807	1570	786	1505
	ν_8	$\delta_a(BF_3)$(O.P.)	512	29	511	16	480	19	459
	ν_9	tw(BF_3)(O.P.)(I.M)	42	0.01	187	0.0001	41	0.006	——[c]
	ν_{10}	ring pucker	16	[b]	62	[b]	10	[b]	——[c]
b_g	ν_{11}	$\nu_a(BF_2)$(I.P)	1640	——[b]	1538	——[b]	1554	——[b]	——[c]
	ν_{12}	$\delta(BF_3)$(I.P.)	502	——[b]	398	——[b]	472	——[b]	——[c]
	ν_{13}	tw(BF_2)(I.P)(I.M)	43	——[b]	304	——[b]	42	——[b]	——[c]
b_u	ν_{14}	ν(BF)(O.P.)	1603	1059	1202	887	1509	859	1484
	ν_{15}	$\nu s(BF_3)$(O.P.)	939	0.8	901	311	885	0.9	820
	ν_{16}	T(BF_3)(O.P.)(I.M)	748	385	647	496	689	269	678
	ν_{17}	$\delta(BF_3)$(O.P.)	508	33	457	12	480	21	459
	ν_{18}	ring stretch (O.P)(I.M)	35	I	317	24	51	2	——[c]

[a]A~ band intensity, [b]infrared inactive, [c]band not observed in this region, IP~in-phase, OP~ out-of-Phase and IM~ intermolecular mode

d Ref: 130

[a]A= band intensity, [b]infrared inactive, [c] band not observed in this region, IP= in-phase, O.P= out-of-phase, I.M=intermolecular mode

[d] Ref: 130

The calculated/experimental wavenumber ratios of the $(^{11}BF_3)_2$ and $(^{10}BF_3)_2$ dimer are shown in Table 5.1.5 and 5.1.6 respectively. Table 5.1.5 shows that both the HF and DFT methods overestimate the experimental data by ca.10% and ca. 3% on average, respectively, while the MP2 fit the experimental values. This trend is also observed for the $(^{10}BF_3)_2$ isotopomer. Since the MP2 method predicts the values which are closest to the experimental ones, we are therefore justified to base our investigations on the MP2 method for further discussion. The correspondence between each of the dimer modes and its counterpart in the monomer in all three levels of theory is presented in Table 5.1.7, in which the monomer-dimer wavenumbers shifts are reported. This table indicates that all the BF-stretching vibrations derived from the monomer ν_1 mode are red shifted, although only the ν_{15} mode of the dimer is infrared inactive. All the dimer modes correlating with ν_2 mode of the monomer are also red-shifted. At the (MP2) levels of theory, the antisymmetric BF_3-stretching vibration undergoes the largest changes on dimerization, splitting into a pair of bands (ν_1 and ν_{14}) which are shifted to the red, and one bands (ν_{11}) is red-shifted. The infrared active modes of the dimer correlating with the degenerate BF_3-bending mode (ν_8 and ν_{17}) also experience the same shifts and suffer only minimal displacements, while the inactive vibration ν_4 and ν_{12} modes, are also shifted by amount less than 90 cm^{-1} in either direction. It is noted that the largest wavenumber shifts of the infrared active bands on dimerization are those associated with the BF bonds actually involved in the interaction (ν_7,ν_{14} and ν_{16}) as predicted by Friedrich and Person's theory of EDA interaction [78]. The same is true for the infrared inactive ν_1 band, which is the ν_{15} of the dimer, the in-phase coupled stretching mode of the two bonded BF groups. The infrared spectra of the $(BF_3)_2$ are thus predicted to consist of two bands derived from the antisymmetric stretching mode, one displaced to approximately 340 cm^{-1} to the red and the other one to ca. 25 cm^{-1} to the blue relative to the monomer; two bands, ν_8 and ν_{17}, one shifted to higher wavenumbers and the other one to lower wavenumbers of the monomer out-of-plane bending mode by almost the same amount, two bands one correlating with the symmetric stretching mode of the monomer, ν_{15}, being shifted to the red and the other one correlating to the out-of-plane bending absorption of the monomer , ν_{16}, being also shifted to the red by ca. 67 cm^{-1}.

Table 5.1.5 Ratios of the computed to the experimental wavenumbers observed in nitrogen matrices of the intramolecular modes of the $^{11}(BF_3)$ dimer.

	[a]Level of theory		
Mode	HF/6-31G(d, p)	MP2/6-31G(d, p)	DFT/6-31G(d, p)
ν_7	1.10	1.04	0.96
ν_8	1.11	1.11	1.04
ν_{14}	1.09	0.81	1.01
ν_{15}	1.07	1.08	1.08
ν_{16}	1.15	0.97	1.02
ν_{17}	1.06	0.99	1.04
Mean Average	1.10	1.00	1.03

Table 5.1.6 Ratios of the computed to the experimental wavenumbers observed in nitrogen matrices of the intramolecular modes of the $^{10}(BF_3)$ dimer.

	[a]Levels of theory		
	HF/6-31G(d, p)	MP2/6-31G(d, p)	DFF/6-31G(d, p)
ν_7	1.11	1.05	1.04
ν_8	1.12	1.11	1.05
ν_{14}	1.08	0.80	1.02
ν_{15}	1.10	0.95	1.02
ν_{16}	1.11	1.00	1.05
Mean Average	1.10	1.00	1.03

[a]Ratio=$\tilde{\upsilon}_{calc} / \tilde{\upsilon}_{expt}$

The computed infrared intensities for the $(^{10}BF_3)_2$ and $(^{11}BF_3)_2$ species are gathered in Table 5.1.8. The symmetric BF_3-stretching mode, ν_{15}, and the three intermolecular modes, ν_9, ν_{10} and ν_{18} have negligible intensities. Thus, only five infrared active bands of the C_{2h} dimer would be expected to be observed at best. The intensity ratio of the infrared active bands of $(^{11}BF_3)_2$ to the corresponding bands of $^{11}BF_3$ are presented in Table 5.1.9. These ratios are all clustered around a value of 1 to 5. The increase in intensity on dimerization are consistent with the prediction of the Friedrich and Pearson theory [78] while the modest values of the ratio testify to the weakness of the interaction.

The Raman intensities and depolarization ratio of the a_g and b_g modes of the $(^{11}BF_3)_2$ dimer, computed as part of the vibrational analysis [79] are listed in Table 5.1.10, and those of the monomer [80] are listed in Table 4.6. Raman intensities have received relatively little attention, compared with their infrared counterparts, as diagnostic parameters for analysis of molecular interactions, either experimentally or theoretically [76]. Nevertheless, it is instructive to compare the changes in the Raman intensities of the monomer band resulting to the formation of the dimer, as was done for the infrared bands in Table 5.1.9. The intensity ratios are found to lie in the range from 1.7 to 2.9, exactly as was observed for the infrared intensity ratios. Moreover the fact that none of the Raman intensities is increased by a substantial amount as a result of the dimerization process confirms to the evidence provided by the infrared intensity behaviour that the interaction is a weak one.

Table 5.1.7 Comparison of the calculated wavenumbers of the $^{11}BF_3$ dimer with those of the corresponding modes of the $^{11}BF_3$ monomer calculated at the HF, MP2 and DFT levels of theory.

HF/6-31G(d, p)					MP2/6-31G(d, p)					DFT/6-31G(d, p)				
dimer		monomer			dimer		monomer			dimer		monomer		
Mode ([a]SS)	$\tilde{\upsilon}/cm^{-1}$	Mode ([a]SS)	$\tilde{\upsilon}/cm^{-1}$	[b]Shifts $\Delta\tilde{\upsilon}/cm^{-1}$	Mode ([a]SS)	$\tilde{\upsilon}/cm^{-1}$	Mode ([a]SS)	$\tilde{\upsilon}/cm^{-1}$	[b]Shifts $\Delta\tilde{\upsilon}/cm^{-1}$	Mode ([a]SS)	$\tilde{\upsilon}/cm^{-1}$	Mode ([a]SS)	$\tilde{\upsilon}/cm^{-1}$	Shifts $\Delta\tilde{\upsilon}/cm^{-1}$
$\nu_1(a_g)$	1542	$\nu_3(e')$	1575	-33	$\nu_1(a_g)$	1262	$\nu_3(e')$	1497	-235	$\nu_1(a_g)$	1449	$\nu_3(e')$	1448	1
$\nu_2(a_g)$	936	$\nu_1(a')$	943	-7	$\nu_2(a_g)$	753	$\nu_1(a')$	889	-136	$\nu_2(a_g)$	881	$\nu_1(a')$	889	-8
$\nu_3(a_g)$	732	$\nu_2(a'')$	738	-6	$\nu_3(a_g)$	625	$\nu_2(a'')$	699	-74	$\nu_3(a_g)$	669	$\nu_2(a'')$	685	-16
$\nu_4(a_g)$	509	$\nu_4(e')$	508	1	$\nu_4(a_g)$	534	$\nu_4(e')$	481	53	$\nu_4(a_g)$	481	$\nu_4(e')$	479	2
$\nu_7(a_u)$	1599	$\nu_3(e')$	1575	24	$\nu_7(a_u)$	1522	$\nu_3(e')$	1497	25	$\nu_7(a_u)$	1514	$\nu_3(e')$	1448	66
$\nu_8(a_u)$	510	$\nu_4(e')$	508	2	$\nu_8(a_u)$	508	$\nu_4(e')$	481	27	$\nu_8(a_u)$	477	$\nu_4(e')$	479	-2
$\nu_{11}(b_g)$	1582	$\nu_3(e')$	1575	7	$\nu_{11}(b_g)$	1483	$\nu_3(e')$	1497	-14	$\nu_{11}(b_g)$	1455	$\nu_3(e')$	1448	7
$\nu_{12}(b_g)$	500	$\nu_4(e')$	508	-8	$\nu_{12}(b_g)$	395	$\nu_4(e')$	481	-86	$\nu_{12}(b_g)$	470	$\nu_4(e')$	479	-9
$\nu_{14}(b_u)$	1546	$\nu_3(e')$	1575	-29	$\nu_{14}(b_u)$	1163	$\nu_3(e')$	1497	-334	$\nu_{14}(b_u)$	1455	$\nu_3(e')$	1448	7
$\nu_{15}(b_u)$	939	$\nu_1(a')$	943	-4	$\nu_{15}(b_u)$	882	$\nu_1(a')$	889	-7	$\nu_{15}(b_u)$	885	$\nu_1(a')$	889	-4
$\nu_{16}(b_u)$	717	$\nu_2(a'')$	738	19	$\nu_{16}(b_u)$	632	$\nu_2(a'')$	699	-67	$\nu_{16}(b_u)$	662	$\nu_2(a'')$	685	-23
$\nu_{17}(b_u)$	506	$\nu_4(e')$	508	-2	$\nu_{17}(b_u)$	455	$\nu_4(e')$	481	-26	$\nu_{17}(b_u)$	477	$\nu_4(e')$	479	-2

[a](SS)~ Symmetry Species

[b]Shifts=$(\tilde{\upsilon}/cm^{-1})_{dimer}-(\tilde{\upsilon}/cm^{-1})_{monomer}$

Table 5.1.8 Calculated intensities of the infrared active modes of the two isotopic variants of the boron trifluoride dimer of symmetry C_{2h} computed at the HF, MP2 and DFT levels of theory using the 6-31G(d, p) split-valence polarized basis set.

		HF/6-31G(d, p)		MP2/6-31G(d, p)		DFT/6-31G(d, p)	
Symmetry species	Mode	Intensity /km mol^{-1} $(^{10}BF_3)_2$	Intensity /km mol^{-1} $(^{11}BF_3)_2$	Intensity /km mol^{-1} $(^{10}BF_3)_2$	Intensity /km mol^{-1} $(^{11}BF_3)_2$	Intensity /km mol^{-1} $(^{10}BF_3)_2$	Intensity /km mol^{-1} $(^{11}BF_3)_2$
a_u	ν_7	1007	928	744	807	724	786
	ν_8	29	29	16	16	19	19
	ν_9	0.0	0.0	0.4	10^{-3}	0.01	0.01
	ν_{10}	0.01	0.01	0.6	0.5	10^{-3}	10^{-3}
b_u	ν_{14}	1059	976	801	887	792	859
	ν_{15}	0.8	0.6	254	311	0.8	0.9
	ν_{16}	385	355	500	496	247	269
	ν_{17}	33	33	13	13	19	21
	ν_{18}	0.01	0.01	24	24	2	2

Table 5.1.9 Ratios of the intensities of the infrared active bands of the $^{11}BF_3$ dimer to those of the corresponding modes of the $^{11}BF_3$ monomer at the HF, MP2 and DFT levels of theory using the 6-31G(d, p) split-valence polarized basis set.

HF/6-31G(d, p)					MP2/6-31G(d, p)				DFT/6-31G(d, p)			
$^{11}(BF_3)_2$		$^{11}BF_3$			$^{11}(BF_3)_2$	$^{11}BF_3$			$^{11}(BF_3)_2$	$^{11}BF_3$		
Mode (^{a}SS)	Intensity /km mol^{-1}	mode (^{a}SS)	Intensity /km mol^{-1}	$\frac{A_{dimer}}{A_{monomer}}$	Intensity /km mol^{-1}	mode (^{a}SS)	Intensity /km mol^{-1}	$\frac{A_{dimer}}{A_{monomer}}$	Intensity /km mol^{-1}	mode (^{a}SS)	Intensity /km mol^{-1}	$\frac{A_{dimer}}{A_{monomer}}$
$\nu_7(a_u)$	928	$\nu_3(e')$	485	1.91	744	$\nu_3(e')$	409	1.82	786	$\nu_3(e')$	352	2.81
$\nu_8(a_u)$	29	$\nu_4(e')$	16	1.81	16	$\nu_4(e')$	13	1.23	19	$\nu_4(e')$	11	1.73
$\nu_{14}(b_u)$	976	$\nu_3(e')$	485	2.01	801	$\nu_3(e')$	409	1.96	859	$\nu_3(e')$	382	2.25
$\nu_{15}(b_u)$	0.6	$\nu_1(a_1')$	0	-	254	$\nu_1(a_1')$	0	-	0.9	$\nu_1(a_1')$	0	-
$\nu_{16}(b_u)$	355	$\nu_1(a''_2)$	149	2.38	500	$\nu_1(a''_2)$	101	4..95	269	$\nu_1(a''_2)$	56	4.80
$\nu_{17}(b_u)$	33	$\nu_4(e')$	16	2.06	13	$\nu_4(e')$	13	1.00	21	$\nu_4(e')$	11	1.90

(^{a}SS)= symmetry species

5.1.10 Ratios of the intensities of the Raman-active bands of the $(^{11}BF_3)_2$ dimer to those corresponding modes of the $^{11}BF_3$ monomer at the HF level of theory, using the 6-31G(d, p) split-valence polarizes basis set.

$^{11}(BF_3)_2$		$^{11}BF_3$		
Mode (Symmetry species)	Intensity ($10^2 m^4 kg^{-1}$)	Mode (symmetry species)	Intensity ($10^2 m^4 kg^{-1}$)	A(dimer) / A(monomer)
$\nu_1(a_g)$	0.1489	$\nu_3(e')$	0.0529	2.81
$\nu_2(a_g)$	2.3189	$\nu_1(a_1')$	1.2051	1.92
$\nu_3(a_g)$	0.0599	$\nu_2(a''_2)$	0	-
$\nu_4(a_g)$	0.4815	$\nu_4(e')$	0.2571	1.87
$\nu_{11}(b_g)$	0.1029	$\nu_3(e')$	0.0259	1.95
$\nu_{12}(b_g)$	0.4541	$\nu_4(e')$	0.2571	1.77

5.2 The Carbon Monoxide dimer

In recent years the studies of molecular interactions involving boron trifluoride as an electron acceptor (Lewis acid), with a variety of carbon [81-83], nitrogen [84-86], oxygen [81,84,87-88], sulphur [84,89-91] and some halogen electron donors have been carried out. For the studies mentioned above, the matrix isolation infrared spectroscopic technique was used to determine the effect on the spectrum of the interaction of boron trifluoride molecule with the electron donor. As early as 1913, to prepare a chemically bound $(CO)_2$ species have proven unsuccessful. Since carbon monoxide dimer, as a simple molecular associated species has not been the subject of the previous theoretical studies this prompted us to further investigate this interesting molecular species.

5.2.1 The optimised geometrical parameters of the carbon monoxide dimer

Figure 5.2 shows the optimized structure of the CO dimer. This is a true global minimum structure. The absence of a negative eigenvalue lends strong support to the identification of this dimer as the most preferred configuration. Table 5.2.1 presents the values of the converged geometrical parameters of the carbon monoxide dimer. The numbering of atoms and the orientation of the axis are illustrated in fig 5.2. The CO monomer bond length calculated at the HF, MP2 and DFT levels of theory is (CO) equal to 111.4, 115.1 and 113.8 pm respectively. Table 5.2.1 shows that the non-bonded (CO) bond length of the two carbon monoxide subunits in the dimer are completely unchanged from the monomer value in all the three levels of theory. The intermolecular bond length $r(O_2...C_3)$, is 383.7, 363.4 and 399.7 pm for HF, MP2 and DFT methods respectively, is a value obviously indicative of genuine van der Waals interaction. The $O\hat{C}O$ bond angle of the carbon monoxide deviates from linearity by ca.21.5 degrees for both HF and MP2 calculations and by more than 45 degrees for DFT. Such large deviations from linearity as demonstrated by the three levels of theory clearly indicate that the interaction is taking place through the anti-bonding π orbitals of the other subunit.

5.2.2 The dimerization energy and the BSSE

The computed dimerization energy of the carbon monoxide dimer is given in Table 5.2.2. The weakness of the dimerization of carbon monoxide is also confirmed by the calculated value of 0.10 kJ mol^{-1} for the HF, 2.99 kJ mol^{-1} for the MP2 and 2.34 kJ mol^{-1} for the DFT methods after correcting the interaction energy for BSSE as seen in Table 5.2.2. It is also noted in this table that in the MP2 calculation the BSSE contribution is virtually absent.

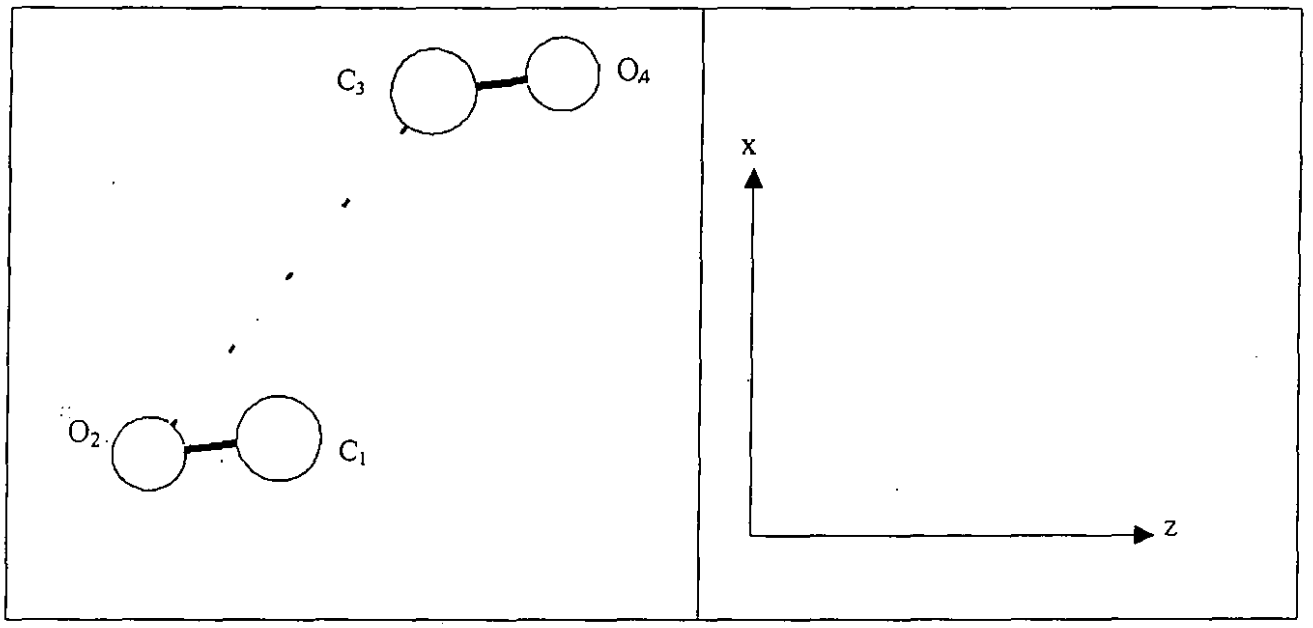

Figure 5.2 shows the optimized structure of the carbon monoxide dimer, the numbering of the atoms together with the orientation of the axis.

Table 5.2.1 The optimized geometrical parameters of the $(CO)_2$ calculated at the HF, MP2 and DFT levels of theory using the 6-31G(d, p) split-valence polarized basis set

		Level of theory		
Species	Parameters	HF	MP2	DFT
$(CO)_2$	$r(C_1O_2)$/pm	111.4	115.1	113.8
	$r(O_2...C_3)$/pm	383.7	363.4	399.7
	$r(C_3O_4)$/pm	111.4	115.1	113.8
	$C_1\hat{O}_2C_3$ /deg	76.8	75.0	44.7
	$O_2\hat{C}_3O_4$ /deg	158.5	158.4	134.5

Table 5.2.2 The dimerization energies and the basis set superposition errors of the $(CO)_2$ calculated at the HF, MP2, and DFT levels of theory using the 6-31G(d, p) split-valence polarized basis set

			Level of theory		
Species	Point group	Energy/kJ mol^{-1}	HF	MP2	DFT
$(CO)_2$	C_s	ΔE $(_{uncorrected})$	-1.40	-2.99	-3.36
		BSSE	1.30	0.00	0.02
		ΔE $(_{corrected})$	-0.10	-2.99	-2.34

Table 5.2.3 The computed and the experimental wavenumbers of the $(CO)_2$ dimer calculated at the HF, MP2, and DFT levels of theory using the 6-31G(d, p) split-valence polirized basis set.

			Level of theory			
Symmetry Species	Mode	Approximate description	HF $\tilde{\upsilon}/cm^{-1}$	MP2 $\tilde{\upsilon}/cm^{-1}$	DFT $\tilde{\upsilon}/cm^{-1}$	[a]Experimental $\tilde{\upsilon}/cm^{-1}$
a′	ν_1	ν(CO) (E.A)	2442	2121	2211	[c]
	ν_2	ν (CO) (E.D.)	2438	2119	2209	2138
	ν_3	libration(in-phase) (I.M.)	68	72	113	[b]
	ν_4	inter-unit stretch (I.M)	45	56	39	[b]
	ν_5	libration (out-of-phase)(I.M)	20	16	15	[b]
a″	ν_6	out-of-phase libration (I.M.)	35	29	31	[b]

[a]Ref: 130

[b] band not observed in this region, [c] overlapping bands

Table 5.2.4 The intensities of the $(CO)_2$ calculated at the HF, MP2 and DFT levels of theory using the 6-31G(d, p) basis set

			Levels of theory		
Symmetry species	Mode	Approximate description	HF A/km mol^{-1}	MP2 A/km mol^{-1}	DFT A/km mol^{-1}
a′	ν_1	ν(CO) (E.A)	147	27	-
	ν_2	ν (CO) (E.D.)	131	26	145
	ν_3	libration(in-phase) (I.M.)	0.8	0.01	-
	ν_4	inter-unit stretch (I.M)	0.1	0.03	-
	ν_5	libration (out-of-phase)(I.M)	0.3	0.07	0.3
a″	ν_6	out-of-phase libration (I.M.)	0.3	0.04	0.0

5.2.3 Vibrational wavenumbers and band intensities of the carbon monoxide dimer

The HF, MP2 and DFT harmonic vibrational and the experimental wavenumbers for the carbon monoxide dimer, together with the approximate description of the normal modes, are given in table 5.2.3. The calculated/experimental wavenumber ratios indicate that the experimental wavenumbers are consistently overestimated by ca. 14% and 3% for HF and DFT methods respectively and is underestimated by 1% for MP2 level of computation. Our assignments confirm the interpretation of Davies and Hallam [92] of the infrared spectra of carbon monoxide isolated in argon matrices as supported by our ab initio calculations. It is also confirmed from Table 5.2.3 that the carbon monoxide dimer shown in fig.5.2, is a true global energy minimum on the potential energy surface (PES) due to the absence of negative frequencies in all three levels of theory.

Table 5.2.4 shows the intensities of the carbon monoxide dimer calculated at the HF, MP2 and DFT levels of theory, using the 6-31G(d, p) basis set. It is clearly observed in this table that the calculated intensities for the v_1 and v_2 modes of the dimer are almost identical at the HF and MP2 levels. However, the DFT theoretical results are inconsistent with the predicted trend. The identical trend was also noted for the calculated vibrational wavenumbers of these two modes (see Table 5.2.3) at all three levels of computation. This suggests that only one absorption band is expected to be observed due to the overlapping of these two bands.

Table 5.2.5 shows the wavenumber shifts and intensity enhancements on dimerization of the carbon monoxide calculated at all the three levels of theory studied here. As indicated in Table 5.2.5 and Table 5.2.6 respectively only negligible wavenumber shifts and small intensity enhancements accompany the dimerization of carbon monoxide. Ab initio theoretical calculations at all the three levels of theory qualitatively predict that the matrix isolation infrared spectra of the carbon monoxide dimer should show two CO stretching absorption bands of comparable intensity to that of the monomer CO stretching vibration; these two bands overlapping and both being slightly shifted by $2cm^{-1}$ to the blue relative to the monomer wavenumber position.

Table 5.2.5 Comparison of the calculated wavenumbers of the $(CO)_2$, with those of the corresponding modes of the monomer, calculated at the HF, MP2 and DFT using the 6-31G(d, p) basis set.

HF/6-31G(d, p)					**MP2/6-31G(d, p)**					**DFT/6-31G(d, p)**				
dimer		monomer			dimer		monomer			dimer		monomer		
mode ([a]SS)	$\tilde{\upsilon}/cm^{-1}$	mode ([a]SS)	$\tilde{\upsilon}/cm^{-1}$	Shifts [b]$\Delta\tilde{\upsilon}/cm^{-1}$	mode ([a]SS)	$\tilde{\upsilon}/cm^{-1}$	mode ([a]SS)	$\tilde{\upsilon}/cm^{-1}$	Shifts [b]$\Delta\tilde{\upsilon}/cm^{-1}$	mode ([a]SS)	$\tilde{\upsilon}/cm^{-1}$	mode ([a]SS)	$\tilde{\upsilon}/cm^{-1}$	Shifts [b]$\Delta\tilde{\upsilon}/cm^{-1}$
$\nu_1(a')$	2442	$\nu(\delta)$	2439	3	$\nu_1(a')$	2121	$\nu(\delta)$	2119	2	$\nu_1(a')$	2211	$\nu(\delta)$	2209	2
$\nu_2(a')$	2438	$\nu(\delta)$	2439	-1	$\nu_2(a')$	2119	$\nu(\delta)$	2119	0	$\nu_2(a')$	2209	$\nu(\delta)$	2209	0

([a]SS) is the symmetry species

[b]$\Delta\tilde{\upsilon} = \tilde{\upsilon}_{dimer} - \tilde{\upsilon}_{monomer}$

Table 5.2.6 Comparison of the calculated band intensities of the $(CO)_2$, with those of the corresponding modes of the monomer, calculated at the HF, MP2 and DFT levels of theory using the 6-31G(d, p) basis set

HF/6-31G(d, p)					MP2/6-31G(d, p)					DFT/6-31G(d, p)				
dimer		monomer			dimer		monomer			dimer		monomer		
mode (^{a}SS)	A/km mol^{-1}	mode (^{a}SS)	A/km mol^{-1}	A^b/A^c	mode (^{a}SS)	A/km mol^{-1}	mode (^{a}SS)	A/km mol^{-1}	A^b/A^c	mode (^{a}SS)	A/km mol^{-1}	mode (^{a}SS)	A/Km mol^{-1}	A^b/A^c
$\nu_1(a')$	147	$\nu(\delta)$	138	1.06	$\nu_1(a')$	27	$\nu(\delta)$	26	1.04	$\nu_1(a')$	0.0	$\nu(\delta)$	70	0.0
$\nu_2(a')$	131	$\nu(\delta)$	138	0.95	$\nu_2(a')$	26	$\nu(\delta)$	26	1.00	$\nu_2(a')$	145	$\nu(\delta)$	70	2.07

5.3 The Carbon dioxide dimer

Most experimental studies of the carbon dioxide dimer including those by matrix isolation IR in noble gases [93] and deuterium [94] matrices, high resolution gas-phase IR [95] and molecular beam (MB) spectroscopy [96-99], have concluded that the structure is best represented as a slipped parallel dimer of C_{2h} symmetry, stabilized by weak quadrupole-quadrapole interactions. A variety of theoretical predictions [100-109] concur with the experimental evidence that the true structure has an offset parallel geometry, with the T-shaped structure more representing a transition state connecting two equivalent slipped parallel dimers through a synchronized inter-conversion mechanism occurring in the plane of the complex. However, one author proposed a structure midway between the C_{2h} and C_{2v} models [110], but this conclusion has not found any additional support. For the purpose of this investigation two isomers would be considered, one of C_{2h} symmetry and the other one of C_{2v} symmetry, at the three different levels of computation.

5.3.1 The optimized geometrical parameters

The geometry optimizations of the dimers of carbon dioxide structures of the C_{2h} and the perpendicular $C_1...O_2$ bonded species belonging to the C_{2v} point group are illustrated in fig 5.3; and they were performed at the HF, MP2 and DFT levels of computation. The optimized geometrical parameters of the CO_2 dimers are shown in Table 5.3.1. The computed bond length of the carbon dioxide monomer is equal to 114.3 (for HF), 118.0 (MP2) and 116.9 pm (DFT). For both structures, and at all levels of theory, the free CO bond shortens marginally on dimerization, while the bonded CO bond length increases slightly, or remains unchanged at the perpendicular C_{2v} symmetry. The linearity of the interacting monomer is not affected. The carbon dioxide remains unchanged on dimerization at all levels, at both structures. At the T-shaped structure the intermolecular bond length, $r(C_1....O_2)$ is equal to 311.5, 294.9 and 302.0 pm for HF, MP2 and DFT methods respectively. Similarly, for the slipped parallel the intermolecular bond length $r(C_2...O_4)$ is 329.4 (for HF), 347.2 (MP2) and 354.6 pm (DFT) and these values are slightly high indicating some type of van der Waals interaction.

and these values are slightly high indicating some type of van der Waals interaction.

5.3.2 The dimerization energies

The computed dimerization energies of the two carbon dioxide dimers are given in Table 5.3.2. In fact, various calculations and emperical schemes for estimating dissociation energies for the carbon dioxide dimer predict a value of 4-8 kJ mol^{-1}, yielding the staggered side-by-side structure (C_{2h}) to be more stable than the T-shaped structure (C_{2v}) [100,111,112]. These results from Table 5.3.2 also shows that, at all levels, before correcting for BSSE, the staggered structure (C_{2h}) is more stable than the T-shaped structure (C_{2v}), confirming the findings of the majority of various studies [101, 102, 103, 104,109]. Correction for BSSE has the effect of virtually equalizing the interaction of both dimers at all levels. BSSE represents a large contribution to the uncorrected interaction energies as was also observed by Bone and Handy [104]. The vibrational analyses, based on these predictions, confirm the T-shaped to be the transition state.

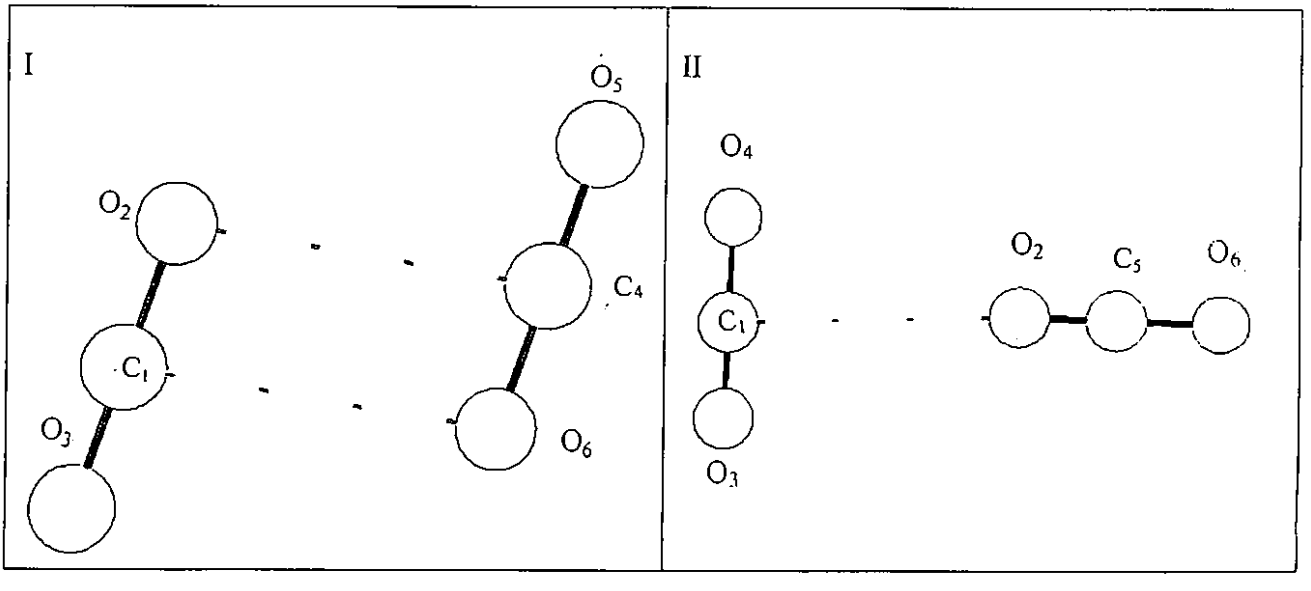

Figure 5.3 shows the optimized structure of the carbon dioxide dimer of the C_{2h} (I) and C_{2v} (II) symmetry together with the numbering of the atoms

Table 5.3.1 The optimized geometrical parameters of the $(CO_2)_2$ calculated at the HF, MP2 and DFT levels of theory using the 6-31G(d, p) split-valence polarized basis set.

		Level of theory		
Species	Parameters	HF	MP2/	DFT
$(CO_2)_2$ C_{2h}	$r(C_1O_2)$/pm	114.3	117.9	116.9
	$r(O_3C_1)$/pm	114.5	118.0	117.0
	$r(O_2 \ldots C_4)$/pm	329.4	347.2	354.6
	$O_3\hat{C}_1O_2$/deg	180.0	180.0	180.0
	$O_5\hat{C}_4O_6$/deg	180.0	180.0	180.0
$(CO_2)_2$ C_{2v}	$r(C_1 \ldots O_2)$/pm	311.5	294.9	302.0
	$r(C_1O_3)$/pm	114.3	117.9	116.9
	$r(C_5O_1)$/pm	114.2	117.9	116.8
	$O_3\hat{C}_1O_4$/deg	179.2	179.4	179.2
	$O_2\hat{C}_5O_6$/deg	180.0	180.0	180.0
	$O_2\hat{C}_1O_4$/deg	90.0	90.0	90.0

Table 5.3.2 The dimerization energies and the basis set superposition errors of the $(CO_2)_2$ calculated at the HF, MP2, and DFT levels of theory using the 6-31G(d, p) split-valence polarized basis set.

			Level of theory		
Species	Point group	Energy/kJ mol^{-1}	HF	MP2	DFT
$(CO_2)_2$	C_{2h}	ΔE (uncorrected)	-4.93	-7.93	-6.75
		BSSE	2.37	5.68	4.42
		ΔE (corrected)	-2.56	-2.25	-2.33
$(CO_2)_2$	C_{2v}	ΔE (uncorrected)	-3.71	-5.98	-1.94
		BSSE	1.33	3.55	1.93
		ΔE (corrected)	-2.38	-2.35	-0.01

5.3.3. Vibrational wavenumbers and band intensities

The computed wavenumbers together with the experimental wavenumbers of the intramolecular modes of the $(CO_2)_2$ observed in nitrogen matrices and the intensities of the slipped parallel (C_{2h}) and T-shaped (C_{2V}) dimer structures are reported in Tables 5.3.3 and 5.3.4 respectively. The normal modes of the slipped parallel dimer transform as

$\Gamma_{vib}=5a_g+2a_u+b_g+4b_u$

and those of T-shaped structure as

$\Gamma_{vib}=5a_1+3b_1+4b_2$

In the case of the slipped parallel dimer the monomer modes couple to produce a combination of antisymmetric stretches (in-phase, ν_1, and out-of-phase, ν_9) symmetric stretches (in-phase, ν_2, and out-of-phase, ν_{10}) and bends (in-plane) out-of-phase, ν_3, in plane, out-of-plane, ν_{11}, out-of-plane, out-of-phase, ν_6), with equal contributions from each monomer unit. The intermolecular modes, ν_4, ν_5, ν_7 and ν_{12}, may be identified with the coupled in-plane libration (R_y (con)), the inter-monomer stretching (T_z), the libration (R_x (con)) and the out-phase in-plane libration (R_y (anti)), respectively.

Due to the non-equivalence of the two monomer units in the T-shaped dimer, the intramolecular normal modes of the dimer are more conveniently described as the uncoupled antisymmetric stretches of the ED, ν_1, and the EA, ν_9, the in-plane bends of the EA, ν_4, and the ED, ν_{10}, the out-of plane bends of the EA, ν_6, and the ED, ν_7. The symmetric stretching modes of the two monomer units are coupled to a certain extent, however, and ν_2 and ν_3 are described as the in-phase and out-of-phase combination of those motions respectively. The intermolecular modes are inter-monomer stretching, ν_5 (T_z), the out-of-plane libration, ν_8 (R_x (anti)), and out-of-phase, ν_{12}, (R_y (anti)) in-plane libration. The ν_9 mode are predicted to have a negative eigenvalue at all the levels of theory. This confirms that the T-shaped structure is a transition state.

Table 5.3.3 The computed and the experimental wavenumbers of the $(CO_2)_2$ dimer calculated at the HF, MP2, and DFT levels of theory using the 6-31G(d, p) split-valence polarized basis set.

				Level of theory			
Dimer	Symmetry Species	Mode	Approximate description	HF $\tilde{\nu}$/cm^{-1}	MP2 $\tilde{\nu}$/cm^{-1}	DFT $\tilde{\nu}$/cm^{-1}	[a]Expt $\tilde{\nu}$/cm^{-1}
Slipped parallel structure (C_{2h}) :							
$(CO_2)_2$	a_g	ν_1	$\nu_a(CO_2)$ (IP)	2583	2453	2445	___[b]
		ν_2	$\nu_s(CO_2)$ (IP)	1518	1337	1335	___[b]
		ν_3	$\delta(CO_2)$ (OP)	748	642	633	___[b]
		ν_4	R_y (con)	101	109	113	___[b]
		ν_5	T_z	39	48	49	___[b]
	a_u	ν_6	γ(OCO)(OP)	750	644	635	664
		ν_7	R_x (con)	27	27	38	___[b]
	b_g	ν_8	γ(OCO)(IP)	743	641	631	___[b]
	b_u	ν_9	$\nu_a(CO_2)$ (OP)	2585	2455	2448	2340
		ν_{10}	$\nu_s(CO_2)$(OP)	1518	1337	1336	1442
		ν_{11}	δ(OCO)(OP)	744	640	632	657
		ν_{12}	R_y (anti)	22	32	27	___[b]
T-shaped structure (C_{2v}) :							
$(CO_2)_2$	a_1	ν_1	$\nu_a(CO_2)$ (E.D)	2588	2450	2440	
		ν_2	$\nu_s(CO_2)$ (IP)	1520	1336	1375	
		ν_3	$\nu_s(CO_2)$ (OP)	1518	1335	1373	
		ν_4	δ(OCO)(EA)	744	634	638	
		ν_5	T_z	48	65	51	
	b_1	ν_6	γ(OCO)(EA)	2585	2448	2438	
		ν_7	γ(OCO)(ED)	744	634	638	
		ν_8	R_x(anti)	62	58	48	
	b_2	ν_9	$\nu_a(CO_2)$ (EA)	-15	-16	-15	
		ν_{10}	δ(OCO)(ED)	749	638	642	
		ν_{11}	R_y(con)	744	635	639	
		ν_{12}	R_y (anti)	13	7	10	

[a]Ref: 130

[b] band not observed in this region

IP is the in-phase, OP is the out-of-phase, ED is the electron donor, EA is the electron acceptor

Table 5.3.4 Ratios of the computed to the experimental wavenumbers observed in nitrogen matrices of the intramolecular modes of the carbon dioxide dimer (C_{2h}).

	[a]Levels of theory		
Mode	HF	MP2	DFT
ν_6	1.12	0.97	0.98
ν_9	1.10	1.05	1.05
ν_{10}	1.05	0.93	0.98
ν_{11}	1.15	1.98	0.98
Mean Average	1.11	0.99	1.00

[a]Ratio=$\tilde{\upsilon}_{calc} / \tilde{\upsilon}_{expt}$

Table 5.3.4 shows the calculated/experimental wavenumber ratios of the carbon dioxide dimer of the slipped parallel configuration. This table shows that the HF level overestimates the experimental values by ca. 11% on average, while the MP2 is underestimated by ca. 1% on average and DFT levels of computation ideally fit the experimental values. Since the DFT method is more reliable than the other two methods, then we are going to focus our investigation on the DFT method. Table 5.3.5 shows the wavenumbers of the selected bands of the staggered parallel dimer and those of the corresponding monomer from which they were derived. This table indicates that the antisymmetric CO_2-stretching vibration undergoes the changes on dimerization, splitting into a pair of bands (ν_1 and ν_9), where the ν_1 mode is red shifted while the ν_9 mode remains unperturbed. The infrared active mode ν_2 of the monomer correlates with the degenerate CO_2-bending modes (ν_2, ν_6, ν_8 and ν_{11}) of the dimer and shifted by amounts less than $5cm^{-1}$ on either direction. The symmetric CO_2-stretching of the monomer undergoes smallest changes on dimerization, splitting into a pair of bands (ν_2 and ν_{10}), where the ν_2 mode is blue shifted and ν_9 mode remains unchanged.

The intensity of the ν_9 mode of the staggered side-by-side carbon dioxide dimer structure of C_{2h} symmetry is higher than that of the parent monomer at the DFT, while that of the ν_{10} mode of the dimer has as its counterpart in the monomer the infrared inactive ν_1 mode (Table 5.3.7). The intensity of the bending mode of the dimer, ν_6 and ν_{11}, are both about twice as higher as the monomer bending intensity. These calculated trends are also consistent with the type of interaction involved on dimerization of carbon dioxide being very weak. Table 5.3.7 shows that the intensity ratios are ranging from 0.98 to 2.90 at all the levels of theory, which emphasise the fact that the interaction is a weak one.

Finally, from the quantitative point of view, the spectrum of the carbon dioxide dimer of C_{2h} symmetry should show only one band close to the monomer antisymmetric stretching vibration, and two bending bands of relative moderate intensity and the other one which is close to the monomer symmetric stretching vibration will be weakly observed since the inactivity is uplifted. Unfortunately the intermolecular modes will be impossible to observe in this work, since they are below the available range of observation of most commercial instruments.

Table 5.3.5 Comparison of the calculated wavenumber of the $(CO_2)_2$, with those of the corresponding modes of the monomer, calculated at the HF, MP2 and DFT levels of theory using the 6-31G(d, p) basis set

HF/6-31G(d, p)				MP2/6-31G(d, p)				DFT/6-31G(d, p)			
Dimer		Monomer		Dimer		Monomer		Dimer		Monomer	
mode (^{a}SS)	$\tilde{\upsilon}/cm^{-1}$	mode (^{a}SS)	$\tilde{\upsilon}/cm^{-1}$ Shifts $\Delta\tilde{\upsilon}/cm^{-1}$	mode (^{a}SS)	$\tilde{\upsilon}/cm^{-1}$	mode (^{a}SS)	$\tilde{\upsilon}/cm^{-1}$ Shifts $\Delta\tilde{\upsilon}/cm^{-1}$	mode (^{a}SS)	$\tilde{\upsilon}/cm^{-1}$	mode (^{a}SS)	$\tilde{\upsilon}/cm^{-1}$ Shifts $\Delta\tilde{\upsilon}/cm^{-1}$
Slipped parallel structure (C_{2h}) :											
$\nu_1(a_g)$	2585	$\nu_3(\Sigma^-_u)$	2585 -2	$\nu_1(a_g)$	2453	$\nu_3(\Sigma^-_u)$	2455 -2	$\nu_1(a_g)$	2445	$\nu_3(\Sigma^-_u)$	2448 -3
$\nu_2(a_g)$	1518	$\nu_1(\Sigma^-_g)$	1519 -1	$\nu_2(a_g)$	1337	$\nu_1(\Sigma^-_g)$	1337 0	$\nu_2(a_g)$	1335	$\nu_1(\Sigma^-_g)$	1336 -1
$\nu_3(a_g)$	748	$\nu_2(\Pi_u)$	746 2	$\nu_3(a_g)$	642	$\nu_2(\Pi_u)$	742 0	$\nu_3(a_g)$	633	$\nu_2(\Pi_u)$	633 0
$\nu_6(a_u)$	750	$\nu_2(\Pi_u)$	746 4	$\nu_6(a_u)$	644	$\nu_2(\Pi_u)$	742 2	$\nu_6(a_u)$	635	$\nu_2(\Pi_u)$	633 2
$\nu_8(b_g)$	743	$\nu_2(\Pi_u)$	746 -3	$\nu_8(b_g)$	641	$\nu_2(\Pi_u)$	742 -1	$\nu_8(b_g)$	631	$\nu_2(\Pi_u)$	633 -2
$\nu_9(b_u)$	2585	$\nu_3(\Sigma^-_u)$	2585 0	$\nu_9(b_u)$	2455	$\nu_3(\Sigma^-_u)$	2455 0	$\nu_9(b_u)$	2448	$\nu_3(\Sigma^-_u)$	2448 0
$\nu_{10}(b_u)$	1518	$\nu_1(\Sigma_g)$	1519 -1	$\nu_{10}(b_u)$	1337	$\nu_1(\Sigma_g)$	1337 0	$\nu_{10}(b_u)$	1336	$\nu_1(\Sigma_g)$	1336 0
$\nu_{11}(b_u)$	744	$\nu_2(\Pi_u)$	746 -2	$\nu_{11}(b_u)$	640	$\nu_2(\Pi_u)$	742 -2	$\nu_{11}(b_u)$	632	$\nu_2(\Pi_u)$	633 -1

Table 5.3.6 Comparison of the calculated intensities of the $(CO_2)_2$ with those of the corresponding modes of the monomer, calculated at the HF, MP2 and DFT levels of theory using the 6-31G(d, p) basis set

HF/6-31G(d, p)					MP2/6-31G(d, p)					DFT/6-31G(d, p)				
Dimer		Monomer			Dimer		Monomer			Dimer		Monomer		
mode ([a]SS)	A/km mol^{-1}	mode ([a]SS)	A/km mol^{-1}	A^b/A^c	mode ([a]SS)	A/km mol^{-1}	mode ([a]SS)	A/km mol^{-1}	A^b/A^c	mode ([a]SS)	A/km mol^{-1}	mode ([a]SS)	A/km mol^{-1}	A^b/A^c
Slipped parallel structure (C_{2h}) :														
$\nu_6(a_u)$	134	$\nu_2(\Pi_u)$	69	1.94	$\nu_6(a_u)$	49	$\nu_2(\Pi_u)$	26	1.88	$\nu_6(a_u)$	67	$\nu_2(\Pi_u)$	30	2.23
$\nu_9(b_u)$	967	$\nu_3(\Sigma^-_u)$	985	0.98	$\nu_9(b_u)$	887	$\nu_3(\Sigma^-_u)$	453	1.96	$\nu_9(b_u)$	923	$\nu_3(\Sigma^-_u)$	576	1.60
$\nu_{10}(b_u)$	0.3	$\nu_1(\Sigma_g)$	0	-	$\nu_{10}(b_u)$	0.5	$\nu_1(\Sigma_g)$	0	-	$\nu_{10}(b_u)$	0.2	$\nu_1(\Sigma_g)$	0	-
$\nu_{11}(b_u)$	155	$\nu_2(\Pi_u)$	64	2.42	$\nu_{11}(b_u)$	66	$\nu_2(\Pi_u)$	26	2.54	$\nu_{11}(b_u)$	87	$\nu_2(\Pi_u)$	30	2.90

[a]SS- symmetric species, A^b is the band intensity of the dimer and A^c is the band intensity of the monomer

Table 5.3.7 The intensities of the CO_2 dimer calculated at the HF, MP2 and DFT levels of theory using the 6-31G(d, p) basis set

				Level of theory		
Dimer	Symmetry species	Mode	Approximate description	HF km mol^{-1}	MP2 km mol^{-1}	DFT km mol^{-1}
$(CO_2)_2$ C_{2h}	a_u	ν_6	γ(OCO)(OP)	134	49	67
	b_u	ν_9	$\nu_a(CO_2)$ (OP)	967	887	923
		ν_{10}	$\nu_a(CO_2)$(OP)	0.3	0.5	0.2
		ν_{11}	δ(OCO)(OP)	155	66	87
		ν_{12}	R_y (anti)	0.2	0.2	0.1
$(CO_2)_2$ C_{2v}	a_1	ν_1	$\nu_a(CO_2)$ (E.D)	1055	492	592
		ν_2	ν_s (CO_2) (IP)	0.2	0.1	0.1
		ν_3	ν_s (CO_2) (OP)	0.04	0.002	0.002
		ν_4	δ(OCO)(EA)	93	41	46
		ν_5	T_z	0.1	0.1	0.1
	b_1	ν_6	γ(OCO)(EA)	963	442	530
		ν_7	γ(OCO)(ED)	65	24	29
		ν_8	R_x(anti)	0.03	0.03	0.03
	b_2	ν_9	$\nu_s(CO_2)$ (EA)	0.002	0.003	0.002
		ν_{10}	δ(OCO)(ED)	122	27	43
		ν_{11}	R_y(con)	14	23	17
		ν_{12}	R_y(anti)	0.001	0.0003	0.001

ED is the electron donor, EA is the electron acceptor, OP is the out-of-phase, IP is the in-phase

5.4. The Water dimer

The water dimer is probably the most important van der Waals dimer and accordingly has received much experimental [113-115] and theoretical [116, 117, 118, 119, 120-123] attention. The earliest matrix isolation experiment in nitrogen matrices [114] suggested a cyclic dimer configuration since the authors observed only two bands in the OH stretching and one in the HOH bending regions. Further matrix studies by Fredin *et al* [124] at higher resolution located more dimer bands in the monomer stretching region, suggesting a linear bonded dimer configuration. This result was also consistent with the argon matrix spectrum [113, 115, 125]. All theoretical calculations on the dimer [116, 118, 119, 126, 122-128] determined the linear bonded structure to be most stable at the HF level of theory. Recent studies by Maguet *et al* [129] found the bifurcated dimer to be a local minimum at the self-consistent field (SCF) level of theory; however, Marsden and co-workers [128] could not reproduce their findings at the same level of theory and with the same basis function, hence concluded that the bifurcated structure is not a minimum energy structure. The recent studies by Nxumalo *et al* [130] also confirmed that the linear dimer is the true global minimum structure at the HF level using the 6-31G(d, p) basis set. In this work we report the results of our ab initio studies of the water dimer at the HF, MP2 and DFT levels, using the 6-31G(d, p) split-valence polarized basis set.

5.4.1 The optimized geometrical parameters of the water dimer

The optimized geometrical parameters of the linear water dimer including those of the monomer, calculated using the 6-31G(d, p) split-valence polarized basis set [77, 134, 135, 136] are collected in Table 4.1 (see chapter 4, page 22) and 5.4.1 at all the levels of theory, respectively. The results show that the non-bonded OH bond length of the linear dimer is virtually unchanged relative to the monomer, but the bonded OH bond length undergoes a substantial increase. The two HOH bond angles of the dimer suffer very little change at all the levels of computation. The hydrogen bonded $H_2...O_1$ distance is 203.9, 196.6 and 193.1pm for HF, MP2 and DFT methods respectively. The $O_3\hat{H}_2...O_1$ bond angle deviates from linearity by 8, 15 and 17 degrees for HF, MP2 and DFT methods respectively. The calculated O-O distance obtained at this levels of theory are in excellent

accord with the experimental value of 299 pm obtained by Dyke *et al* [203] with the exception of the MP2 method, where the theoretical value is less than the experimental value by an incremenet of not more than 10 pm.

5.4.2 The dimerization energies and BSSEs

The dimerization energies calculated at the HF, MP2 and DFT levels of theory, before and after correction for basis set superposition error (BSSE), is given in Table 5.4.2. From this table one can see that there is a slight difference between the uncorrected dimerization energies on either method. However, BSSE accounts for about 36% of the hydrogen bond energy of the linear dimer at the HF and 23% at the DFT and 34% at the MP2 methods. After correction for BSSE, this dimer is predicted to have the higher association energy, confirming the findings of the majority of various investigators including Nxumalo, Yeo and Ford *et al* [130, 131].

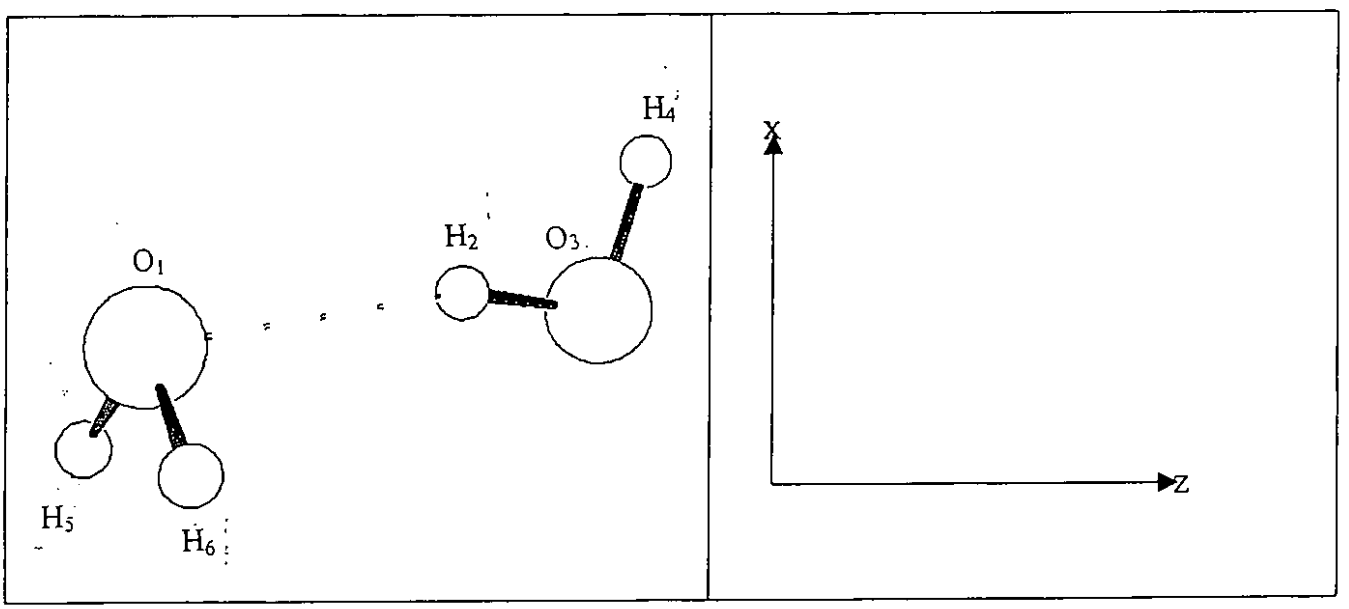

Figure 5.4 shows the optimized structure of the water dimer together with the numbering of the atoms

Table 5.4.1 The optimized geometrical parameters of the $(H_2O)_2$ calculated at the HF, MP2 and DFT levels of theory using the 6-31G(d, p) split-valence polarized basis set

		Level of theory		
Species	Parameters	HF	MP2	DFT
$(H_2O)_2$	$r(O_3H_2)$/pm	94.8	96.7	97.3
	$r(O_3H_4)$/pm	94.2	96.0	96.4
	$r(O_1H_5)$/pm	94.4	96.3	96.7
	$r(H_2...O_1)$/pm	203.9	196.6	193.1
	$H_2\hat{O}_3H_4$/deg	105.9	104.1	104.1
	$H_5\hat{O}_1H_6$/deg	106.3	104.1	104.1
	$O_3H_2...O_1$/deg	172.2	165.5	163.0
	$H_5\hat{O}_1...H_2$/deg	107.5	98.5	96.0
	$H_6\hat{O}_1...H_2$/deg	107.5	98.5	96.0

Table 5.4.2 The dimerization energies and the basis set superposition errors of the $(H_2O)_2$ dimer calculated at the HF, MP2, and DFT levels of theory using the 6-31G(d, p) basis set

			Level of theory		
Species	Point group	Energy/kJ mol^{-1}	HF	MP2	DFT
$(H_2O)_2$	C_s	ΔE $(_{uncorrected})$	-36.33	-29.81	-31.80
		BSSE	12.99	10.20	7.41
		ΔE $(_{corrected})$	-23.34	-19.61	-24.39

5.4.3 The vibrational wavenumbers and band Intensities

The computed wavenumber, together with the experimental wavenumbers and the band intensities of the linear water dimer, at all the levels of computation, are shown in Table 5.4.3 and 5.4.4 respectively. It is noted that one of the bending modes of the DFT method, ν_{12}, is calculated to have an imaginary frequency.

The ratios of the computed to the experimental wavenumbers of the intramolecular modes of the water dimer observed in nitrogen matrices are presented in Table 5.4.5. This table shows that the HF method overestimates the experimental wavenumbers by ca. 13% on average while the MP2 and DFT levels of computation also overestimate the experimental wavenumbers by ca. 7% and 5% on average, respectively. From Table 5.4.5 it has been observed that the results of the DFT method are close to the experimental results and, therefore we are going to focus our predictions on the MP2 method. The correlation between the dimer and the monomer modes are listed in Table 5.4.6. The OH stretching mode of the dimer (ν_1) of electron acceptor (E.A.) is red shifted, while the bonded OH-stretching counterpart, (ν_3), suffer a red shifts (74 cm^{-1}). The bending mode of the dimer (ν_4) is blue shifted. The *HÔH* bending mode (ν_5) of the dimer is also red shifted but only slightly from the monomer value at this method. This is typical behaviour for a hydrogen bonded interaction [2, 131]. The OH_2-stretching mode of the dimer ν_2 of the electron donor (E.D.) is red shifted ($15cm^{-1}$) while the ν_9 mode of the dimer is also slightly shifted to the red by ca. 23 cm^{-1}.

The ratios of the intensities of the water dimer to the corresponding bands of the H_2O monomer are presented in Table 5.4.7. This table shows that the symmetric OH_2-stretching intensities of the electron acceptor (EA), ν_3, mode show intensity enhancement. The increase in intensity on dimerization is consistent with the prediction of the Friedrich and Person theory[78]. This behaviour is also predictable for hydrogen bonding situations [131,132].

Qualitatively, the matrix isolation infrared spectrum of the linear hydrogen bonded water dimer, in the monomer fundamental regions, should consist of two fairly strong bands to the OH-stretching being shifted to the red and two bands one of relative high intensity at the significantly lower position than the monomer ν_1, one bending absorption band close to the monomer ν_2 and the second, being shifted to higher wavenumbers and both having similar intensity.

Table 5.4.3 The computed and the experimental wavenumbers of the $(H_2O)_2$ calculated at the HF, MP2, and DFT levels of theory using the 6-31G(d, p) split-valence polirized basis set.

				Level of theory			
Dimers	Symmetry Species	Mode	Approximate description	HF $\tilde{\upsilon}/cm^{-1}$	MP2 $\tilde{\upsilon}/cm^{-1}$	DFT $\tilde{\upsilon}/cm^{-1}$	[a]Expt $\tilde{\upsilon}/cm^{-1}$
$(H_2O)_2$	a′	ν_1	ν(OH) (free)(EA)	4238	4000	3880	3699
		ν_2	ν_s (OH_2) (ED)	4142	3877	3793	3627
		ν_3	ν_s (OH) (bonded)(EA)	4099	3818	3687	3549
		ν_4	δ(HOH)(EA)	1797	1714	1693	1619
		ν_5	δ(HOH)(ED)	1768	1680	1661	1601
		ν_6	δ(OH...O)(I.M)	377	427	449	___[b]
		ν_7	ν(H...O) (I.M)	180	204	222	___[b]
		ν_8	ω(OH_2)(E.D)(I.M)	138	139	137	___[b]
	a″	ν_9	ν_a(OH_2) (ED)	4238	4007	3900	3725
		ν_{10}	τ(OH...O) (I.M)	612	660	672	___[b]
		ν_{11}	tw(OH_2) (ED) (I.M)	143	158	171	___[b]
		ν_{12}	τ(OH) (EA) (I.M)	119	79	-34	___[b]

[a]Ref: 130

[b] bands not observed in this region

Table 5.4.4 The band intensities of the $(H_2O)_2$ calculated at the HF, MP2 and DFT levels of theory using the 6-31G(d, p) split-valence polarized basis set.

				Level of theory		
Dimers	Symmetry Species	Mode	Approximate description	HF km mol^{-1}	MP2 km mol^{-1}	DFT km mol^{-1}
$(H_2O)_2$	a′	ν_1	ν(OH) (free)(EA)	105	78	45
		ν_2	ν_s (OH_2) (ED)	27	13	9
		ν_3	ν_s (OH) (bonded)(EA)	181	202	253

Table 5.4.4 Continued

	ν_4	δ(HOH)(EA)	99	76	72
	ν_5	δ(HOH)(ED)	112	76	64
	ν_6	δ(OH...O)(I.M)	89	33	25
	ν_7	ν(H...O) (I.M)	126	155	160
	ν_8	$\omega(OH_2)$(E.D)(I.M)	249	262	257
a″	ν_9	$\nu_a(OH_2)$ (ED)	89	60	47
	ν_{10}	τ(OH...O) (I.M)	203	139	113
	ν_{11}	$tw(OH_2)$ (ED) (I.M)	118	166	187
	ν_{12}	τ(OH) (EA) (I.M)	95	58	29

EA= electron acceptor, ED= electron donor and IM= intermolecular mode

Table 5.4.5 Ratios of the computed to the experimental wavenumbers of the intramolecular modes of the water dimer observed in nitrogen matrices.

	[a]Levels of theory		
Mode	HF/6-31G(d, p)	MP2/6-31G(d, p)	DFT/6-31G(d, p)
ν_1	1.15	1.08	1.05
ν_2	1.14	1.07	1.05
ν_3	1.15	1.08	1.04
ν_4	1.11	1.06	1.05
ν_5	1.10	1.05	1.04
ν_9	1.13	1.08	1.05
Mean Average	1.13	1.07	1.05

[a]Ratio= $\tilde{\upsilon}_{cal} / \tilde{\upsilon}_{exp}$

Table 5.4.6 Comparison of the calculated wavenumbers of the $(H_2O)_2$ with those of the corresponding modes of the monomer, calculated at the HF, MP2 and DFT levels of theory using the 6-31G(d, p) basis set.

HF/6-31G(d, p)					MP2/6-31G(d, p)					DFT/6-31G(d, p)				
Dimer		Monomer			Dimer		Monomer			Dimer		Monomer		
mode ([a]SS)	$\tilde{\upsilon}/cm^{-1}$	mode ([a]SS)	$\tilde{\upsilon}/cm^{-1}$	Shifts [b]$\Delta\tilde{\upsilon}/cm^{-1}$	mode ([a]SS)	$\tilde{\upsilon}/cm^{-1}$	mode ([a]SS)	$\tilde{\upsilon}/cm^{-1}$	Shifts [b]$\Delta\tilde{\upsilon}/cm^{-1}$	mode ([a]SS)	$\tilde{\upsilon}/cm^{-1}$	mode ([a]SS)	$\tilde{\upsilon}/cm^{-1}$	Shifts [b]$\Delta\tilde{\upsilon}/cm^{-1}$
$\nu_1(a')$	4238	$\nu_3(b)$	4249	11	$\nu_1(a')$	4000	$\nu_3(b)$	4030	-30	$\nu_1(a')$	3880	$\nu_3(b)$	3912	-32
$\nu_2(a')$	4142	$\nu_1(a_1)$	4102	40	$\nu_2(a')$	3877	$\nu_1(a_1)$	3892	-15	$\nu_2(a')$	3793	$\nu_1(a_1)$	3786	7
$\nu_3(a')$	4099	$\nu_1(a_1)$	4102	-3	$\nu_3(a')$	3818	$\nu_1(a_1)$	3892	-74	$\nu_3(a')$	3818	$\nu_1(a_1)$	3892	-74
$\nu_4(a')$	1797	$\nu_2(a_2)$	1743	44	$\nu_4(a')$	1714	$\nu_2(a_2)$	1682	32	$\nu_4(a')$	1714	$\nu_2(a_2)$	1682	32
$\nu_5(a')$	1768	$\nu_2(a_2)$	1743	15	$\nu_5(a')$	1680	$\nu_2(a_2)$	1682	-2	$\nu_5(a')$	1680	$\nu_2(a_2)$	1682	-2
$\nu_9(a'')$	4255	$\nu_3(b)$	4249	6	$\nu_9(a'')$	4007	$\nu_3(b)$	4030	-23	$\nu_9(a'')$	4007	$\nu_3(b)$	4030	-2

([a]SS) stands for symmetric species

[b]$\Delta\nu=(\tilde{\upsilon}/cm^{-1})_{dimer}-(\tilde{\upsilon}/cm^{-1})_{monomer}$

Table 5.4.7 Comparison of the calculated intensities of the $(H_2O)_2$ with those of the corresponding modes of the monomer, calculated at the HF, MP2 and DFT levels of theory using the 6-31G(d, p) basis set

HF/6-31G(d, p)					MP2/6-31G(d, p)					DFT/6-31G(d, p)				
Dimer		Monomer			Dimer		Monomer			Dimer		Monomer		
mode ([a]SS)	A/km mol^{-1}	mode ([a]SS)	[b]A/km mol^{-1}	[b]A/[c]A	mode ([a]SS)	[b]A/km mol^{-1}	mode ([a]SS)	[b]A/km mol^{-1}	[b]A/[c]A	mode ([a]SS)	[b]A/km mol^{-1}	mode ([a]SS)	[b]A/km mol^{-1}	[b]A/[c]A
$\nu_1(a')$	105	$\nu_3(b)$	15	7.00	$\nu_1(a')$	78	$\nu_3(b)$	34	2.29	$\nu_1(a')$	45	$\nu_3(b)$	20	2.25
$\nu_2(a')$	27	$\nu_1(a_1)$	94	0.29	$\nu_2(a')$	13	$\nu_1(a_1)$	4	3.25	$\nu_2(a')$	9	$\nu_1(a_1)$	2	4.50
$\nu_3(a')$	181	$\nu_1(a_1)$	94	1.93	$\nu_3(a')$	202	$\nu_1(a_1)$	4	50.5	$\nu_3(a')$	253	$\nu_1(a_1)$	2	126.5
$\nu_4(a')$	99	$\nu_2(a_2)$	73	1.36	$\nu_4(a')$	76	$\nu_2(a_2)$	78	0.97	$\nu_4(a')$	72	$\nu_2(a_2)$	70	1.03
$\nu_5(a')$	112	$\nu_2(a_2)$	73	1.53	$\nu_5(a')$	76	$\nu_2(a_2)$	78	0.97	$\nu_5(a')$	64	$\nu_2(a_2)$	70	0.91
$\nu_9(a'')$	89	$\nu_3(b)$	15	5.93	$\nu_9(a'')$	155	$\nu_3(b)$	34	4.56	$\nu_9(a'')$	47	$\nu_3(b)$	20	2.35

([a]SS) stands for symmetric species

[b]A is the intensity of the dimer and [c]A is the intensity of the monomer

5.5 The nitrous oxide dimer

The structure of the nitrous oxide dimer has not enjoyed such thorough examination. Early gas phase vibrational predissociation [133] and molecular beam (MB) experiments [134,135] were unable to resolve the true structure. More recent high-resolution gas-phase measurements, however, have shown the slipped-parallel geometry of C_{2h} symmetry with the molecule dipoles aligned anti parallel to one another to be preferred [136-139]. Some evidence also has been presented based on gas-phase IR band shape measurements [140] in favour of a C_s configuration T-shaped structure bonded through the nitrogen of the electron donor (ED) molecule. Some very detailed spectra of the variables isotopic forms of nitrous oxide trapped in argon matrices have been presented, and the authors have assigned a number of bands to the dimer. Calculations of the vibrational predissociation lifetimes proved to be inconclusive [141,142, 143] although ab initio computations appear to support a centrosymmetric slipped parallel geometry [109, 144, 145]. The recent studies by Nxumalo *et al*[109] also emphasized that the C_{2h} isomer is the true global minimum structure. For the purpose of this investigation two isomers would be considered, one of C_{2h} symmetry and the other one of C_s symmetry, at the three different levels of computation.

5.5.1 Optimized geomtrical parameters of the nitrous oxide dimer

The geometrical parameters of the nitrous oxide dimers of the staggered parallel (C_{2h}) and perpendicular T-shaped (C_s) structures have been fully optimized by the energy gradient method [146] commonly known as BERNY optimization method [79] without setting any constraint of the bond length and bond angle. The structures are shown in figure 5.4. The optimized geometrical parameters of these molecular species calculated at the three levels of computation are shown in Table 5.5.1. The computed bond length of the nitrous oxide monomer is r(ON) equal to 117.8 pm (for HF), 119.3 pm (MP2) and 119.2 pm (DFT); r(NN) equal to 109.2 pm (for HF), 117.2 (MP2) and 113.4 pm (DFT) which are slightly changed on dimerization. The intermolecular bond length, r(N_1...O_6), is 353.5, 297.7 and 310.8 pm for HF, MP2 and DFT respectively, which is a value obviously indicative of genuine van der Waals interaction. The nitrous oxide monomer bond angles calculated at all the levels is equal to 180 degree and remain unchanged on dimerization.

Similarly, for the T-shaped nitrous oxide dimer both the bond distances r(ON) and r(NN) remain virtually unchanged at the three levels of computation on dimerization. The intermolecular bond length, $r(N_1...N_2)$ is 327.1, 295.7 and 313.2 pm for the HF, MP2 and DFT respectively, which again confirm to the dominance of van der Waals interaction.

5.5.2 The dimerization Energy and the BSSE

The dimerization energies for the slipped parallel and T-shaped nitrous oxide dimers, calculated at the HF, MP2 and DFT levels of computation; before and after correcting for BSSEs, are presented in Table 5.5.2. It is shown in Table 5.32 that the slipped parallel structure is more stable than the perpendicular T-shaped structure before and after correction for BSSEs. One of the interesting features to be noted is that the BSSE for the T-shaped conformer accounts for about 50% of the dimerization energy at all levels but with the exception of the DFT method. In the view of this trend this renders the staggered parallel structure to be more stable than the T-shaped conformation. This aggrees with the findings of Huang and Miller [147] who established that the nitrous oxide dimer has a slipped parallel geometry which possesses the centre of symmetry.

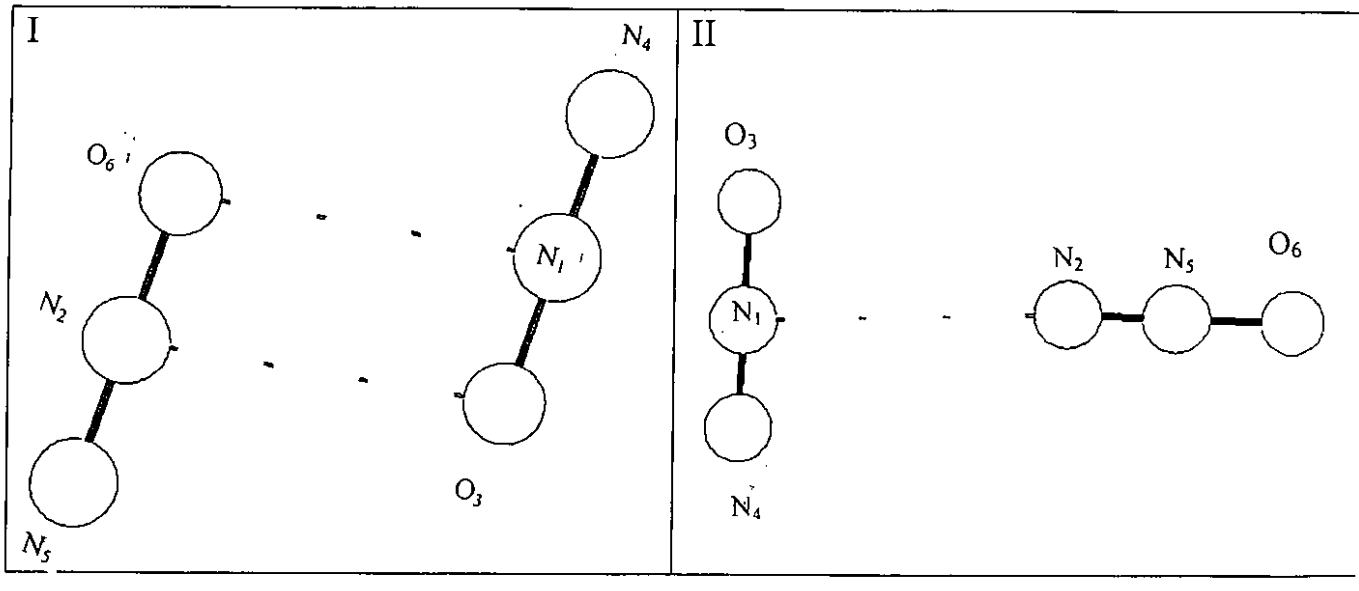

Figure 5.4 shows the optimized structure of the nitrous oxide dimer of the C_{2h} (I) and C_s (II) symmetry together with the numbering of atoms.

Table 5.5.1 The optimized geometrical parameters of the $(N_2O)_2$ calculated at the HF, MP2 and DFT levels of theory using the 6-31G(d, p) split-valence polarized basis set

		Levels of theory		
Species	Parameters	HF	MP2	DFT
$(N_2O)_2$ C_2h	$r(N_1N_4)$/pm	109.2	117.2	113.3
	$r(N_1O_3)$/pm	117.8	119.1	119.4
	$r(N_1...O_6)$/pm	353.5	297.7	310.8
	$O_6\hat{N}_2N_5$/deg	180.0	180.0	180.0
	$O_3\hat{N}_1N_4$/deg	180.0	180.0	180.0
$(N_2O)_2$ Cs	$r(N_1...N_2)$/pm	327.1	295.7	313.2
	$r(N_1N_4)$/pm	109.2	117.2	113.4
	$r(N_1O_3)$/pm	117.8	119.3	119.2
	$r(N_2N_5)$/pm	109.2	117.2	113.4
	$r(N_5O_6)$/pm	117.7	119.2	119.2
	$O_3\hat{N}_1N_4$/deg	180.0	180.0	180.0
	$N_2\hat{N}_5O_6$/deg	180.0	180.0	180.0

Table 5.5.2 The dimerization energies and the basis set superposition errors of the $(N_2O)_2$ calculated at the HF, MP2, and DFT levels of theory using the 6-31G(d, p) split-valence polarized basis set

			Level of theory		
Species	Point group	Energies/kJ mol^{-1}	HF	MP2	DFT
$(N_2O)_2$	C_{2h}	ΔE (uncorrected)	-6.93	-6.86	-5.49
		BSSE	3.02	4.71	1.26
		ΔE (corrected)	-3.91	-2.80	-4.23
$(N_2O)_2$	Cs	ΔE (uncorrected)	-1.79	-7.19	-4.23
		BSSE	1.32	4.39	1.90
		ΔE (corrected)	-0.47	-2.80	-2.33

5.5.3 Vibrational wavenumbers and band intensities of the dimer

The vibrational wavenumbers for the nitrous oxide dimer of the slipped parallel structure, together with the approximate description of the normal modes, is given in Table 5.5.3. In the case of this dimer, the normal modes distribute among the symmetry species according to

$\Gamma_{vib}=5a_u+2a_u+b_g+4b_u$

Due to the equivalence of both monomer units in each case the intramolecular modes are completely coupled, as was found in the carbon dioxide dimer, with ν_1 and ν_9 being the NN-stretching, ν_2 and ν_{10} the NO-stretching, ν_3 and ν_{11} the in-plane-bending and ν_6 and ν_8 the out-of-plane bending librations, ν_5 is the inter-monomer stretching and ν_7 is the out-of plane libration combinations. The weakness of the coupling, however, is indicated by the separations of the in-phase and out-of phase components of each pair, none of those separations, at either levels of theory exceeds 27cm^{-1}

The calculated/experimental wavenumber ratios for the IR active dimer bands are listed in Table 5.5.5. This table shows that both the HF and DFT levels overestimate the experimental wavenumbers by ca. 15% and 4% respectively, while the MP2 method underestimates the experimental wavenumbers by ca. 1%. Since the results of the DFT approach are closed to the experimenatal ones, then we are going to base our predictions upon the DFT method. The correspondence between each of the dimer modes and its counterpart in the monomer in all the levels of theory is presented in Table 5.5.6, in which monomer-dimer wavenumber shifts are reported. The stretching mode wavenumber shifts for nitrous oxide dimer, in which the interaction is between the NN bonds, are smaller. The NO-stretching mode undergoes smaller changes on dimerization on either side, splitting into a pair of bands (ν_2 and ν_{10}), except that the NO-stretching (ν_2) is considerable blue shifted (27cm^{-1}) at this method. The NNO-bending (ν_3, ν_6, ν_8 and ν_{10}) modes of the N_2O fragment are all shifted by small amounts on either direction. The observed wavenumber shifts from the infrared active modes are not more than 6cm^{-1}, but those of infrared inactive are slightly high. The corresponding modes of the in-phase and the out-of-phase are shifted in the range of less than 27cm^{-1} thus confirming that the dimer is weakly bound.

In the perpendicular T-shaped nitrous oxide dimer, the normal modes transform as

$\Gamma_{vib}=9a'+3a''$

The intermolecular modes (ν_1-ν_6, ν_{10} and ν_{11}) are fully uncoupled, and then are consequently localized as either the ED or the EA (see Table 5.5.3). This is again an analogous situation to that for the corresponding carbon dioxide dimer of the C_{2v} symmetry, except that in the latter case the symmetric CO_2-stretches are described as in-phase or out -of-phase; since in the nitrous oxide dimers there are no symmetric stretching vibrations, this description is inappropriate here. The vibrational wavenumbers of the nitrous oxide dimer of the T-shaped (C_s) structure together with the approximate description of the normal modes, are given in Table 5.5.3. It is noted that one of the infrared active modes calculated by the DFT method, ν_{12}, is found to have an imaginary frequency. This is indicative of the T-shaped structure representing a transition state [148]. The correspondence between each of the dimer modes and its counterpart in the monomer in all the levels of theory is presented in Table 5.5.6, in which the monomer-dimer wavenumber shifts are reported. The shifts of the intermolecular vibration of the perpendicular dimer of the T-shaped structure are all predicted to be positive, except for that of ν_6 at all levels of computation. At the HF method, the ν_6 mode on dimerization remain unperturbed, while at the MP2 and DFT methods are shifted to the opposite direction by $3cm^{-1}$ and $1cm^{-1}$ respectively. Moreover, the shifts are larger for the electron donor (ED) molecule than for the electron acceptor (EA). Again, none of the wavenumber shifts exceed 10 cm^{-1}, thus emphasizing that the dimer is also weakly bound.

The ratio of the intensities of the infrared active bands of $(N_2O)_2$ dimer to the corresponding bands of N_2O is presented in Table 5.5.7. These ratios are all cluttered around a value of 3.0 at all the levels of computation, while ν_9 and ν_{10} modes undergo intensity increases on dimerization. Table 5.5.6 shows that at all levels of computation close to the NN stretching mode (ν_1) of the monomer band is expected to be observed; another band is expected to be observed next to the NO stretching mode (ν_2). Finally two bands are expected next NNO bending mode (ν_3). Thus, all in all, only four infrared

active bands of the C_{2h} dimer would be expected to be observed at best at all the levels of theory.

The spectrum of the T-shaped dimer should contain two NN-stretching and two NO-stretching bands, all very close to the monomer absorption. In a similar fashion, there should be four NNO-bending modes, also very close to the monomer vibration and having intensities not quite different from those of the monomer. All four of the intermolecular modes which are infrared active, are expected to be either weakly observed or not observed at all due to their negligible intensities.

Table 5.5.3 The computed and the experimental wavenumbers of the $(N_2O)_2$ calculated at the HF, MP2, and DFT levels of theory using the 6-31G(d, p) split-valence polarized basis set

				Levels of theory			
Dimers	Symmetry Species	Mode	Approximate description	HF $\tilde{\upsilon}/cm^{-1}$	MP2 $\tilde{\upsilon}/cm^{-1}$	DFT $\tilde{\upsilon}/cm^{-1}$	[a]Expt $\tilde{\upsilon}/cm^{-1}$
Slipped parallel structure (C_{2h}) :							
$(N_2O)_2$	a_g	ν_1	ν(NN) (IP)	2636	2234	2373	____[b]
		ν_2	ν(NO) (IP)	1397	1289	1341	____[b]
		ν_3	δ(NNO) (OP)	690	570	603	____[b]
		ν_4	R_y(con)	47	111	99	____[b]
		ν_5	T_z(NNO) (IP)	13	54	43	____[b]
	a_u	ν_6	τ(NNO) (IP)	691	575	604	591
		ν_7	R_z(anti)	11	26	25	____[b]
	b_g	ν_8	τ(NNO)(OP)	690	574	603	____[b]
	b_u	ν_9	ν(NN) (OP)	2630	2240	2376	2240
		ν_{10}	ν(NO) (O.P)	1395	1288	1338	1286
		ν_{11}	δ(NNO) (IP)	689	572	603	584
		ν_{12}	R_y(anti)	27	47	36	____[b]
T-shaped structure (C_{2v}) :							
$(N_2O)_2$	a′	ν_1	ν(NN) (ED)	2635	2257	2378	
		ν_2	ν(NN) (EA)	2634	2251	2374	
		ν_3	ν(NO) (ED)	1400	1293	1348	
		ν_4	ν(NO) (EA)	1395	1291	1346	
		ν_5	δ(NNO) (ED)	690	576	605	
		ν_6	δ(NNO) (EA)	689	572	603	
		ν_7	T_z	60	76	65	
		ν_8	R_y (con)	42	74	51	
		ν_9	R_y (anti)	12	8	27	
	a″	ν_{10}	γ(NNO) (ED)	694	582	609	
		ν_{11}	γ(NNO) (EA)	690	576	605	
		ν_{12}	R_y(anti)	26	33	-8	

Ref: 130, [b] band not observed in this region

Table 5.5.4 The band intensities of the $(N_2O)_2$ calculated at the HF, MP2 and DFT levels of theory using the 6-31G(d, p) basis set

				Levels of theory		
Dimers	Symmetry Species	Mode	Approximate description	HF A/km mol^{-1}	MP2 A/km mol^{-1}	DFT A/km mol^{-1}
Slipped parallel structure (C_{2h}) :						
$(N_2O)_2$	a_u	ν_6	τ(NNO) (IP)	39	9	17
		ν_7	R_z (anti)	1	0.04	0.1
	b_u	ν_9	ν(NN) (OP)	1042	497	589
		ν_{10}	ν(NO) (O.P)	341	24	113
		ν_{11}	δ(NNO) (IP)	40	13	28
T-shaped structure (C_s) :						
$(N_2O)_2$	a′	ν_1	ν(NN) (ED)	527	275	329
		ν_2	ν(NN) (EA)	477	253	302
		ν_3	ν(NO) (ED)	170	8	51
		ν_4	ν(NO) (EA)	162	9	51
		ν_5	δ(NNO) (ED)	19	5	10
		ν_6	δ(NNO) (EA)	26	8	12
		ν_7	T_z	0.9	0.03	0.1
		ν_8	R_y(con)	0.04	0.03	0.03
		ν_9	R_y (anti)	0.6	0.02	0.1
	a″	ν_{10}	γ(NNO) (ED)	25	5	11
		ν_{11}	γ(NNO) (EA)	14	4	8
		ν_{12}	R_y (anti)	0.5	0.02	0.005

EA is the electron acceptor and ED is an electron donor

Table 5.5.5 Ratios of the computed to the experimental wavenumber observed in nitrogen matrices of the intramolecular modes of the nitrous oxide dimer (C_{2h}).

	[a]Level of theory		
Mode	HF	MP2	DFT
ν_6	1.17	0.97	1.02
ν_9	1.17	1.00	1.06
ν_{10}	1.08	1.00	1.04
ν_{11}	1.18	0.98	1.03
Mean Average	1.15	0.99	1.04

[a]Ratio= $\tilde{\upsilon}_{cal} / \tilde{\upsilon}_{expt}$

Table 5.5.6 Comparison of the calculated wavenumbers of the $(N_2O)_2$ with those of the corresponding modes of the monomer, calculated at the HF, MP2 and DFT levels of theory using the 6-31G(d, p) basis set.

HF/6-31G(d, p)					MP2/6-31G(d, p)					DFT/6-31G(d, p)				
Dimer		Monomer			Dimer		Monomer			Dimer		Monomer		
mode ([a]SS)	$\tilde{\upsilon}/cm^{-1}$	mode ([a]SS)	$\tilde{\upsilon}/cm^{-1}$	Shifts [b]$\Delta\tilde{\upsilon}/cm^{-1}$	mode ([a]SS)	$\tilde{\upsilon}/cm^{-1}$	mode ([a]SS)	$\tilde{\upsilon}/cm^{-1}$	Shifts [b]$\Delta\tilde{\upsilon}/cm^{-1}$	mode ([a]SS)	$\tilde{\upsilon}/cm^{-1}$	mode ([a]SS)	$\tilde{\upsilon}/cm^{-1}$	Shifts [b]$\Delta\tilde{\upsilon}/cm^{-1}$
Slipped parallel structure (C_{2h}) :														
$\nu_1(a_g)$	2636	$\nu_1(\Sigma^+)$	2633	3	$\nu_1(a_g)$	2234	$\nu_1(\Sigma^+)$	2247	3	$\nu_1(a_g)$	2374	$\nu_1(\Sigma^+)$	2371	3
$\nu_2(a_g)$	1397	$\nu_2(\Sigma^+)$	1393	4	$\nu_2(a_g)$	1289	$\nu_2(\Sigma^+)$	1289	0	$\nu_2(a_g)$	1371	$\nu_2(\Sigma^+)$	1344	27
$\nu_3(a_g)$	690	$\nu_3(\Pi_u)$	689	1	$\nu_3(a_g)$	570	$\nu_3(\Pi_u)$	575	-5	$\nu_3(a_g)$	603	$\nu_3(\Pi_u)$	604	-1
$\nu_6(a_u)$	691	$\nu_3(\Pi_u)$	689	2	$\nu_6(a_u)$	575	$\nu_3(\Pi_u)$	575	0	$\nu_6(a_u)$	604	$\nu_3(\Pi_u)$	604	0
$\nu_8(b_g)$	690	$\nu_3(\Pi_u)$	689	2	$\nu_8(b_g)$	574	$\nu_3(\Pi_u)$	575	-1	$\nu_8(b_g)$	603	$\nu_3(\Pi_u)$	604	-1
$\nu_9(b_u)$	2630	$\nu_1(\Sigma^+)$	2633	-3	$\nu_9(b_u)$	2240	$\nu_1(\Sigma^+)$	2247	-7	$\nu_9(b_u)$	2376	$\nu_1(\Sigma^+)$	2371	5
$\nu_{10}(b_u)$	1395	$\nu_2(\Sigma^+)$	1393	2	$\nu_{10}(b_u)$	1288	$\nu_2(\Sigma^+)$	1289	-1	$\nu_{10}(b_u)$	1338	$\nu_2(\Sigma^+)$	1344	-6
$\nu_{11}(b_u)$	689	$\nu_2(\Pi)$	689	0	$\nu_{11}(b_u)$	572	$\nu_2(\Pi)$	575	-3	$\nu_{11}(b_u)$	603	$\nu_2(\Pi)$	604	-1
T-shaped structure (Cs) :														
$\nu_1(a')$	2635	$\nu_1(\Sigma^+)$	2633	2	$\nu_1(a')$	2257	$\nu_1(\Sigma^+)$	2247	10	$\nu_1(a')$	2378	$\nu_1(\Sigma^+)$	2371	7
$\nu_2(a')$	2634	$\nu_1(\Sigma^+)$	2633	1	$\nu_2(a')$	2251	$\nu_1(\Sigma^+)$	2247	4	$\nu_2(a')$	2374	$\nu_1(\Sigma^+)$	2371	3
$\nu_3(a')$	1400	$\nu_2(\Sigma^+)$	1393	7	$\nu_3(a')$	1293	$\nu_2(\Sigma^+)$	1289	4	$\nu_3(a')$	1348	$\nu_2(\Sigma^+)$	1344	-4
$\nu_4(a')$	1395	$\nu_1(\Sigma^+)$	1393	2	$\nu_4(a')$	1291	$\nu_1(\Sigma^+)$	1289	2	$\nu_4(a')$	1346	$\nu_1(\Sigma^+)$	1344	2
$\nu_5(a')$	690	$\nu_3(\Pi)$	689	1	$\nu_5(a')$	576	$\nu_3(\Pi)$	575	1	$\nu_5(a')$	605	$\nu_3(\Pi)$	604	1

Table 5.5.6 continue

HF/6-31G(d, p)				MP2/6-31G(d, p)				DFT/6-31G(d, p)			
Dimer		Monomer		Dimer		Monomer		Dimer		Monomer	
mode (^{a}SS)	$\tilde{\upsilon}/cm^{-1}$	mode (^{a}SS)	$\tilde{\upsilon}/cm^{-1}$ Shifts $^b\Delta\tilde{\upsilon}/cm^{-1}$	mode (^{a}SS)	$\tilde{\upsilon}/cm^{-1}$	mode (^{a}SS)	$\tilde{\upsilon}/cm^{-1}$ Shifts $^b\Delta\tilde{\upsilon}/cm^{-1}$	mode (^{a}SS)	$\tilde{\upsilon}/cm^{-1}$	mode (^{a}SS)	$\tilde{\upsilon}/cm^{-1}$ Shifts $^b\Delta\tilde{\upsilon}/cm^{-1}$
$\nu_6(a')$	689	$\nu_3(\Pi)$	689 0	$\nu_6(a')$	572	$\nu_3(\Pi)$	575 -3	$\nu_6(a')$	603	$\nu_3(\Pi)$	604 -1
$\nu_{10}(a'')$	694	$\nu_3(\Pi)$	689 5	$\nu_{10}(a'')$	582	$\nu_3(\Pi)$	575 5	$\nu_{10}(a'')$	609	$\nu_3(\Pi)$	604 -5
$\nu_{11}(a'')$	689	$\nu_3(\Pi)$	689 1	$\nu_{11}(a'')$	576	$\nu_3(\Pi)$	575 1	$\nu_{11}(a'')$	605	$\nu_3(\Pi)$	604 1

(^{a}SS) stands for symmetry species

$^b\Delta\tilde{\upsilon} = \tilde{\upsilon}_{dimer} - \tilde{\upsilon}_{monomer}$

Table 5.5.7 Comparison of the calculated band intensities of the $(N_2O)_2$ with those of the corresponding modes of the monomer, calculated at the HF, MP2 and DFT levels of theory using the 6-31G(d, p) basis set

HF/6-31G(d, p)					MP2/6-31G(d, p)					DFT/6-31G(d, p)				
Dimer		Monomer			Dimer		Monomer			Dimer		Monomer		
mode ([a]SS)	[b]A/km mol^{-1}	mode ([a]SS)	[b]A/km mol^{-1}	[b]A/[c]A	mode ([a]SS)	[b]A/km mol^{-1}	mode ([a]SS)	[b]A/km mol^{-1}	[b]A/[c]A	mode ([a]SS)	[b]A/km mol^{-1}	mode ([a]SS)	[b]A/km mol^{-1}	[b]A/[c]A
Slipped parallel structure (C_{2h}) :														
$\nu_6(a_u)$	39	$\nu_3(\Pi_u)$	20	1.95	$\nu_6(a_u)$	9	$\nu_3(\Pi_u)$	5	1.80	$\nu_6(a_u)$	17	$\nu_3(\Pi_u)$	9	1.89
$\nu_9(b_u)$	1042	$\nu_1(\Sigma^+)$	490	2.13	$\nu_9(b_u)$	497	$\nu_1(\Sigma^+)$	263	1.89	$\nu_9(b_u)$	589	$\nu_1(\Sigma^+)$	310	1.90
$\nu_{10}(b_u)$	341	$\nu_2(\Sigma^+)$	165	2.07	$\nu_{10}(b_u)$	24	$\nu_2(\Sigma^+)$	8	3.00	$\nu_{10}(b_u)$	113	$\nu_2(\Sigma^+)$	49	2.31
$\nu_{11}(b_u)$	40	$\nu_2(\Pi)$	20	2.00	$\nu_{11}(b_u)$	13	$\nu_2(\Pi)$	5	2.60	$\nu_{11}(b_u)$	28	$\nu_2(\Pi)$	9	3.11
T-shaped structure (C_{2v}) :														
$\nu_1(a')$	527	$\nu_1(\Sigma^+)$	490	1.08	$\nu_1(a')$	275	$\nu_1(\Sigma^+)$	263	1.05	$\nu_1(a')$	329	$\nu_1(\Sigma^+)$	310	1.06
$\nu_2(a')$	477	$\nu_1(\Sigma^+)$	490	0.97	$\nu_2(a')$	253	$\nu_1(\Sigma^+)$	263	0.96	$\nu_2(a')$	302	$\nu_1(\Sigma^+)$	310	0.97
$\nu_3(a')$	170	$\nu_2(\Sigma^+)$	164	1.04	$\nu_3(a')$	8	$\nu_2(\Sigma^+)$	8	1.00	$\nu_3(a')$	51	$\nu_2(\Sigma^+)$	49	1.04
$\nu_4(a')$	162	$\nu_1(\Sigma^+)$	164	0.99	$\nu_4(a')$	9	$\nu_1(\Sigma^+)$	8	1.13	$\nu_4(a')$	51	$\nu_1(\Sigma^+)$	49	1.04
$\nu_5(a')$	19	$\nu_3(\Pi)$	20	0.95	$\nu_5(a')$	5	$\nu_3(\Pi)$	5	1.00	$\nu_5(a')$	10	$\nu_3(\Pi)$	9	1.11

Table 5.5.7 Continue

HF/6-31G(d, p)					MP2/6-31G(d, p)					DFT/6-31G(d, p)				
Dimer		Monomer			Dimer		Monomer			Dimer		Monomer		
mode (^{a}SS)	^{b}A/km mol^{-1}	mode (^{a}SS)	^{b}A/km mol^{-1}	^{b}A/^{c}A	mode (^{a}SS)	^{b}A/km mol^{-1}	mode (^{a}SS)	^{b}A/km mol^{-1}	^{b}A/^{c}A	mode (^{a}SS)	^{b}A/km mol^{-1}	mode (^{a}SS)	^{b}A/km mol^{-1}	^{b}A/^{c}A
$\nu_6(a')$	26	$\nu_3(\Pi)$	20	1.30	$\nu_6(a')$	8	$\nu_3(\Pi)$	5	1.60	$\nu_6(a')$	12	$\nu_3(\Pi)$	9	1.33
$\nu_{10}(a'')$	25	$\nu_3(\Pi)$	20	1.25	$\nu_{10}(a'')$	5	$\nu_3(\Pi)$	5	1.00	$\nu_{10}(a'')$	11	$\nu_3(\Pi)$	9	1.22
$\nu_{11}(a'')$	14	$\nu_3(\Pi)$	20	0.70	$\nu_{11}(a'')$	4	$\nu_3(\Pi)$	5	0.80	$\nu_{11}(a'')$	8	$\nu_3(\Pi)$	9	0.89

(^{a}SS) stands for symmetric species, ^{b}A is the intensity of the dimer and ^{c}A is the intensity of the monomer

Table 5.5.7 Continue

HF/6-31G(d, p)					MP2/6-31G(d, p)					DFT/6-31G(d, p)				
Dimer		Monomer			Dimer		Monomer			Dimer		Monomer		
mode (^{a}SS)	^{b}A/km mol^{-1}	mode (^{a}SS)	^{b}A/km mol^{-1}	^{b}A/^{c}A	mode (^{a}SS)	^{b}A/km mol^{-1}	mode (^{a}SS)	^{b}A/km mol^{-1}	^{b}A/^{c}A	mode (^{a}SS)	^{b}A/km mol^{-1}	mode (^{a}SS)	^{b}A/km mol^{-1}	^{b}A/^{c}A
$\nu_6(a')$	26	$\nu_3(\Pi)$	20	1.30	$\nu_6(a')$	8	$\nu_3(\Pi)$	5	1.60	$\nu_6(a')$	12	$\nu_3(\Pi)$	9	1.33
$\nu_{10}(a'')$	25	$\nu_3(\Pi)$	20	1.25	$\nu_{10}(a'')$	5	$\nu_3(\Pi)$	5	1.00	$\nu_{10}(a'')$	11	$\nu_3(\Pi)$	9	1.22
$\nu_{11}(a'')$	14	$\nu_3(\Pi)$	20	0.70	$\nu_{11}(a'')$	4	$\nu_3(\Pi)$	5	0.80	$\nu_{11}(a'')$	8	$\nu_3(\Pi)$	9	0.89

(^{a}SS) stands for symmetric species, ^{b}A is the intensity of the dimer and ^{c}A is the intensity of the monomer

5.6. The Sulphur dioxide dimer

Mainly as a result of the current interest in sulphur dioxide as a major pollutant in emissions from factory and power plants stacks and from motor car exhausts and its consequent role is introduced for the remote detection and monitoring of these gases. Many of these methods involve the observation of the infrared and ultraviolet absorption and emission spectra of sulphur dioxide [149]. In attempts to a better understanding of the infrared spectrum, this substance has been studied by a number of authors in cryogenetic matrices [150-154]. Most studies have focussed on the spectra of the various isotopic monomer species. Nelson [155], Matrumura [156], Taleb-Bendiab [157] and their co-workers have described the radiofrequency and microwave spectra of a number of isotopic variants of SO_2 dimer in the gas phase. They concluded that the equilibrium structure of the dimer has a plane of symmetry with the two monomer units being non-equivalent, and that the dimer undergoes a high barrier tunnelling motion with a period of 14μs [155], similar to that proposed for H_2O dimer by Coudert and Hougen [158]. In our ab initio calculations we considered a linear structure of the sulphur dioxide dimer.

5.6.1 The geometrical parameters of sulphur dioxide dimer

The ab initio calculations [159] of the nature of the 1:1 SO_2 dimer indicate that the most probable structure possesses the C_s symmetry configuration (see fig 5.6). Table 5.6.1 presents the values of the converged geometrical parameters of the sulphur dioxide dimer. The sulphur dioxide monomer bond length calculated at all the levels of theory studied here is equal to 141.4 (for HF), 147.8 (MP2) and 146.3 pm (DFT). Table 5.6.1 shows that the bond length of the sulphur dioxide in the subunit in the dimer is slightly changed at the both the HF and MP2 approaches and remains unchanged at the DFT method. The $\hat{OSO}$ bond angles shorten slightly on dimerization. The intermolecular bond length r(S...O) is 372.1, 344.6 and 359.6 pm for HF, MP2 and DFT levels of computation, respectively.

5.6.2 The dimerization energies

The dimerization energies for the SO_2 dimer of Cs symmetry, before and after correcting for BSSEs by the full counterpoise method [77] are listed in

Table 5.6.2. In the HF level of theory, the dimerization energy of SO_2 dimer, after BSSE correction are virtually indistinguishable. The same order is reproduced in the MP2 and DFT levels of computation. The BSSE contributions to the uncorrected energies about 29% at the HF, this contribution increases to about 64% and 66% at both the DFT and MP2 levels of computation, respectively.

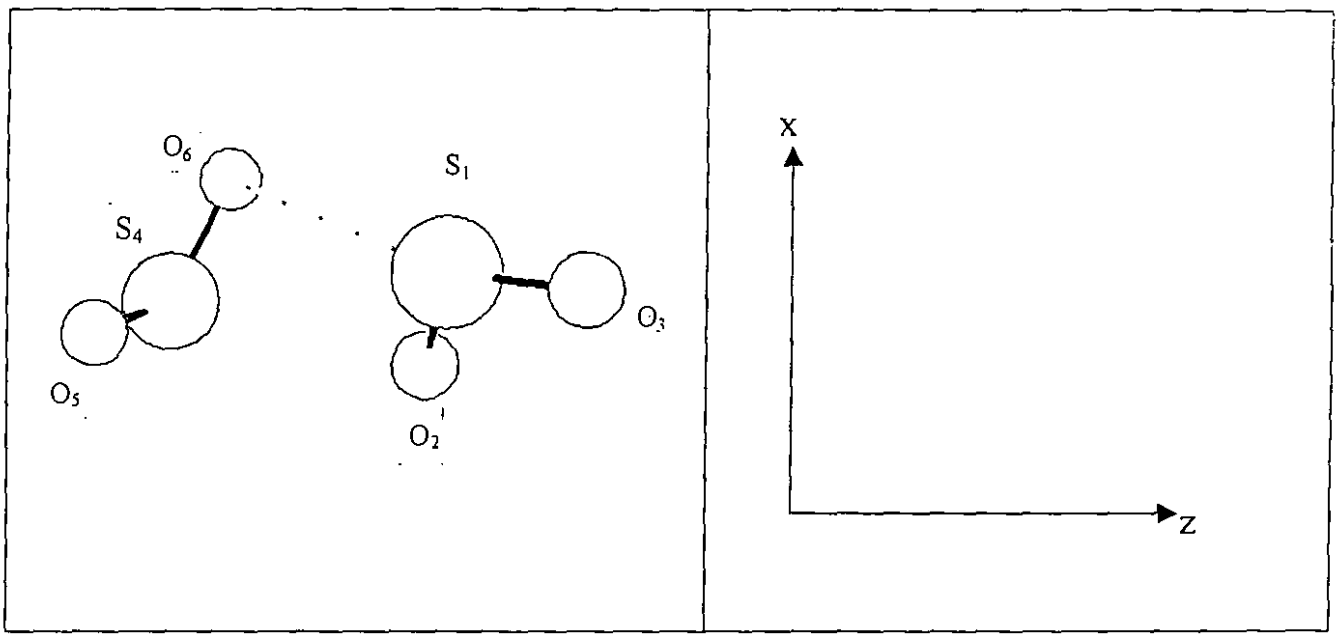

Figure 5.6 shows the structure of the linear sulphur dioxide dimer of C_s symmetry

Table 5.6.1 The optimized geometrical parameters of the $(SO_2)_2$ calculated at the HF, MP2 and DFT levels of theory using the 6-31G(d, p) split-valence polarized basis set

		Level of theory		
Species	Parameters	HF	MP2	DFT
$(SO_2)_2$	$r(S_1...O_5)$/pm	372.1	344.6	356.9
	$r(S_4O_5)$/pm	141.5	147.9	146.3
	$r(S_1O_2)$/pm	141.7	147.9	146.3
	$r(S_4O_6)$/pm	141.5	147.9	146.3
	$r(S_1O_3)$/pm	141.7	147.9	146.3
	$O_5\hat{S}_4O_6$/deg	118.1	119.1	118.4
	$O_2\hat{S}_1O_3$/deg	118.1	119.1	118.4

Table 5.6.2 The dimerization energies and the basis set superposition errors of the $(SO_2)_2$ calculated at the HF, MP2, and DFT levels of theory using the 6-31G(d, p) split-valence polarized basis set

			Level of theory		
Species	Point group	Energy/kJ mol^{-1}	HF	MP2	DFT
$(SO_2)_2$	C_s	ΔE $(_{uncorrected})$	-13.35	-14.41	-11.15
		BSSE	3.86	9.48	7.51
		ΔE $(_{corrected})$	-9.49	-4.93	-3.64

5.6.3 The vibrational wavenumbers and the band intensities

The vibrational wavenumbers for the sulphur dioxide dimer, together with the approximate description of normal modes, are given in Table 5.6.3. This table shows that at all the three levels of theory one imaginary frequency was calculated at the ν_{12} mode of the electron donor. In the SO_2 dimer, the normal modes distributions transform as

$\Gamma_{vib}=8a'+4a''$

Table 5.6.4 shows the intensities of the sulphur dioxide dimer. It is noted at this table that the ν_{12} mode of the electron donor showed a very negligible intensity at the DFT level. The intermolecular dimer intensities are all predicted to be below about 50 km mol^{-1}, in a region which is not readily accessible to most commercial infrared spectrometers. The ratios of the computed to the experimental wavenumbers of the intramolecular modes of the SO_2 dimer observed in nitrogen matrices are presented in Table 5.6.5. This table shows that the HF level of theory overestimates the experimental infrared wavenumber by ca. 16% on average while both the MP2 and DFT methods underestimate the experimental wavenumbers by ca. 5% and ca. 2% on average, respectively. Since the DFT approach results are close to the experimental ones as it gives a slight underestimation, therefore we are going to base our predictions upon this method. The confirmation of the reliability of the assignment of the intramolecular dimer modes is provided in Table 5.6.6, in which the wavenumber shifts between the sulphur dioxide monomer and the sulphur dioxide dimer are reported. The theoretical predictions are that on dimerization, the antisymmetric SO stretching undergoes smallest changes, splitting into a pair of bands of the electron acceptor ν_1 mode and electron donor ν_9 mode, which are all red shifted. The symmetric SO stretching mode of the monomer correlates with the ν_2 and ν_3 modes of the dimer and is shifted to the blue at both modes. The ν_4 mode of the dimer correlates with the out-of-phase combination of the bending mode of the monomer units and displaced by 8 cm^{-1} to the blue of the monomer position. The ν_5 mode is the corresponding in-phase combination that is red shifted by 1cm^{-1} from the monomer band. The fact that none of the

theoretical shifts exceed $11cm^{-1}$, confirms to the extreme weakness of the interaction in the SO_2 dimer. The magnitudes of the shifts also show close agreement with the experimental values, this evidence taken alongside the consistency in the values of the calculated/experimental wavenumber ratios (see Table 5.6.5), provides a convincing argument that the experimental infrared spectrum of the sulphur dioxide dimer observed in nitrogen matrices agrees closely with that predicted by ab initio [159]. This also confirms that the structure of the dimer deduced from the gas phase microwave spectrum [155-157] is also the preferred structure in cryogenic matrices.

The comparison of the calculated intensities of the sulphur dioxide dimer with those of the corresponding modes of the monomer, calculated at the HF, MP2 and DFT using the 6-31G(p, d) is shown in Table 5.6.7. This table shows that the range of these ratios is from 0.36 to 1.47 at all the levels of computation. The relatively small intensity changes of the monomer modes on dimerization are also indicative of a very weak interaction. The intermolecular dimer intensities are all predicted to be below about 50 km mol^{-1}, in a region which is not readily accessible to most commercial infrared spectrometers. Therefore these intensities data are not expected to be of any value in assisting with the assignments of the experimental spectra.

The spectrum of the open bonded SO_2 dimer should contain six SO-stretching bands, two very modest in intensity and another two having significantly weaker intensities; two of these will appear slightly below the monomer symmetric SO_2-stretching vibration. Likewise, there should be two SO-bending modes, one shifted very little from the parent monomer band and the other one noticeably blue shifted, both having intensities not remarkable different from those of the monomer. All six intramolecular modes will be infrared active. All in all, the six bands of the SO_2 dimer would be expected to be observed at best

Table 5.6.3 The computed and the experimental wavenumbers of the $(SO_2)_2$ calculated at the HF, MP2 and DFT, using the 6-31G(d, p) split-valence polarized basis set

			Levels of theory			
Symmetry Species	Mode	approximate description	HF $\tilde{\upsilon}/cm^{-1}$	MP2 $\tilde{\upsilon}/cm^{-1}$	DFT $\tilde{\upsilon}/cm^{-1}$	[a]Experimental $\tilde{\upsilon}/cm^{-1}$
a'	ν_1	$\nu_a(SO_2)$ (ED)	1558	1301	1329	1349
	ν_2	$\nu_s(SO_2)$ (EA)	1360	1081	1142	1156
	ν_3	$\nu(SO_2)$ (ED)	1355	1080	1140	1154
	ν_4	$\delta(SO_2)$ (OP)	602	494	510	527
	ν_5	$\delta(SO_2)$ (IP)	591	485	501	524
	ν_6	$w(SO_2)$ (EA)	116	97	91	___[b]
	ν_7	ν(O...S)	71	67	58	___[b]
	ν_8	$\tau(SO_2)$ (ED)	32	51	39	___[b]
a''	ν_9	$\nu_a(SO_2)$ (EA)	1559	1304	1331	1346
	ν_{10}	$t_w(SO_2)$ (EA)	97	73	71	____[b]
	ν_{11}	$\tau(SO_2)$ (EA)	29	41	31	____[b]
	ν_{12}	$\tau(SO_2)$ (ED)	-13	-11	-14	____[b]

[a]Ref: 130

[b] band no observed in this region

Table 5.6.4 The band intensities of the $(SO_2)_2$ calculated at the HF, MP2 and DFT levels of theory using the 6-31G(d, p) basis set

				Levels of theory		
Dimers	Symmetry Species	Mode	Approximate description	HF A/ km mol^{-1}	MP2 A/km mol^{-1}	DFT A/km mol^{-1}
$(SO_2)_2$	a'	ν_1	$\nu_a(SO_2)$ (ED)	370	99	192
		ν_2	$\nu_s(SO_2)$ (EA)	103	18	38
		ν_3	$\nu(SO_2)$ (ED)	23	13	21
		ν_4	$\delta(SO_2)$ OP)	91	31	39

Table 5.6.4 continue

	ν_5	$\delta(SO_2)$ (IP)	31	42	35
	ν_6	$w(SO_2)$ (EA)	17	8	6
	ν_7	ν(O...S)	13	5	6
	ν_8	$\tau(SO_2)$ (ED)	16	10	16
a"	ν_9	$\nu_a(SO_2)$ (EA)	315	79	160
	ν_{10}	$t_w(SO_2)$ (EA)	4	0.03	1
	ν_{11}	$\tau(SO_2)$ (EA)	22	11	15
	ν_{12}	$\tau(SO_2)$ (ED)	0.4	4	0.0002

Table 5.6.5 Ratios of the computed to the experimental wavenumbers observed in of the nitrogen matrices of the intramolecular modes of the sulphur dioxide dimer.

	[a] **Level of theory**		
Mode	HF	MP2	DFT
ν_1	1.15	0.97	0.99
ν_2	1.18	0.93	0.99
ν_3	1.17	0.94	0.99
ν_4	1.14	0.94	0.97
ν_5	1.13	0.93	0.96
ν_9	1.16	0.97	0.99
Mean Average	1.16	0.95	0.98

[a]Ratio= $\widetilde{\upsilon}_{cal} / \widetilde{\upsilon}_{exp\,t}$

Table 5.6.6 Comparison of the calculated band intensities of the $(SO_2)_2$ with those of the corresponding modes of the monomer, calculated at the HF, MP2 and DFT levels using the 6-31G(d, p) basis set

HF/6-31G(d, p)					MP2/6-31G(d, p)					DFT/6-31G(d, p)				
Dimer		Monomer			Dimer		Monomer			Dimer		Monomer		
mode ([a]SS)	ν/cm^{-1}	mode ([a]SS)	$\tilde{\upsilon}/cm^{-1}$	Shifts [b]$\Delta\tilde{\upsilon}/cm^{-1}$	mode ([a]SS)	$\tilde{\upsilon}/cm^{-1}$	mode ([a]SS)	$\tilde{\upsilon}/cm^{-1}$	Shifts [b]$\Delta\tilde{\upsilon}/cm^{-1}$	mode ([a]SS)	$\tilde{\upsilon}/cm^{-1}$	mode ([a]SS)	$\tilde{\upsilon}/cm^{-1}$	Shifts [b]$\Delta\tilde{\upsilon}/cm^{-1}$
$\nu_1(a')$	1558	$\nu_3(b)$	1569	-11	$\nu_1(a')$	1301	$\nu_3(b)$	1305	-4	$\nu_1(a')$	1329	$\nu_3(b)$	1336	-7
$\nu_2(a')$	1360	$\nu_1(a_1)$	1359	1	$\nu_2(a')$	1081	$\nu_1(a_1)$	1077	4	$\nu_2(a')$	1142	$\nu_1(a_1)$	1139	3
$\nu_3(a')$	1355	$\nu_1(a_1)$	1359	-4	$\nu_3(a')$	1080	$\nu_1(a_1)$	1077	3	$\nu_3(a')$	1139	$\nu_1(a_1)$	1139	0
$\nu_4(a')$	602	$\nu_2(a_1)$	592	10	$\nu_4(a')$	494	$\nu_2(a_1)$	486	8	$\nu_4(a')$	510	$\nu_2(a_1)$	502	8
$\nu_5(a')$	591	$\nu_2(a_1)$	592	-1	$\nu_5(a')$	485	$\nu_2(a_1)$	486	-1	$\nu_5(a')$	501	$\nu_2(a_1)$	502	-1
$\nu_9(a'')$	1559	$\nu_3(b)$	1569	-10	$\nu_9(a'')$	1304	$\nu_3(b)$	1305	-1	$\nu_9(a'')$	1331	$\nu_3(b)$	1336	-5

([a]SS) stand for symmetry species

[b] $\Delta\tilde{\upsilon} = \tilde{\upsilon}_{dimer} - \tilde{\upsilon}_{monomer}$

Table 5.6.7 Comparison of the calculated wavenumbers of the $(SO_2)_2$ with those of the corresponding modes of the monomer, calculated at the HF, MP2 and DFT levels of theory using the 6-31G(d, p) basis set

HF/6-31G(d, p)					MP2/6-31G(d, p)					DFT/6-31G(d, p)				
Dimer		Monomer			Dimer		Monomer			Dimer		Monomer		
mode ([a]SS)	A/km mol^{-1}	mode ([a]SS)	A/km mol^{-1}	[b]A/[c]A	mode ([a]SS)	A/km mol^{-1}	mode ([a]SS)	A/km mol^{-1}	[b]A/[c]A	mode ([a]SS)	A/km mol^{-1}	mode ([a]SS)	A/km mol^{-1}	[b]A/[c]A
$\nu_1(a')$	370	$\nu_3(b)$	322	1.15	$\nu_1(a')$	99	$\nu_3(b)$	79	1.25	$\nu_1(a')$	192	$\nu_3(b)$	165	1.16
$\nu_2(a')$	103	$\nu_1(a_1)$	64	1.61	$\nu_2(a')$	18	$\nu_1(a_1)$	13	1.38	$\nu_2(a')$	38	$\nu_1(a_1)$	28	1.36
$\nu_3(a')$	23	$\nu_1(a_1)$	64	0.36	$\nu_3(a')$	15	$\nu_1(a_1)$	13	1.15	$\nu_3(a')$	21	$\nu_1(a_1)$	28	0.75
$\nu_4(a')$	91	$\nu_2(a_1)$	62	1.47	$\nu_4(a')$	31	$\nu_2(a_1)$	32	0.97	$\nu_4(a')$	39	$\nu_2(a_1)$	34	1.15
$\nu_5(a')$	31	$\nu_2(a_1)$	62	0.50	$\nu_5(a')$	42	$\nu_2(a_1)$	32	1.31	$\nu_5(a')$	35	$\nu_2(a_1)$	34	1.03
$\nu_9(a'')$	315	$\nu_3(b)$	322	0.98	$\nu_9(a'')$	79	$\nu_3(b)$	79	1.00	$\nu_9(a'')$	160	$\nu_3(b)$	165	0.97

([a]SS) stands for symmetry species [b]A is the intensity of the dimer and [c]A is the intensity of the monomer

CHAPTER SIX

Theoretical predictions of the geometries, energies and the vibrational spectra of the hetero-dimers.

6.1 The boron trifluoride-carbon monoxide molecular complex

In the past few years, high-resolution infrared spectroscopic studies of gaseous, binary van der Waals complexes have contributed a wealth of important information on the structures of the complexes and on the nature of the molecular interactions responsible for their existance.[160-164] Most of these studies have involved the excitation, usually by means of a suitable laser, of an intramolecular vibrational mode associated with one of the monomer components of the complex. The resulting vibration-rotation spectra yield the relative orientations of the interacting monomer species, the changes in their internal geometries resulting from complex formation, and the wavenumber shifts of those modes rising from association. Molecular complexes containing boron trifluoride, as the electron acceptor has been known from early X-ray [165-167] and solid-state infrared and Raman [168-170] studies of aggregates of BF_3 with the nitrogen donors. Resulting from advances in experimental techniques, there have been reports in the literature of the characterization of a number of such complexes containing boron trifluoride in the gas phase. Those of interest to us include the complexes of BF_3 with CO [171,172], CO_2, H_2O[173, 174], N_2O[175], O_2[130], O_3 and SO_2[176, 177].

6.1.1 The optimized geometrical parameters

Fig 6.1 shows the structure of the boron trifluoride-carbon monoxide complex of C_{3v} symmetry with the orientation of the axis and the numbering of atoms. The structure was drawn from the standard orientation of the optimized structure using the Oak Ridge Thermal Ellipsoidal Programme (ORTEP) [34]. The optimized structural parameters of the BF_3.CO complex are presented in Table 6.1.1. The computed bond lengths of the boron trifluoride and carbon monoxide monomer are presented in Table 4.1 (see chapter 4, page 22). The carbon monoxide monomer bond length calculated at the HF, MP2 and DFT levels is r(CO) equal to 111.4, 115.1 and 113.8 pm respectively. It is noted from Table 4.1 that the OC bond length of the

not significantly changed on complexation. The boron trifluoride monomer bond angle calculated at all the levels of theory is $F\hat{B}F$ equal to 120 degrees and remains unchanged on complexation. The intermolecular bond length r(B...O), is 279.0, 268.9 and 274.2 pm for the HF, MP2 and DFT methods respectively and this high value implies a weak interaction.

6.1.2 The complexation energy

The interaction energy of the BF_3.CO complex before and after correcting for the BSSEs by the full counterpoise methods [77] is listed in Table 6.1.2. The BSSEs account for about 41 % of the interaction energy of the complex at the HF method, while at the MP2 and DFT methods, the BSSE accounts for about 79% and 64 %, respectively. The interaction found in all the three levels of computation is weak and is also confirmed by the high value of the interaction distance (see table 6.1.1).

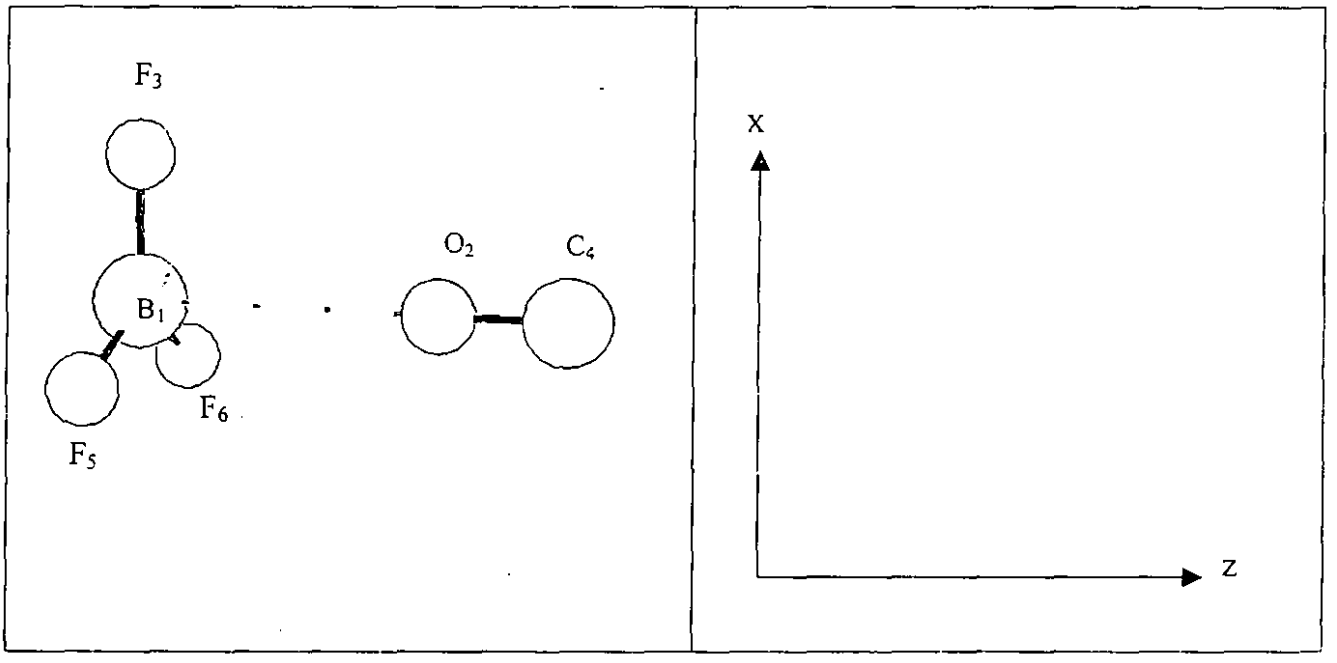

Figure 6.1 shows the optimized structure of the boron trifluoride-carbon monoxide molecular complex together with the numbering of atoms.

Table 6.1.1 The optimized geometrical parameters of the BF_3.CO complex calculated at the HF, MP2 and DFT levels of theory using the 6-31G(d, p) split-valence polarized basis set.

	Level of theory		
Parameters	HF/6-31G(d, p)	MP2/6-31G(d, p)	DFT/6-31G(d, p)
$r(B_1 \ldots O_2)$/pm	279.0	268.9	274.2
$r(B_1F_3) = r(B_1F_5)$/pm	130.2	132.4	131.8
$r(O_2C_6)$pm	111.5	115.1	113.9
$B_1\ldots\hat{O}_2C_6$/deg	180.0	180.0	180.0
$O_2\ldots\hat{B}_1F_3 = O_2\ldots\hat{B}_1F_5$/deg	90.6	90.5	90.5
$F_4\hat{B}_1F_5$/deg	120.0	120.0	118.8

Table 6.1.2 Interaction energy and basis set superposition error of the boron trifluoride-carbon monoxide complex calculated at the HF, MP2 and DFT levels of theory using the 6-31G(d, p) basis set.

	Level of theory		
Energy/kJ mol^{-1}	HF/6-31G(d, p)	MP2/6-31G(d, p)	DFT/6-31G(d, p)
$\Delta E_{(uncorrected)}$	-6.96	-12.78	-7.18
BSSE	2.84	10.07	4.61
$\Delta E_{(corrected)}$	-4.12	-2.71	-2.57

6.1.3 The vibrational wavenumbers and band intensities

The HF, MP2 and DFT harmonic vibrational analyses for the boron trifluoride-carbon monoxide complex, together with the approximate description of the normal modes and the experimental wavenumbers are given Table 6.1.3. The computed intensities of the BF_3.CO complex are also shown in Table 6.1.4. The intermolecular intensities are all predicted to be below 20 km mol^{-1}, in a region which is not readily accessible to the most commercial infrared spectrometers. The ratios of the calculated to the experimental wavenumbers of the intramolecular modes of the complex are shown in Table 6.1.5. This table shows that the HF, MP2 and DFT levels of computation overestimate the experimental wavenumber by ca. 9, 1 and 2% on average, respectively. Since the results of the MP2 approach are close to the experimental ones, then we are going to focus our predictions upon the MP2 method. Comparison of the complex wavenumbers with those of the isolated monomers is given in Table 6.1.6. This table shows that the wavenumber shifts of the modes of the boron trifluoride fragment on complexation are small (except perhaps for the counterpart of the out-of-plane BF_3 bending mode) and are all red shifted with the exception of the ν_1 mode of the complex which is blue shifted. On the other hand, the carbon monoxide stretching mode is predicted to be shifted to the blue by 1 cm^{-1}. Thus, observation of the spectrum of the complex in the CO stretching region should yield an unambiguous assignment of the most probable structure of the complex formed between boron trifluoride and carbon monoxide.

A comparison of the band intensities of the modes of the complex with those of the parent monomer is also presented in Table 6.1.6. Here, we represent the intensity changes on complexation as intensity ratios (in contrast to the wavenumber changes, which are quoted as differences) because infrared intensities, even with the same molecular species, may span several orders of magnitude, and arithmetic differences for weak modes, which may be small in absolute terms, may represent changes by factor of perhaps 2 or 3 when expressed as ratios. Table 6.1.6 shows that no intensity ratios resulting from complexation lie outside the range of 0.91-2.44 in all the levels of computations, hence no complex mode intensities

differ from their parent monomer mode intensities by factors greater than 3, which is typical of weakly bound aggregates.

In qualitative terms, the ab initio calculation predicts that the matrix isolation infrared spectra of the BF_3.CO complex should yield two BF-stretching bands in the monomer fundamental BF-stretching region. Both vibrations will be slightly red shifted, with the symmetric BF-stretching mode being weakly observed, the antisymmetric BF-stretching vibration being of similar intensity as the monomer ν_3 bands. Two BF-bending bands should be observed at a lower wavenumber than the monomer.

Table 6.1.3 The computed and the experimental wavenumbers of the BF_3.CO complex calculated at the HF, MP2, and DFT levels of theory using the 6-31G(d, p) split-valence polarized basis set.

			Level of theory			
Symmetry Species	Mode	Approximate description	HF $\tilde{\upsilon}/cm^{-1}$	MP2 $\tilde{\upsilon}/cm^{-1}$	DFT $\tilde{\upsilon}/cm^{-1}$	[a]Experimental $\tilde{\upsilon}/cm^{-1}$
a_1	ν_1	ν(CO)	2427	2120	2202	2151
	ν_2	$\nu_s(BF_3)$	940	886	888	1434
	ν_3	$\delta_s(BF_3)$	726	686	672	678
	ν_4	ν(B...O)	80	88	74	---[b]
e	ν_5	$\nu_a(BF_3)$	1571	1494	1488	1490
	ν_6	$\delta_a(BF_3)$	508	482	479	650
	ν_7	l(CO)	72	78	68	474
	ν_8	$l(BF_3)$	28	34	31	471

[a] Ref: 130

[b] band not observed in this region

Table 6.1.4 The computed band intensities of the BF_3.CO complex calculated at the HF,MP2, and DFT levels of theory using the 6-31G(d, p) split-valence polirized basis set.

			Level of theory		
Symmetry Species	Mode	Approximate description	HF A/km mol^{-1}	MP2 A/km mol^{-1}	DFT A/km mol^{-1}
a_1	ν_1	ν(CO)	173	42	94
	ν_2	$\nu_s(BF_3)$	0.5	0.3	0.4
	ν_3	$\delta_s(BF_3)$	203	156	136
	ν_4	ν(B...O)	1	0.5	0.5
e	ν_5	$\nu_a(BF_3)$	467	393	368
	ν_6	$\delta_a(BF_3)$	16	12	10
	ν_7	l(CO)	0.1	0.1	0.03
	ν_8	$l(BF_3)$	0.3	0.05	10^{-4}

Table 6.1.5 Ratios of the computed to the experimental wavenumber observed in nitrogen matrices of the intramolecular modes of the boron trifluoride carbon monoxide complex.

	[a]Levels of theory		
Mode	HF	MP2	DFT
ν_1	1.13	0.99	1.02
ν_2	1.10	1.04	1.04
ν_3	1.04	0.98	0.96
ν_5	1.10	1.04	1.04
ν_6	1.08	1.02	1.02
Mean Average	1.09	1.01	1.02

[a]Ratio=$\tilde{\upsilon}_{calc} / \tilde{\upsilon}_{expt}$

Table 6.1.6 Comparison of the predicted wavenumbers and band intensities of the boron trifluoride-carbon monoxide complex and of those of the individual parent monomer at the HF, MP2 and DFT Levels of theory using the 6-31G (d, p) split-valence polarized basis set.

	$BF_3.CO$			BF_3			CO				
Levels of Theory	mode (symmetry species)	$\tilde{\upsilon}/cm^{-1}$	A/km mol^{-1}	mode (symmetry species)	$\tilde{\upsilon}/cm^{-1}$	A/km mol^{-1}	mode (symmetry species)	$\tilde{\upsilon}/cm^{-1}$	A/km mol^{-1}	$^{a}\Delta\tilde{\upsilon}/cm^{-1}$	$\frac{A_{complex}}{A_{monomer}}$
HF/6-31G(d, p)	$\nu_1(a_1)$	2427	173				ν(OO)	2439	138	-12	1.25
	$\nu_2(a_1)$	940	0.5	$\nu_1(a'_1)$	943	-				-3	-
	$\nu_3(a_1)$	726	203	$\nu_2(a''_2)$	738	149				-12	1.36
	$\nu_5(e)$	1571	67	$\nu_3(e')$	1575	485				-4	0.96
	$\nu_6(e)$	508	16	$\nu_4(e')$	738	16				0	1.00
MP2/6-31G(d, p)	$\nu_1(a_1)$	2120	42				ν(OO)	2119	26	1	1.62
	$\nu_2(a_1)$	886	0.3	$\nu_1(a'_1)$	889	-				-3	-
	$\nu_3(a_1)$	686	156	$\nu_2(a''_2)$	699	101				-13	1.54
	$\nu_5(e)$	1494	393	$\nu_3(e')$	1497	409				-3	0.96
	$\nu_6(e)$	482	12	$\nu_4(e')$	481	13				1	0.92
DFT/6-31G(d, p)	$\nu_1(a_1)$	2220	94				ν(OO)	2209	70	-7	1.34
	$\nu_2(a_1)$	888	0.4	$\nu_1(a'_1)$	889					-1	-
	$\nu_3(a_1)$	672	136	$\nu_2(a''_2)$	685					-13	2.43
	$\nu_5(e)$	1488	368	$\nu_3(e')$	1448					40	0.96
	$\nu_6(e)$	479	10	$\nu_4(e')$	479					0	0.91

[a] $\Delta\tilde{\upsilon} = (\tilde{\upsilon} / cm^{-1})_{complex} - (\tilde{\upsilon} / cm^{-1})_{monomer}$

6.2. The boron trifluoride-carbon dioxide molecular complex

The ab initio studies of some binary Lewis acid-base complexes of boron trifluoride with some oxygen [178,179], nitrogen [180,181], sulphur [179], fluorine [182] and carbon [130] bases has been observed that these complexes display a wide range of structural, electronic, energetic and vibrational properties. In particular, the ways in which the vibrational spectrum of the boron trifluoride is perturbed as a result of complexation with such bases may be corrected with the physical properties of the bases. Carbon dioxide is known to form molecular complexes in the gas phase, which may be of several types. The structure of $BF_3.CO_2$ in the gas phase has been reported briefly in a study of BF_3.NCCN among other complexes by Leopold *et al* [175], who concluded that the $BF_3.CO_2$ was an asymmetric rotor, consistent with a non-linear B...OCO arrangement, as suggested by a lone pair-directed interaction, according to the structural rules applying to hydrogen-bonded complexes proposed by Legon and Millen [183]. In this work we report the results of our ab initio studies on B...O bonded conformer of the 1:1 $BF_3.CO_2$ complex, using the HF, MP2 and DFT methods.

6.2.1 The optimized geometrical parameters of the $BF_3.CO_2$ complex

The ab initio calculations of the nature of the 1:1 $BF_3.CO_2$ complex indicate that the most probable structure possesses a C_s symmetry, with the OCO fragment eclipsing one of the BF bonds. This optimized structure is in good agreement with that determined using the gas phase, and is shown in fig 6.2. The normal modes of vibration of such an aggregate transform as

$\Gamma_{vib}=10a'+5a''$

under the C_s symmetry. Table 6.2.1 present the values of the converged geometrical parameters of the boron trifluoride-carbon dioxide complex of C_s symmetry structure. The carbon dioxide monomer bond length calculated at the HF, MP2 and DFT levels of theory is r(CO) equal to 114.3, 118.0 and 116.9 pm, respectively. Table 6.2.1 shows that the bond length of the carbon dioxide subunit in the molecular complex is slightly changed from the monomer value, with a factor of not more than 0.3 pm in all the levels of theory. The $O_2\hat{C}_4O_5$ bond angle of the carbon dioxide deviates from linearity

theory. The $O_2\hat{C}_4O_5$ bond angle of the carbon dioxide deviates from linearity by small amount, while the $F\hat{B}F$ bond angle of the monomer is not affected at all on complexation. The intermolecular bond length r(B...O) is 271.4, 262.3 and 272.3 for the HF, MP2 and DFT methods respectively, which is a value indicative of a weakly bound complex (van der Waals interaction).

6.2.2 The complexation energy and the BSSEs

The binding energy of the complex studied here has been determined as uncorrected and corrected interaction energies, with their association BSSEs and are shown in Table 6.2.2. After correction for the BSSE this complex is predicted to have lower association energy. The interaction found in all the three levels of computation is weakly bound.

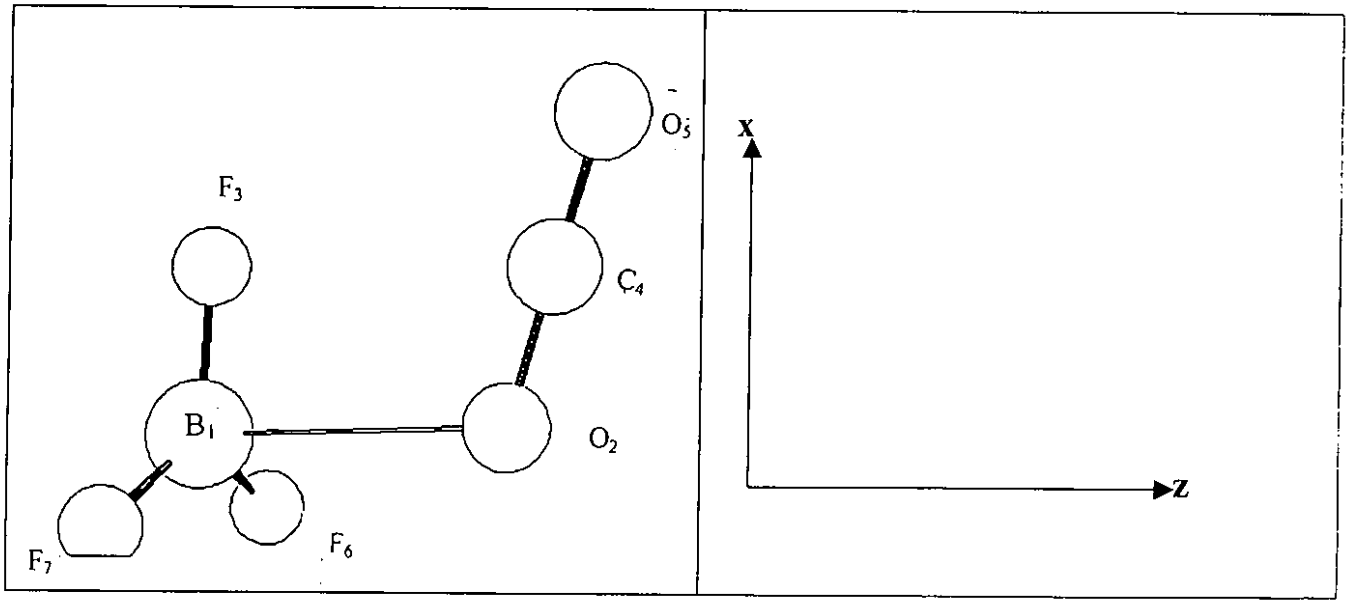

Figure 6.2. Optimized structure of the boron trifluoride-carbon dioxide complex and the numbering of the atoms.

Table 6.2.1 The optimized geometrical parameters of the $BF_3.CO_2$ complex calculated at the HF, MP2 and DFT levels of theory using the 6-31G(d, p) split-valence polarized basis set

	Levels of theory		
Parameters	HF	MP2	DFT
$r(B_1 \ldots O_2)$/pm	271.4	262.3	272.6
$r(B_1F_3)$/pm	130.5	133.0	132.3
$r(O_2 \ldots O_4)$/pm	114.6	118.3	117.2
$r(C_4O_5)$/pm	114.0	117.6	116.6
$r(B_1F_6)=r(B_1F_7)$/pm	130.1	132.3	131.7
$O_2 \ldots \hat{B}_1F_3$/deg	85.4	85.4	82.1
$O_2\hat{C}_4O_5$/deg	179.6	179.5	179.4
$O_2 \ldots \hat{B}_1F_6 = O_2 \ldots \hat{B}_1F_7$/deg	93.6	93.7	95.1
$B_1 \ldots \hat{O}_2C_4$/deg	130.8	114.3	114.0
$F_6\hat{B}_1F_7$/deg	120.0	120.0	120.0

Table 6.2.2 Interaction energy and basis set superposition error of the boron trifluoride carbon monoxide complex calculated at the HF, MP2 and DFT using the 6-31G(d, p) split-valence polarized basis set.

	Level of theory		
Energy/kJ mol^{-1}	HF	MP2	DFT
$\Delta E_{(uncorrected)}$	-9.73	-15.40	-11.30
BSSE	3.12	10.85	7.35
$\Delta E_{(corrected)}$	-6.61	-4.55	-3.95

6.2.3 The vibrational wavenumbers and the band intensities of the complex

The computed and the experimental wavenumbers of the boron trifluoride-carbon dioxide complex are listed in Table 6.2.3, along with the approximate description of the modes of vibration. The computed intensities of the boron trifluoride-carbon dioxide complex are shown in Table 6.2.4. This table shows that all the intermolecular mode intensities are very low. The ratios of the calculated to the experimental wavenumbers of intramolecular modes of the boron trifluoride-carbon dioxide observed in nitrogen matrices are presented in Table 6.2.5. This table shows that the HF and DFT methods overestimate the experimental wavenumbers by 10 and 1% on average respectively while the MP2 approach ideally fit the experimental values. Since the MP2 approach is more reliable than the other two methods, then we are going to focus our predictions on the MP2 method. The correlation between each of the modes of the molecular complex and its counterparts in the monomer are presented in Table 6.2.6, in which the monomer-complex wavenumbers shifts are reported. None of these shifts exceeds 51cm^{-1} in either direction. The antisymmetric CO_2 stretching mode of the complex (ν_1) is red shifted at this method (MP2). Both components of the degenerate bending vibration (ν_6 and ν_{12}) are red shifted. For the antsymmetric (ν_2 and ν_{11}) modes, both modes are shifted to the blue of the monomer. The bending (ν_7 and ν_{13}) modes of the BF_3 fragment are unperturbed, while for the corresponding symmetric bending mode of BF_3, the wavenumber is perturbated to substantially higher values. Nevertheless, for such fairly weakly bonded complexes such as the $BF_3.CO_2$, the theoretical computed wavenumber shifts resulting from complexation are not always found to have the same signs with those observed experimentally [130]. However, all the shifts observed are red shifted with the exception of ν_7 and ν_{13} modes of the complex.

Table 6.2.6 also shows the ratio of the intensities of the infrared active bands of the $BF_3.CO_2$ to the corresponding bands of the BF_3 and CO_2 monomers. These ratios are all around a factor of 2.0 at all the levels of theory. This table also shows that the symmetric BF_3-stretching mode (ν_1) is expected to be weakly observed at all the levels of computation.

Our calculations qualitatively predict that the spectrum of the $BF_3.CO_2$ complex should yield two BF-stretching bands, one appearing close to the monomer antisymmetric BF-stretching band and the other one will be weakly observed near the symmetric BF_3-vibration. In the same manner they should be three BF-bending vibration for the B...O bonded species; two virtually unshifted from the parent monomer bands and one noticeable red shifted; the latter band should be the most intense absorption in the spectrum.

Table 6.2.3 The computed and the experimental wavenumbers of the $BF_3.CO_2$ complex calculated at the HF, MP2, and DFT levels of theory using the 6-31G(d, p) split-valence polarized basis set.

			Levels of theory			
Symmetry Species	Mode	Approximate description	HF $\tilde{\upsilon}/cm^{-1}$	MP2 $\tilde{\upsilon}/cm^{-1}$	DFT $\tilde{\upsilon}/cm^{-1}$	[a]Experimental $\tilde{\upsilon}/cm^{-1}$
a′	ν_1	$\nu_a(CO_2)$	2587	2447	2436	2352
	ν_2	$\nu_a(BF_3)$	1561	1477	1471	1436
	ν_3	$\nu_s(CO_2)$	1587	1334	1372	1424
	ν_4	$\nu_s(BF_3)$	938	883	885	852
	ν_5	$\delta_s(BF_3)$	748	673	665	681
	ν_6	$\delta(CO_2)$	719	640	643	653
	ν_7	$\delta_a(BF_3)$	508	481	480	476
	ν_8	$l(BF_3)$	123	140	180	___[b]
	ν_9	ν(B...O)	66	78	51	___[b]
	ν_{10}	$l(BF_3)$	19	43	39	___[b]
a″	ν_{11}	$\nu_a(BF_3)$	1577	1502	1495	1454
	ν_{12}	$\gamma(BF_3)$	743	633	638	655
	ν_{13}	$\delta_a(BF_3)$	508	481	478	476
	ν_{14}	$l(BF_3)$	71	73	49	___[b]
	ν_{15}	$l(CO_2)$	17	21	19	___[b]

[a] Ref: 130, [b] band not observed in this region

Table 6.2.4 The computed band intensities of the $BF_3.CO_2$ complex calculated at the HF, MP2, and DFT levels of theory using the 6-31G(d, p) split-valence polarized basis set

			Levels of theory		
Symmetry Species	Mode	Approximate description	HF A/km mol^{-1}	MP2 A/km mol^{-1}	DFT A/km mol^{-1}
a′	ν_1	$\nu_a(CO_2)$	1069	1069	592
	ν_2	$\nu_a(BF_3)$	463	379	366
	ν_3	$\nu_s(CO_2)$	1	2	0.9

Table 6.2.4 Continued

			Levels of theory		
Symmetry Species	Mode	Approximate description	HF A/km mol^{-1}	MP2 A/km mol^{-1}	DFT A/km mol^{-1}
	ν_4	$\nu_s(BF_3)$	1	0.7	0.5
	ν_5	$\delta_s(BF_3)$	67	171	138
	ν_6	$\delta(CO_2)$	225	30	38
	ν_7	$\delta_a(BF_3)$	15	12	10
	ν_8	$l(BF_3)$	0.4	0.8	0.3
	ν_9	ν(B...O)	0.6	0.9	0.4
	ν_{10}	$l(BF_3)$	0.1	0.3	0.7
a"	ν_{11}	$\nu_a(BF_3)$	467	391	367
	ν_{12}	$\gamma(BF_3)$	66	24	29
	ν_{13}	$\delta_a(BF_3)$	15	11	10
	ν_{14}	$l(BF_3)$	0.02	0.1	0.001
	ν_{15}	$l(CO_2)$	0.0002	$2x10^{-3}$	0.0

Table 6.2.5 Ratios of the computed to the experimental wavenumber of the intramolecular modes of the boron trifluoride carbon dioxide complex observed in nitrogen matrices.

	[a]Levels of theory		
Mode	HF	MP2	DFT
ν_1	1.10	1.04	1.04
ν_2	1.09	1.02	1.02
ν_3	1.11	0.94	0.96
ν_4	1.10	1.04	1.04
ν_5	1.10	0.99	0.98
ν_6	1.10	0.98	0.98
ν_7	1.07	1.01	1.01
ν_{11}	1.08	1.03	1.03
ν_{12}	1.13	0.97	0.97
ν_{13}	1.07	1.01	1.00
Mean Average	1.10	1.00	1.01

[a]Ratio=$\tilde{\upsilon}_{calc} / \tilde{\upsilon}_{expt}$

Table 6.1.6 Comparison of the predicted wavenumbers and the band intensities of the boron trifluoride-carbon dioxide complex and of those of the individual parent monomer at the HF, MP2 and DFT Levels of theory using the 6-31G (d, p) split-valence polarized basis set.

	$BF_3.CO_2$			BF_3			CO_2				
Levels of Theory	mode (symmetry species)	$\tilde{\upsilon}\,/cm^{-1}$	A/km mol^{-1}	mode (symmetry species)	$\tilde{\upsilon}\,/cm^{-1}$	A/km mol^{-1}	mode (symmetry species)	$\tilde{\upsilon}\,/cm^{-1}$	A/km mol^{-1}	$^{a}\Delta\tilde{\upsilon}\,/cm^{-1}$	$\frac{A_{complex}}{A_{monomer}}$
HF/6-31G(d, p)	$\nu_1(a')$	2587	1069				$\nu_3(\Sigma u)$	2585	985	2	1.09
	$\nu_2(a')$	1561	463	$\nu_3(e')$	1575	485				-14	0.95
	$\nu_3(a')$	1519	1				$\nu_1(\Sigma g)$	1519	0	0	-
	$\nu_4(a')$	938	1	$\nu_1(a'_1)$	943	0				-5	-
	$\nu_5(a')$	748	67	$\nu_2(a''_2)$	699	149				49	0.45
	$\nu_6(a')$	719	225				$\nu_2(\Pi u)$	746	69	-25	3.26
	$\nu_7(a')$	508	15	$\nu_4(e')$	508	16				0	0.94
	$\nu_{11}(a'')$	1577	467	$\nu_3(e')$	1575	485				2	0.96
	$\nu_{12}(a'')$	743	66				$\nu_2(\Pi u)$	746	69	-3	0.96
	$\nu_{13}(a'')$	508	15	$\nu_4(e')$	738	16				0	0.94
MP2/6-31G(d, p)	$\nu_1(a')$	2447	1069				$\nu_3(\Sigma u)$	2455	453	-8	2.36
	$\nu_2(a')$	1447	379	$\nu_3(e')$	1528	409				-51	0.93
	$\nu_3(a')$	1334	2				$\nu_1(\Sigma g)$	1337	0	-7	-
	$\nu_4(a')$	883	1	$\nu_1(a'_1)$	889	0				-6	-
	$\nu_5(a')$	673	171	$\nu_2(a''_2)$	699	101				-26	1.69

Table 6.1.6 Comparison of the predicted wavenumbers and the band intensities of the boron trifluoride-carbon dioxide complex and of those of the individual parent monomer at the HF, MP2 and DFT Levels of theory using the 6-31G (d, p) split-valence polarized basis set.

	$BF_3.CO_2$			BF_3			CO_2				
Levels of Theory	mode (symmetry species)	$\tilde{\upsilon}/cm^{-1}$	A/km mol^{-1}	mode (symmetry species)	$\tilde{\upsilon}/cm^{-1}$	A/km mol^{-1}	mode (symmetry species)	$\tilde{\upsilon}/cm^{-1}$	A/km mol^{-1}	$^{a}\Delta\tilde{\upsilon}/cm^{-1}$	$\frac{A_{complex}}{A_{monomer}}$
HF/6-31G(d, p)	$\nu_1(a')$	2587	1069				$\nu_3(\Sigma u)$	2585	985	2	1.09
	$\nu_2(a')$	1561	463	$\nu_3(e')$	1575	485				-14	0.95
	$\nu_3(a')$	1519	1				$\nu_1(\Sigma g)$	1519	0	0	-
	$\nu_4(a')$	938	1	$\nu_1(a'_1)$	943	0				-5	-
	$\nu_5(a')$	748	67	$\nu_2(a''_2)$	699	149				49	0.45
	$\nu_6(a')$	719	225				$\nu_2(\Pi u)$	746	69	-25	3.26
	$\nu_7(a')$	508	15	$\nu_4(e')$	508	16				0	0.94
	$\nu_{11}(a'')$	1577	467	$\nu_3(e')$	1575	485				2	0.96
	$\nu_{12}(a'')$	743	66				$\nu_2(\Pi u)$	746	69	-3	0.96
	$\nu_{13}(a'')$	508	15	$\nu_4(e')$	738	16				0	0.94
MP2/6-31G(d, p)	$\nu_1(a')$	2447	1069				$\nu_3(\Sigma u)$	2455	453	-8	2.36
	$\nu_2(a')$	1447	379	$\nu_3(e')$	1528	409				-51	0.93
	$\nu_3(a')$	1334	2				$\nu_1(\Sigma g)$	1337	0	-7	-
	$\nu_4(a')$	883	1	$\nu_1(a'_1)$	889	0				-6	-
	$\nu_5(a')$	673	171	$\nu_2(a''_2)$	699	101				-26	1.69

Table 6.1.6 continue

	$\nu_6(a')$	640	30				$\nu_2(\Pi u)$	642	26	-2	1.15
	$\nu_7(a')$	481	12	$\nu_4(e')$	481	13				0	0.92
	$\nu_{11}(a'')$	1502	391	$\nu_3(e')$	1528	409				-26	0.96
	$\nu_{12}(a'')$	633	24				$\nu_2(\Pi u)$	642	26	-9	0.92
	$\nu_{13}(a'')$	481	11	$\nu_4(e')$	481	13				0	0.85
DFT/6-31G(d, p)	$\nu_1(a')$	2436	592				$\nu_3(\Sigma u)$	2448	576	-12	1.03
	$\nu_2(a')$	1471	366	$\nu_3(e')$	1448	382				23	0.96
	$\nu_3(a')$	1372	1				$\nu_1(\Sigma g)$	1336	0	36	-
	$\nu_4(a')$	885	1	$\nu_1(a'_1)$	889	0				-4	-
	$\nu_5(a')$	665	138	$\nu_2(a''_2)$	685	56				-20	2.49
	$\nu_6(a')$	643	38				$\nu_2(\Pi u)$	633	30	10	1.27
	$\nu_7(a')$	480	10	$\nu_4(e')$	479	11				1	0.91
	$\nu_{11}(a'')$	1495	367	$\nu_3(e')$	1448	382				47	1.04
	$\nu_{12}(a'')$	638	29				$\nu_2(\Pi u)$	633	30	5	0.97
	$\nu_{13}(a'')$	478	10	$\nu_4(e')$	479	11				-1	0.91

[a] $\Delta\tilde{\upsilon} = (\tilde{\upsilon}/cm^{-1})_{complex} - (\tilde{\upsilon}/cm^{-1})_{monomer}$

6.3 The boron trrifluoride-water complex

Understanding the nature of interaction between electron donors and acceptors forming complexes has been a subject of considerable interest [184-188]. Addition compounds formed by BF_3 with electron donors such as H_2O[178, 189] have been observed in the gas phase by the combined use of electron energy-loss spectroscopy (E.E.L.S) and u.v. photoelectron spectroscopy (U.P.S.) and the structures and molecular-orbital energies have been determined by means of ab initio molecular-orbital calculations[130, 178, 189]. In another recent investigation by Evans *et al.* [178] characterized the $BF_3.H_2O$ complex through its matrix-isolation infrared spectrum. They confirmed the assignment of their bands by a series of ab initio molecular-orbital calculations of the infrared spectrum of this complex using the 4-31G-basis set. In this study we present the theoretical investigation of the structure of the $BF_3.H_2O$ hetero-dimer by the use of ab initio MO calculations at the Hartree-Fock, second order Møller Plasset and Density Functional Theory methods, using the 6-31G(d, p) split-valence polarized basis set. [190]

6.3.1 Optimized geometrical parameters of the boron trifluoride-water complex

Table 6.3.1 presents the value of the geometrical parameters of the boron trifluoride-water complex of the C_s symmetry structure. Figure 6.3 shows the structure of the $BF_3.H_2O$ complex. The boron trifluoride monomer bond length calculated at the HF, MP2 and DFT methods is r(BF) equal to 130.1, 132.2 and 131.8 pm respectively. Table 6.3.1 shows that the BF bond length of the boron trifluoride subunit in the complex is significantly changed from the monomer value on complexation in all the three levels of computation. The water monomer calculated at the HF, MP2 and DFT method is r(OH) equal to 94.0, 96.1 and 96.5 pm respectively. It is also observed that the OH bond length of the H_2O is not significantly changed from the monomer value, while the *HÔH* bond angle undergoes small changes in the complex at all the levels of computation. The intermolecular bond length $r(B_1...O_2)$, is 193.4, 180.3 and 184.2 pm for the HF, MP2 and DFT methods, respectively.

6.3.2 The energies of the boron trifluoride-water complex

The interaction energy of the complex was determined from the energy of the adduct and of the separate monomer units, and was corrected for the basis set superposition error (BSSE) by the full counterpoise method [77]. The interaction energy of the complex as uncorrected and corrected interaction energy with the associated BSSEs is shown in Table 6.3.2. It should be noted that the BSSE account for more than half of the binding energy at the HF approach; similarly, at both the MP2 and DFT method the BSSE contribute 60% and 62% of the binding energy respectively.

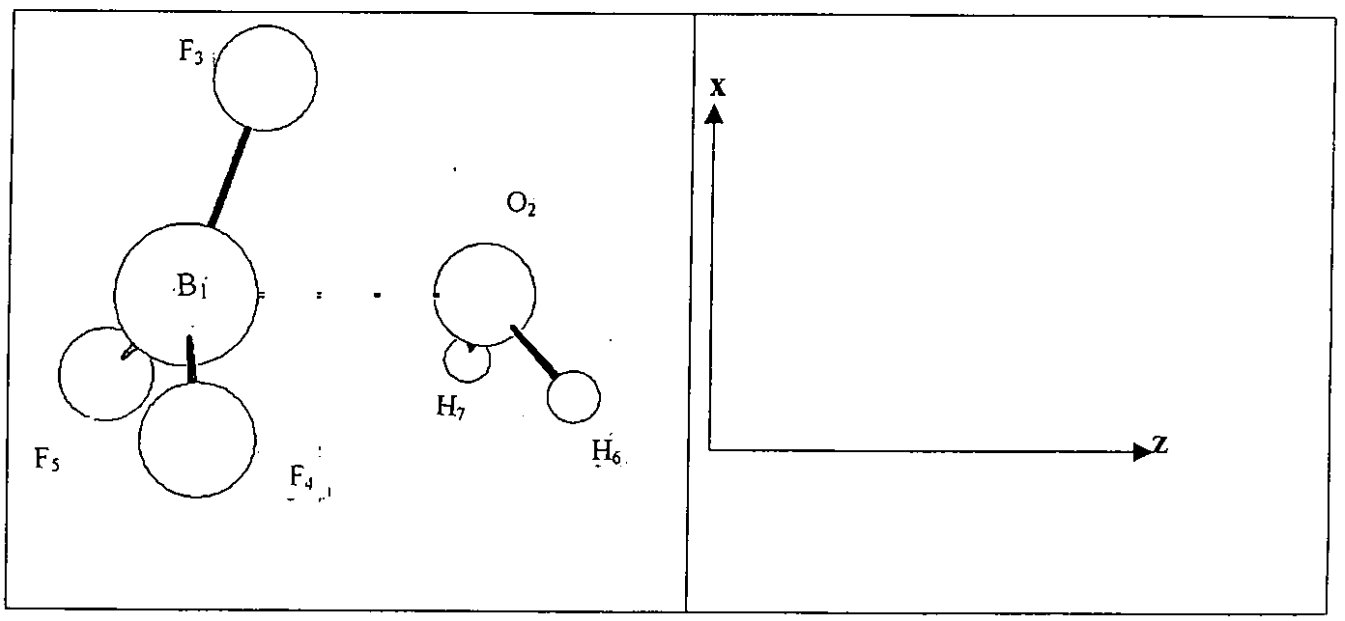

Figure 6.3 shows the opimized structure of the $BF_3...H_2O$ complex together with the numbering of atoms and the orientation of the axis.

Table 6.3.1 The optimized geometrical parameters of the $BF_3.H_2O$ complex calculated at the HF, MP2 and DFT levels of computation using the 6-31G(d, p) split-valence polarized basis set.

	Level of theory		
Parameters	HF	MP2	DFT
$r(B_1...O_2)$/pm	193.4	180.3	184.2
$r(B_1F_3)$/pm	131.8	134.7	133.8
$r(B_1F_4)=r(B_1F_5)$/pm	132.7	136.2	135.3
$r(O_2H_6)=r(OH_7)$/pm	94.6	96.8	96.9
$F_3\hat{B}_1...O_2$ /deg	100.2	102.6	102.3
$O_2...\hat{B}_1F_4 = O_2...\hat{B}_1F_5$ /deg	97.2	98.9	98.4
$F_3\hat{B}_1F_5 = F_3\hat{B}_1F_4$ /deg	118.1	117.2	117.5
$F_4\hat{B}_1F_5$ /deg	117.8	116.5	116.7
$B_1\hat{O}_2H_7 = B_1\hat{O}_2H_6$ / deg	111.9	105.9	105.0
$H_4\hat{O}_2H_5$ /deg	108.4	106.7	106.8

Table 6.3.2 Interaction energies and basis set superposition error of the boron trifluoride-water complex calculated at the HF, MP2 and DFT levels of theory using the 6-31G(d, p) basis set.

	Level of theory		
Energy/kJ mol^{-1}	HF	MP2	DFT
$\Delta E_{(uncorrected)}$	-37.32	-39.93	-38.12
BSSE	19.71	24.03	23.68
$\Delta E_{(corrected)}$	-15.91	-15.90	-14.42

6.3.3 The wavenumbers and the band intensities of the complex

Table 6.3.3 shows the computed and the experimental wavenumbers together with the approximate description of the normal modes of the complex. The computed band intensities of the $BF_3.H_2O$ complex calculated at the HF, MP2 and DFT methods are shown in Table 6.3.4. This table shows that the intermolecular intensities are all low. The ratio of the computed to the experimental wavenumber of the intramolecular modes of the boron trifluoride-water complex observed in nitrogen matrices are shown in Table 6.3.5. This table shows that the HF, MP2 and DFT methods overestimate the experimental wavenumbers by ca. 11, 9 and 6 % on average respectively. Since the results of the DFT approach are close to the experimental ones, we are going to focus our predictions upon the DFT method.

Table 6.3.6 shows the wavenumbers of the selected band of the complex and of those of the individual monomer bands from which they were derived. Correlation in the case of the H_2O moiety is straightforward, since local C_{2v} symmetry is unchanged on complexation. The BF_3 fragment in the complex, however, has C_s symmetry. The correlation of its normal modes with those of the D_{3h} monomer may be made through a hypothetical planar C_{2v} monomer. Table 6.3.6 shows that, while the modes of the H_2O sub-unit in the complex show small wavenumber increases from 19 to 37 cm^{-1} on either direction relative to the monomer, those of the BF_3 fragment shows much larger wavenumber shifts, and mostly in the opposite direction. The perturbation of the BF_3 group by the H_2O fragment is quite significant, however, as the calculated red shifts for ν_3, ν_4, ν_5, ν_6 and ν_{11} shows. The shifts for ν_{12} and ν_{13} are much smaller, indicating a closer corresponding monomer vibration. The predictions made on the basis of the theory of Friedrich and Person [78] concerning the shifts of the BF_3 stretching wavenumbers, which hold for the experimental results, is also borne out by the calculation wavenumbers. The symmetric stretching mode of the BF_3 monomer correlate with the ν_4 mode of the complex and suffer a small red shift compared with the gas phase [191]. The ν_{13} mode of the complex correlates with the monomer ν_4 and a small shift is observed to the blue ($5cm^{-1}$).

The calculated intensities are less useful than the wavenumbers for comparison purposes, since no experimental intensities are available. Moreover, the precision with which the intensities may be calculated is intrinsically lower, typically within a factor of two of the experimental values [70]. The main features of the complex intensities collected in Table 6.3.6, compared with those of the water monomer, are the reversal of the relative intensities of bending and antisymmetric stretching modes and the enormous enhancement of the symmetric stretching mode intensity. The infrared-inactive symmetric stretching mode acquires considerable intensity as it becomes the complex ν_4 mode, as a result of the distortion from planarity. Both the ν_7 and ν_{10} modes undergo intensity increases on complexation, while the enhancement factor for ν_4 mode of the complex is indeterminate since the corresponding mode in the monomer, ν_1, is infrared inactive. Hence, Friedrich and Person predict increases in the BF-stretching band intensities on complex formation, the increase being in proportion to the extent of interaction [78]. These calculated intensity data, along with those on the wavenumber shifts, are entirely consistent with the formation of a weak $BF_3...H_2O$ charge transfer complex, and provide valuable corroborative information for the experimental results.

Our calculations qualitatively predicted that the spectrum of the $BF_3.H_2O$ complex should yield three BF-stretching bands, two appearing close to the monomer antisymmetric BF-stretching band and the other one will be weakly observed near the symmetric BF_3-vibration. In the same manner they should be four BF-bending vibration for the B...O bonded species.

Table 6.3.3 The computed and the experimental wavenumbers of the $BF_3.H_2O$ complex calculated at the HF, MP2, and DFT levels of theory using the 6-31G(d, p) split-valence polarized basis set.

			Levels of theory			
Symmetry Species	Mode	Approximate description	HF $\tilde{\upsilon}/cm^{-1}$	MP2 $\tilde{\upsilon}/cm^{-1}$	DFT $\tilde{\upsilon}/cm^{-1}$	[a]Experimental $\tilde{\upsilon}/cm^{-1}$
a'	ν_1	$\nu_s(OH_2)$	4118	3821	3763	3590
	ν_2	$\delta(OH_2)$	1755	1656	1629	1725
	ν_3	$\nu(BF)$	1489	1396	1396	1225
	ν_4	$\nu_s(BF_3)$	907	856	854	863
	ν_5	$\delta_a(BF_3)$	635	657	632	625
	ν_6	$\omega(OH_2)$	522	614	597	460
	ν_7	$\gamma(FBO)$	460	482	456	385
	ν_8	R_y	251	462	254	___[b]
	ν_9	T_y	88	273	234	___[b]
a"	ν_{10}	$\nu_a(OH_2)$	4234	3950	3873	3660
	ν_{11}	$\nu_a(BF_2)$	1475	1359	1353	1240
	ν_{12}	$r(OH_2)$	668	735	687	818
	ν_{13}	R_z	485	460	455	___[b]
	ν_{14}	T	244	267	246	___[b]
	ν_{15}	T_z	66	113	121	___[b]

[a]Ref: 130, [b] band not observed in this region

Table 6.3.4 The computed band intensities of the BF_3. H_2O calculated at the HF, MP2, and DFT levels of theory using the 6-31G(d, p) split-valence polarized basis set.

			Level of theory		
Symmetry Species	Mode	Approximate description	HF A/km mol^{-1}	MP2 A/km mol^{-1}	DFT A/km mol^{-1}
a'	ν_1	$\nu_s(OH_2)$	78	63	47
	ν_2	$\delta(OH_2)$	126	99	89
	ν_3	$\nu(BF)$	483	407	383

Table 6.3.4 continue

			Level of theory		
Symmetry Species	Mode	Approximate description	HF A/km mol^{-1}	MP2 A/km mol^{-1}	DFT A/km mol^{-1}
	ν_4	$\nu_s(BF_3)$	53	366	76
	ν_5	$\delta_a(BF_3)$	223	97	33
	ν_6	$\omega(OH_2)$	236	125	438
	ν_7	τ(FBO)	156	383	48
	ν_8	R_y	22	37	16
	ν_9	T_y	79	71	64
a″	ν_{10}	$\nu_a(OH_2)$	174	151	126
	ν_{11}	$\nu_a(BF_2)$	453	366	343
	ν_{12}	$r(OH_2)$	12	0	0.05
	ν_{13}	R_z	5	8	6
	ν_{14}	γ	8	4	2
	ν_{15}	T_z	58	70	68

Table 6.3.5 Ratios of the computed to the experimental wavenumbers observed in nitrogen matrices of the intramolecular modes of the boron trifluoride water complex.

	[a]Levels of theory		
Mode	HF	MP2	DFT
ν_1	1.12	1.06	1.05
ν_2	1.10	0.96	0.94
ν_3	1.05	1.13	1.14
ν_4	1.15	0.99	0.99
ν_5	1.14	1.05	1.01
ν_6	1.13	1.33	1.29
ν_7	1.16	1.25	1.18
ν_{10}	1.11	1.08	1.06
ν_{11}	1.10	1.10	1.09
ν_{12}	1.13	0.90	0.83
Mean Average	1.11	1.09	1.06

[a]Ratio=$\tilde{\upsilon}_{calc} / \tilde{\upsilon}_{expt}$

Table 6.3.6 Comparison of the predicted wavenumbers and intensities of the Boron trifluoride-water Complex and of those of the individual parent monomer at the HF, MP2 and DFT Levels of theory using the 6-31G (d, p) split-valence polarized basis set.

	$BF_3.H_2O$			BF_3			H_2O				
Levels of Theory	mode (symmetry species)	$\tilde{\upsilon}/cm^{-1}$	A/km mol^{-1}	mode (symmetry species)	$\tilde{\upsilon}/cm^{-1}$	A/km mol^{-1}	mode (symmetry species)	$\tilde{\upsilon}/cm^{-1}$	A/km mol^{-1}	[a]$\Delta\tilde{\upsilon}/cm^{-1}$	$\frac{A_{compex}}{A_{monomer}}$
HF/6-31G(d, p)	$\nu_1(a')$	4118	78				$\nu_1(a')$	4102	94	16	0.83
	$\nu_2(a')$	1755	126				$\nu_2(a_1)$	1753	73	2	1.73
	$\nu_3(a')$	1489	483	$\nu_3(e')$	1575	485				-86	1.00
	$\nu_4(a')$	907	53	$\nu_1(a'_1)$	943	0				-36	-
	$\nu_5(a')$	635	223	$\nu_2(a''_2)$	738	149				-103	1.50
	$\nu_6(a')$	522	236	$\nu_4(e')$	508	16				14	1.58
	$\nu_7(a')$	460	156	$\nu_4(e')$	508	16				-48	9.75
	$\nu_{10}(a'')$	4234	174				$\nu_3(b)$	4249	15	-15	11.60
	$\nu_{11}(a'')$	1475	453	$\nu_3(e')$	1575	485				-100	0.93
	$\nu_{12}(a'')$	668	12	$\nu_2(a''_2)$	738	149				-73	0.08
	$\nu_{13}(a')$	460	5	$\nu_4(e')$	508	16				-48	9.75
MP2/6-31G(d, p)	$\nu_1(a')$	3821	63				$\nu_1(a_1)$	3892	4	-71	15.75
	$\nu_2(a')$	1656	99				$\nu_2(a_1)$	1682	78	-26	1.27
	$\nu_3(a')$	1396	407	$\nu_3(e')$	1497	409				-101	1.00
	$\nu_4(a')$	856	366	$\nu_1(a'_1)$	889	0				-33	-
	$\nu_5(a')$	657	97	$\nu_2(a''_2)$	699	101				-42	1.50

[a] $\Delta\tilde{\upsilon} = (\tilde{\upsilon}/cm^{-1})_{complex} - (\tilde{\upsilon}/cm^{-1})_{monomer}$

Table 6.3.6 Continue

Levels of Theory	$BF_3.H_2O$ mode (symmetry species)	$\tilde{\upsilon}/cm^{-1}$	A/km mol^{-1}	BF_3 mode (symmetry species)	$\tilde{\upsilon}/cm^{-1}$	A/km mol^{-1}	H_2O mode (symmetry species)	$\tilde{\upsilon}/cm^{-1}$	A/km mol^{-1}	$^{a}\Delta\tilde{\upsilon}/cm^{-1}$	$\frac{A_{compex}}{A_{monomer}}$
	$\nu_6(a')$	614	125	$\nu_4(e')$	481	13				133	1.58
	$\nu_7(a')$	460	156	$\nu_4(e')$	481	13				1	9.75
	$\nu_{10}(a'')$	4234	174				$\nu_3(b)$	4030	34	-80	11.60
	$\nu_{11}(a'')$	1475	453	$\nu_3(e')$	1197	409				-138	0.93
	$\nu_{12}(a'')$	735	12	$\nu_2(a''_2)$	699	101				36	0.08
	$\nu_{13}(a')$	460	5	$\nu_4(e')$	485	13				-25	9.75
DFT/6-31G(d, p)	$\nu_1(a')$	3763	63				$\nu_1(a_1)$	3786	2	-23	15.75
	$\nu_2(a')$	1629	99				$\nu_2(a_1)$	1666	48	-37	1.27
	$\nu_3(a')$	1396	407	$\nu_3(e')$	1448	382				-52	1.00
	$\nu_4(a')$	854	366	$\nu_1(a'_1)$	889	0				-35	-
	$\nu_5(a')$	632	97	$\nu_2(a''_2)$	685	56				-53	1.50
	$\nu_6(a')$	657	125	$\nu_4(e')$	480	11				117	1.58
	$\nu_7(a')$	460	156	$\nu_4(e')$	480	11				-23	9.75
	$\nu_{10}(a'')$	3893	174				$\nu_3(b)$	3912	20	-19	11.60
	$\nu_{11}(a'')$	1353	453	$\nu_3(e')$	1448	382				-95	0.93
	$\nu_{12}(a'')$	687	12	$\nu_2(a''_2)$	685	56				2	0.08
	$\nu_{13}(a'')$	485	5	$\nu_4(e')$	480	11				5	9.75

6.4. The Boron trifluoride-nitrous oxide complex

The complex formed in the gas phase between boron trifluoride and nitrous oxide has been observed experimentally by Leopold *et al.*,[175] by means of rotational spectroscopy using the molecular beam electric resonance technique[175]. The authors deduced that the structure of the $BF_3.N_2O$ complex, like that of the analogous $BF_3.CO_2$ adduct, is an asymmetric rotor. A matrix isolation fourier transform infrared spectroscopic study of the $BF_3.CO_2$ complex in nitrogen and argon matrices has been recorded [192], our results confirmed the finding of Leopold *et al.* [175] that the structure of this species was indeed non-axial. In this work we focus our investigation on the O-bonded structure of the $BF_3.N_2O$ complex using the three different methods, that is HF, MP2 and DFT levels of computation. The experimental wavenumbers values used in this case were observed in nitrogen matrices.

6.4.1 Optimized geometrical parameters of the boron trifluoride-nitrous oxide complex

Fig 6.4 shows the true global minimum structure of the $BF_3.N_2O$ since there was no negative eigenvalue observed in all the levels of theory, and this structure possesses C_s symmetry. The Oxygen atom is bonded to the boron, with the ONN molecule eclipsing the BF bond lying in the symmetry plane (see fig 6.4). Table 4.1 (see chapter 4, page 22) shows the computed geometrical parameters of the nitrous oxide monomer. The nitrous oxide bond length calculated at the HF, MP2 and DFT level of theory is r (ON) equal to 117.8, 119.3 and 119.2 pm respectively. Table 6.4.1 shows that the bond length of the nitrous oxide in the subunit in the molecular complex is slightly changed from the monomer value in all the levels of theory. The nitrous oxide bond length calculated at the HF, MP2 and DFT method is r(NN) equal to 109.2, 117.2 and 113.4 pm respectively, when compared with the bond length of the nitrous oxide in the subunit in the complex is also slightly changed from the monomer value in all the levels of theory. Table 6.4.1 shows that $\hat{NNO}$ bond angle of the boron trifluoride subunits in the molecular complex is completely unchanged from the monomer value at all the levels of theory. The intermolecular bond length r (B...O), is 263.8, 261.9 and 267.4 pm for the HF, MP2 and DFT levels of theory, respectively, and this high value implies a weak interactions (van der Waals interaction).

6.4.2 The complexation energy and the BSSE

The energy for the $BF_3.N_2O$ complex of C_s symmetry before and after correction for BSSE by the full counterpoise method [77] is shown in Table 6.4.2. This table shows that the BSSE accounts for about two thirds of the binding energy, while both the MP2 and DFT method accounts 77 and 71% of the binding energy respectively.

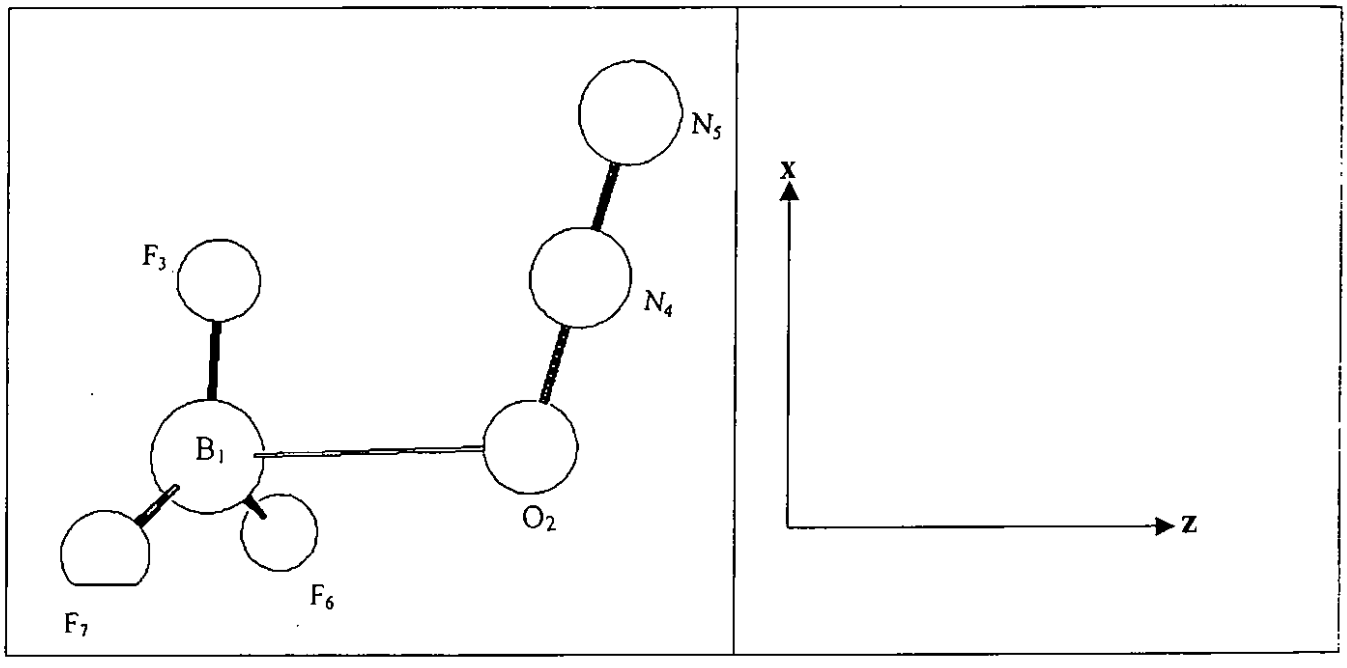

Figure 6.4 shows the optimized structure of the boron trifluoide-nitrous oxide complex together with the numbering of the atoms and the orientation of the axis.

Table 6.4.1 The optimized geometrical parameters of the $BF_3.N_2O$ complex calculated at the HF, MP2 and DFT levels of theory using the 6-31G(d, p) split-valence polarized basis set

	Levels of theory		
Parameters	HF	MP2	DFT
r(B...O)/pm	263.8	261.9	267.4
$r(BF_3)$/pm	130.7	132.9	131.3
$r(BF_6)$=$r(BF_7)$/pm	130.1	132.3	131.7
$r(N_4N_5)$/pm	108.9	116.9	113.2
$r(ON_4)$/pm	118.9	119.7	119.7
$F_3\hat{B}...O_2$/deg	85.2	85.4	83.6
$O...\hat{B}F_6 = O...\hat{B}F_7$ /deg	119.7	93.7	94.6
$F_6\hat{B}F_7$/deg	120.4	120.4	120.3
$B...\hat{O}N_5$/deg	114.6	108.7	110.0
$N_4\hat{N}_5O$/deg	180.0	180.0	180.0

Table 6.4.2 Interaction energy and basis set superposition error of the boron trifluoride-nitrous oxide complex calculated at the HF, MP2 and DFT using the 6-31G(d, p) spit-valence polarized basis set.

	Levels of theory		
Energy/kJ mol^{-1}	HF	MP2	DFT
$\Delta E_{(uncorrected)}$	-12.4	-14.73	-14.42
BSSE	4.7	11.34	10.26
$\Delta E_{(corrected)}$	-7.3	-3.49	-4.16

Table 4.6 and 4.7 (see chapter 4, page 27) lists the computed wavenumbers together with the experimental wavenumbers and infrared band intensities of the BF_3 and N_2O monomers. Table 6.4.3 shows the calculated and the experimental wavenumbers of the eclipsed $BF_3.N_2O$ molecular complex, along with the approximate descriptions of the normal modes, based on the correlation of the vibrations of the complex with those of the parent monomer. The intermolecular modes are described as the stretching of the B...O bond and the librations of the BF_3 and the N_2O units, either symmetric or antisymmetric with respect to symmetry plane, although substantial mixing of these modes occur. The normal modes of the complex structure transform as

$\Gamma_{vib}=10a'+5a''$

The intensities of the boron trifluoride-nitrous oxide complex are shown in Table 6.4.4. This table shows that the intermolecular modes are all predicted to have low intensities and to be observed in the region of the spectrum below about $30cm^{-1}$ and are in any case weak, which is an instrumentally an notoriously difficult region in which to work. The calculated/experimental wavenumber ratios are shown in Table 6.4.5. This table shows that the HF and DFT levels of computation overestimate the experimental wavenumbers by ca. 11 and 3% on average, respectively, while the MP2 approach predict the correct values. This implies that, since the results of the MP2 approachs are close to the experimental ones, therefore, we are going to base our prediction upon the MP2 method.

The wavenumbers of the complex when compared with those of the vibrations of the monomers show only modest changes on complexation, as indicated by the complex-monomer shifts reported in Table 6.4.6. Most monomer modes undergo red shifts on complexation, largest perturbations being those of the BF_3 symmetric bending of BF_3, the NN stretching modes of N_2O and one components of each of the antisymmetric stretching vibration of BF_3 at this method (MP2). The $BF_3.N_2O$ molecular complex (structure) should show 15 fundamental vibrational bands (see Table 6.4.4). The N_2O-stretching mode of the complex (ν_1) is blue shifted. The bending (ν_7 and ν_{13}) modes of the BF_3 remain unpertubed. Both the (ν_6 and ν_{12}) modes of the N_2O fragment are blue shifted by the same margin ($1cm^{-1}$).

At the MP2 method the BF_3 fragment are observed to have high values of wavenumber shifts as compared to the wavenumber shifts caused by the impact of the N_2O fragment.

The ratio of the intensities of the molecular complex are also gathered in Table 6.4.6. This table show that for the symmetric BF_3 stretching of ν_1 mode at all the levels of theory are expected to be weakly observed. The antisymmetric bending mode of BF_3 is remarkably insensitive to the complexation and the same is true for the NO-stretching vibration of N_2O. While the symmetric BF_3 bending mode and the two N_2O stretching modes increase in intensity relative to the monomer intensities, and the remaining mode of the BF_3 fragment decrease in intensity, these changes are not dramatic and, taken in conjunction with the relatively small wavenumber shifts, this emphasize that the interaction is a weak one. The NN stretching, the symmetric BF_3 bending and the antisymmetric BF_3 stretching vibration are all predicted to have high intensities, leading to the relatively high probabilities that they might be observed in the spectra in cryogenic matrix [175].

Two BF-stretching bands should be observed, one appearing close to the monomer antisymmetric BF-stretching band and the other one will be weakly observed near the symmetric BF_3-vibration. In the same manner there should be three BF-bending vibration for the B...O bonded species; two remain unshifted from the parent monomer bands and one noticeably blue shifted; the latter band should be the most intense absorption in the spectrum.

Table 6.4.3 The computed and the experimental wavenumbers of the $BF_3.N_2O$ complex calculated at the HF, MP2, and DFT using the 6-31G(d, p) split-valence polarized basis set.

			Levels of theory			
Symmetry Species	Mode	Approximate description	HF $\tilde{\upsilon}/cm^{-1}$	MP2 $\tilde{\upsilon}/cm^{-1}$	DFT $\tilde{\upsilon}/cm^{-1}$	[a]Experimental $\tilde{\upsilon}/cm^{-1}$
a	ν_1	ν(NN)	2653	2224	2377	2246
	ν_2	$\nu_a(BF_3)$	1554	1479	1472	1401
	ν_3	ν(NO)	1363	1288	1331	1284
	ν_4	$\nu_s(BF_3)$	936	883	884	865
	ν_5	$\delta_s(BF_3)$	709	671	658	651
	ν_6	δ(NNO)	686	576	600	597
	ν_7	$\delta_a(BF_3)$	508	481	480	478
	ν_8	$l(BF_3)$	152	141	135	___[b]
	ν_9	ν(B...O)	76	78	60	___[b]
	ν_{10}	l(NNO)	50	56	50	___[b]
a''	ν_{11}	$\nu_a(BF_3)$	1577	1500	1493	1436
	ν_{12}	γ(NNO)	678	566	597	600
	ν_{13}	$\delta_a(BF_3)$	507	481	478	467
	ν_{14}	$l(BF_3)$	83	70	53	___[b]
	ν_{15}	l(NNO)	22	22	22	___[b]

[a] Ref: 130, [b]band not observed in this region

Table 6.4.4 The computed band intensities of the BF_3. N_2O complex calculated at the HF, MP2, and DFT levels of theory using the 6-31G(d, p) split-valence polarized basis set.

			Levels of theory		
Symmetry Species	Mode	Approximate description	HF A/km mol^{-1}	MP2 A/km mol^{-1}	DFT A/km mol^{-1}
a'	ν_1	ν(NN)	448	298	312
	ν_2	$\nu_a(BF_3)$	449	298	352
	ν_3	ν(NO)	179	19	68

Table 6.4.4 continued

			Levels of theory		
Symmetry Species	Mode	Approximate description	HF A/km mol^{-1}	MP2 A/km mol^{-1}	DFT A/km mol^{-1}
	ν_4	$\nu_s(BF_3)$	2	0.8	1
	ν_5	$\delta_s(BF_3)$	223	175	152
	ν_6	δ(NNO)	31	6	10
	ν_7	$\delta_a(BF_3)$	15	12	10
	ν_8	$l(BF_3)$	2	0.9	0.7
	ν_9	ν(B...O)	2	0.9	0.6
	ν_{10}	l(NNO)	0.6	0.2	0.8
a"	ν_{11}	$\nu_a(BF_3)$	465	390	366
	ν_{12}	γ(NNO)	18	5	8
	ν_{13}	$\delta_a(BF_3)$	15	12	10
	ν_{14}	$l(BF_3)$	0.1	0.01	0.002
	ν_{15}	l(NNO)	0.4	0.002	0.007

Table 6.4.5 Ratios of the computed to the experimental wavenumbers observed in nitrogen matrix of the intramolecular modes of the boron trifluoride-nitrous oxide complex.

	[a]Levels of theory		
Mode	HF	MP2	DFT
ν_1	1.18	0.99	1.06
ν_2	1.11	1.06	1.05
ν_3	1.06	1.03	1.04
ν_4	1.09	1.02	1.02
ν_5	1.15	1.03	1.01
ν_6	1.06	0.96	1.01
ν_7	1.10	1.01	1.01
ν_{11}	1.13	0.94	1.04
ν_{12}	1.09	0.94	1.00
ν_{13}	1.11	1.03	1.02
Mean Average	1.11	1.00	1.03

[a]Ratio=$\tilde{\upsilon}_{calc} / \tilde{\upsilon}_{exp}$

Table 6.4.6 Comparison of the predicted wavenumbers and band intensities of the Boron trifluoride-nitrous oxide Complex and of those of the individual parent monomer at the HF, MP2 and DFT Levels of theory using the 6-31G (d, p) split-valence polarized basis set.

	$BF_3.N_2O$			BF_3			N_2O				
Levels of Theory	mode (symmetry species)	$\tilde{\upsilon}/cm^{-1}$	A/km mol^{-1}	mode (symmetry species)	$\tilde{\upsilon}/cm^{-1}$	A/km mol^{-1}	mode (symmetry species)	$\tilde{\upsilon}/cm^{-1}$	A/km mol^{-1}	$^{a}\Delta\tilde{\upsilon}/cm^{-1}$	$\frac{A_{complex}}{A_{monomer}}$
HF/6-31G(d, p)	$\nu_1(a')$	2653	448				$\nu_1(\Sigma g)$	2633	490	20	0.91
	$\nu_2(a')$	1554	449	$\nu_3(e')$	1575	485				-21	0.93
	$\nu_3(a')$	1363	179				$\nu_2(\Sigma g)$	1393	165	-30	1.08
	$\nu_4(a')$	936	2	$\nu_1(a'_1)$	943	-				-7	-
	$\nu_5(a')$	709	223	$\nu_2(a''_2)$	738	149				-29	1.50
	$\nu_6(a')$	686	31				$\nu_3(\Pi u)$	689	20	-3	1.55
	$\nu_7(a')$	508	15	$\nu_4(e')$	508	16				0	0.94
	$\nu_{11}(a'')$	1577	465	$\nu_3(e')$	1575	485				2	0.96
	$\nu_{12}(a'')$	678	18				$\nu_3(\Pi u)$	689	20	-11	0.90
	$\nu_{13}(a'')$	508	15	$\nu_4(e')$	508	16				0	0.94
MP2/6-31G(d, p)	$\nu_1(a')$	2224	298				$\nu_1(\Sigma g)$	2247	263	-23	1.13
	$\nu_2(a')$	1479	298	$\nu_3(e')$	1497	409				-18	0.73
	$\nu_3(a')$	1288	19				$\nu_2(\Sigma g)$	1289	8	-1	2.38
	$\nu_4(a')$	886	1	$\nu_1(a'_1)$	889	-				-6	-
	$\nu_5(a')$	671	175	$\nu_2(a'_2)$	699	101				-28	1.73
	$\nu_6(a')$	576	6				$\nu_3(\Pi u)$	575	5	1	1.20

Table 6.4.6 continue

$BF_3 . N_2O$				BF_3			N_2O				
Levels of Theory	mode (symmetry species)	$\tilde{\upsilon}/cm^{-1}$	A/km mol^{-1}	mode (symmetry species)	$\tilde{\upsilon}/cm^{-1}$	A/km mol^{-1}	mode (symmetry species)	$\tilde{\upsilon}/cm^{-1}$	A/km mol^{-1}	$^{a}\Delta\tilde{\upsilon}/cm^{-1}$	$\frac{A_{complex}}{A_{monomer}}$
	$\nu_7(a')$	481	12	$\nu_4(e')$	481	13				0	0.92
MP2/6-31G(d, p)	$\nu_{11}(a'')$	1500	390	$\nu_3(e')$	1497	409				3	0.95
	$\nu_{12}(a'')$	566	5				$\nu_3(\Pi u)$	575	5	1	1.00
	$\nu_{13}(a'')$	481	12	$\nu_4(e')$	481	13				0	0.92
DFT/6-31G(d, p)	$\nu_1(a')$	2377	312				$\nu_1(\Sigma g)$	2371	310	6	1.01
	$\nu_2(a')$	1472	352	$\nu_3(e')$	1448	382				24	0.92
	$\nu_3(a')$	1331	68				$\nu_2(\Sigma g)$	1344	49	-13	1.39
	$\nu_4(a')$	884	1	$\nu_1(a'_1)$	889	-				-5	-
	$\nu_5(a')$	658	152	$\nu_2(a'_2)$	685	56				-27	2.71
	$\nu_6(a')$	600	10				$\nu_3(\Pi u)$	604	9	-4	1.11
	$\nu_7(a')$	480	10	$\nu_4(e')$	479	11				1	0.91
	$\nu_{11}(a'')$	1493	366	$\nu_3(e')$	1448	352				45	0.96
	$\nu_{12}(a'')$	597	8				$\nu_3(\Pi u)$	604	9	-7	0.89
	$\nu_{13}(a'')$	478	10	$\nu_4(e')$	479	11				-1	0.91

$^{a}\Delta\tilde{\upsilon} = (\tilde{\upsilon}/cm^{-1})_{complex} - (\tilde{\upsilon}/cm^{-1})_{monomer}$

6.5. The boron trifluoride-oxygen molecular complex

A number of van der Waals complexes containing BF_3 have been studied to date [58, 167, 172, 175, 193, 194, 195-196].In each case the boron atom acts as the binding site in the acidity of boron trifluoride. The BF_3 molecule is relatively complicated in terms of classical valence structure. The elementary picture of simple sp^2 hybridization, single BF bonds, and vacant P_z orbital fails to account quantitatively for many of its properties.[172] There are a similarities between the diatomic BF and the BF bonds in BF_3. The bond lengths are 126.6pm for diatomic BF [197] and 131.0.pm for BF_3 [198]. Bonding in diatomic BF is well studied theoretically and shows considerable similarity to its isoelectronic partners, CO and N_2 in which multiple bonding is present [199] as has frequently been stated [200, 201, 202]. The current study was initiated in order to investigate the nature and strength of the bonding and structural characterization in BF_3 when the bonding partner is O_2.

6.5.1 The optimized geometrical parameters of the complex

Figure 6.5 shows the structure of the boron trifluoride-oxygen complex and this structure posses Cs symmetry, with oxygen bonded to the boron. Table 4.1 (see chapter 4, page 22) shows the computed geometrical parameters of the O_2 monomer. The O_2 monomer bond length calculated at the HF, MP2 and DFT levels of computation is r(OO) equal to 116.8, 124.7 and 121.4 pm respectively. Table 6.5.1 shows that the bond length of the oxygen in the sub-unit in the molecular complex is slightly changed from the monomer value in all the levels of computation. The $F\hat{B}F$ angle remains unchanged at all the levels in the complex. The intermolecular bond length r(B...O) is 272.5, 250.2 and 251.6 pm for the HF, MP2 and DFT methods respectively.

6.5.2 The energy of the boron trifluoride-oxygen molecular complex

The interaction energy of the $BF_3.O_2$ complex before and after correction for BSSE is shown in Table 6.5.2. The interaction found at all the three levels is weak. The BSSE account for about half of the interaction energy of the complex at the HF method, while for both the MP2 and DFT methods it accounts 61 and 60% of the interaction energy respectively.

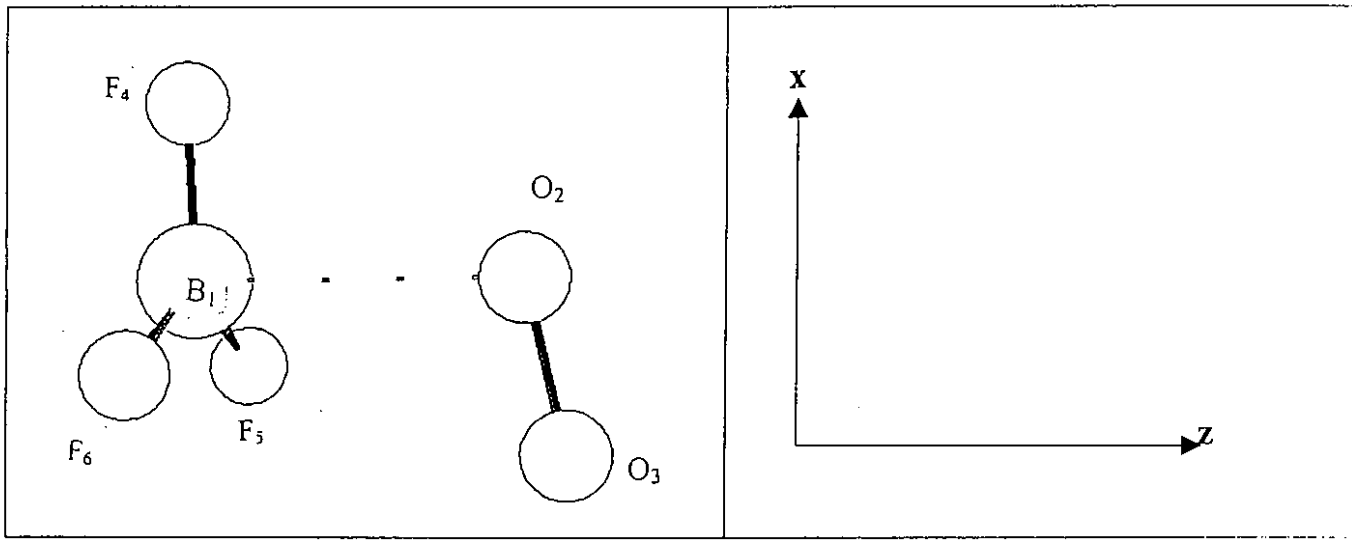

Figure 6.5 shows the optimized structure of the boron trifluoride-oxygen complex together with the numbering of the atoms and the orientation of the axis.

Table 6.5.1 The optimized geometrical parameters of the $BF_3.O_2$ complex calculated at the HF, MP2 and DFT levels of theory using the 6-31G(d, p) split-valence polarized basis set

	Levels of theory		
Parameters	HF	MP2	DFT
r(B...O_2)/pm	272.5	250.2	251.6
r(O_2O_3)/pm	116.5	127.5	121.4
r(B_1F_4)/pm	130.2	132.6	132.1
$B...\hat{O}_2O_3$ /deg	109.6	103.4	110.8
$F_4\hat{B}...O_2$ /deg	92.8	92.5	91.7
$F_5\hat{B}...O_2 = F_6\hat{B}...O_2$ /deg	89.8	91.0	91.5
$F\hat{B}F$ /deg	120.0	120.0	120.0

Table 6.5.2 Interaction energy and basis set superposition error of the boron trifluoride-oxygen complex calculated at the HF, MP2 and DFT levels of theory using the 6-31G(d, p) basis set.

	Levels of theory		
Energy/kJ mol^{-1}	HF	MP2	DFT
$\Delta E_{(uncorrected)}$	-10.93	-18.24	-13.42
BSSE	5.92	11.19	8.00
$\Delta E_{(corrected)}$	-5.01	-7.05	-5.42

6.5.3 The vibrational wavenumbers and the band intensities of the complex

The computed wavenumbers for the boron trifluoride-oxygen complex together with the approximate description of the normal modes are given in Table 6.5.3. The normal modes distribute among the symmetry species according to

$\Gamma_{vib}=8a'+4a''$

The computed intensities of the complex is shown in Table 6.5.4. This table shows that the intensities of the intermolecular modes are small at all the levels of computation. Table 6.5.5 shows that, while the modes of the O_2 sub-unit in the complex show small wavenumber increases relative to the monomer, those of the BF_3 fragment show large wavenumber shifts, and in either direction. The O_2 stretching mode of the molecular complex (ν_1) are blue shifted for both the HF and MP2 methods while the DFT method showed red shift. The antisymmetric stretching (ν_2 and ν_9) modes are blue shifted at both the HF and DFT methods, while in the MP2 is red shifted with ν_2 mode being shifted by quite a substantial amount (294 cm^{-1}). The symmetric stretching ν_3 mode showed small wavenumber shifts in the opposite direction on complexation at all the levels of computation. The symmetric BF_3 bending mode of the complex ν_4 mode is red shifted at all the levels of computation. The BF_3 antisymmetric bending mode of the complex (ν_5 and ν_{10}) showed very small wavenumber shifts in either direction, in all cases, which are not more than $2cm^{-1}$.

The ratio of the intensities of the boron trifluoride-oxygen complex to the corresponding bands of BF_3 and O_2 are presented in Table 6.5.5. This table shows that all the intensities ratios are cluttered around the value of 2.0. The relatively small intensity changes of the monomer modes on the complexation are also indicative of a very weak interaction. Table 6.5.5 shows that for the symmetric BF_3 stretching of the ν_3 mode and the O_2 stretching of ν_1 mode are expected to be weakly observed in all the levels of theory. The antisymmetric BF_3 bending vibration is predicted to have high intensities at all the levels of computation. Two bands are expected to be observed close to the BF_3 antisymmetric stretching mode of the monomer

and another two bands are expected next to the BF_3 antisymmetric bending, finally one band is expected next to the symmetric bending at all the levels of computation.

Table 6.5.3 The computed wavenumbers of the $BF_3.O_2$ molecular complex calculated at the HF, MP2, and DFT levels of theory using the 6-31G(d, p) split-valence polarized basis set

			Levels of theory		
Symmetry Species	Mode	Approximate description	HF $\tilde{\upsilon}/cm^{-1}$	MP2 $\tilde{\upsilon}/cm^{-1}$	DFT $\tilde{\upsilon}/cm^{-1}$
a′	ν_1	ν_s(OO)	1999	1486	1644
	ν_2	ν (BF)	1628	1203	1470
	ν_3	$\nu_s(BF_2)$	939	880	879
	ν_4	$\delta_s(BF_3)$	748	662	643
	ν_5	$\delta_a(BF_3)$	510	481	479
	ν_6	δ(B..OO)	132	157	166
	ν_7	r(B...O)	71	106	91
	ν_8	T_y	43	73	56
a″	ν_9	$\nu_a(BF_2)$	1622	1479	1470
	ν_{10}	δ_a (BF_3)	509	479	475
	ν_{11}	R_x	72	98	81
	ν_{12}	R_y	18	33	12

Table 6.5.4 The computed band intensities of the $BF_3.O_2$ calculated at the HF, MP2, and DFT levels of theory using the 6-31G(d, p) split-valence polarized basis set.

			Levels of theory		
Symmetry Species	Mode	Approximate description	HF A/km mol^{-1}	MP2 A/km mol^{-1}	DFT A/km mol^{-1}
a′	ν_1	ν_s(OO)	0.2	385	0.08
	ν_2	ν (BF)	451	1	370
	ν_3	$\nu_s(BF_2)$	1	2	2
	ν_4	$\delta_s(BF_3)$	199	169	170
	ν_5	$\delta_a(BF_3)$	15	11	9

Table 6.6.4 Continued

			Levels of theory		
Symmetry Species	Mode	Approximate description	HF A/km mol^{-1}	MP2 A/km mol^{-1}	DFT A/km mol^{-1}
	ν_6	δ (B..OO)	1	2	2
	ν_7	r(B...O)	0.3	1	19
	ν_8	T_y	0	0.01	0.01
a″	ν_9	$\nu_a(BF_2)$	471	398	370
	ν_{10}	$\delta_a(BF_3)$	16	12	10
	ν_{11}	R_x	0	0.02	0.01
	ν_{12}	R_y	0	0.03	0.02

Table 6.5.5 Comparison of the predicted wavenumbers and band intensities of the Boron trifluoride-oxygen Complex and of those of the individual parent monomer at the HF, MP2 and DFT Levels of theory using the 6-31G (d, p)

	$BF_3.O_2$			BF_3			O_2				
Levels of Theory	mode (symmetry species)	$\tilde{\upsilon}/cm^{-1}$	A/km mol^{-1}	mode (symmetry species)	$\tilde{\upsilon}/cm^{-1}$	A/km mol^{-1}	mode (symmetry species)	$\tilde{\upsilon}/cm^{-1}$	A/km mol^{-1}	$^{a}\Delta\tilde{\upsilon}/cm^{-1}$	$\frac{A_{complex}}{A_{monomer}}$
HF/6-31G(d, p)	$\nu_1(a')$	1999	0.2				ν(OO)	1998	-	1	-
	$\nu_2(a')$	1628	451	$\nu_3(e')$	1575	485				53	0.93
	$\nu_3(a')$	939	1	$\nu_1(a'_1)$	943	-				-4	-
	$\nu_4(a')$	748	199	$\nu_2(a''_2)$	738	149				-10	1.34
	$\nu_5(a')$	510	15	$\nu_4(e')$	508	16				2	0.94
	$\nu_9(a'')$	1622	471	$\nu_3(e')$	1575	485				47	0.97
	$\nu_{10}(a'')$	509	16	$\nu_4(e')$	508	16				1	1.00
MP2/6-31G(d, p)	$\nu_1(a')$	1486	385				ν(OO)	1409	-	77	-
	$\nu_2(a')$	1203	1	$\nu_3(e')$	1497	409				-294	0.001
	$\nu_3(a')$	880	2	$\nu_1(a'_1)$	889	-				-9	-
	$\nu_4(a')$	662	169	$\nu_2(a''_2)$	699	101				-37	1.67
	$\nu_5(a')$	481	11	$\nu_4(e')$	481	13				0	0.85
	$\nu_9(a'')$	1479	398	$\nu_3(e')$	1497	409				-18	0.97
	$\nu_{10}(a'')$	479	12	$\nu_4(e')$	481	13				-2	0.92

Table 6.5.6 continue

$BF_3.O_2$				BF_3			O_2				
Levels of Theory	mode (symmetry species)	$\tilde{\upsilon}/cm^{-1}$	A/km mol^{-1}	mode (symmetry species)	$\tilde{\upsilon}/cm^{-1}$	A/km mol^{-1}	mode (symmetry species)	$\tilde{\upsilon}/cm^{-1}$	A/km mol^{-1}	$^{a}\Delta\tilde{\upsilon}/cm^{-1}$	$\frac{A_{complex}}{A_{monomer}}$
DFT/6-31G(d, p)	$\nu_1(a')$	1644	0.1				ν(OO)	1660	-	-16	-
	$\nu_2(a')$	1470	370	$\nu_3(e')$	1448	382				22	0.97
	$\nu_3(a')$	879	2	$\nu_1(a'_1)$	889	-				-10	-
	$\nu_4(a')$	643	170	$\nu_2(a''_2)$	685	56				-42	3.04
	$\nu_5(a')$	479	9	$\nu_4(e')$	481	11				-2	0.82
	$\nu_9(a'')$	1470	370	$\nu_3(e')$	1448	382				22	0.97
	$\nu_{10}(a'')$	479	10	$\nu_4(e')$	481	11				-2	0.91

$^{a}\Delta\tilde{\upsilon} = (\tilde{\upsilon}/cm^{-1})_{complex} - (\tilde{\upsilon}/cm^{-1})_{monomer}$

6.6 The boron trifluoride-ozone molecular complex

The boron trifluoride-ozone complex has been studied far less than the other complexes reported in this work. Understanding the nature of interaction between electron donors and electron acceptors forming a complex has been a subject of considerable interest in addition compounds formed by BF_3 with the electron donor such as ozone. This complex has not been observed experimentally up to date as to compare with the other complexes and dimers studied in this work. In this work we report about the results of the 1:1 $BF_3.O_3$ complex calculated at the three different levels.

6.6.1 The optimized geometrical parameters of the boron trifluoride-ozone complex

Figure 6.6.1 shows the true global minimum structure of the boron trifluoride ozone complex and this structure possesses C_s symmetry. Table 6.6.1 present the value of the geometrical parameters of the boron trifluoride-ozone complex. The ozone monomer bond length calculated at the HF, MP2 and DFT levels of computation is r(OO) equal to 126.4, 130.0 and 126.4 pm respectively. It is observed that the r(OO) bond length of the ozone is significantly changed on complexation. The ozone monomer bond angle calculated at the HF, MP2 and DFT levels of computation is r(OOO) equal to 117.9, 116.3 and 117.9 deg respectively. The OOO bond angle is slightly changed from the monomer value. It is observed from Table 6.6.1 that the HF method tends to predict higher bond lengths and shorter bond angles as to compared with other two methods of computation.

6.6.2 The energies of the complex

The energies of the $BF_3.O_3$ complex of C_s symmetry before and after correction for BSSE by the full counterpoise method [77] are listed in Table 6.6.1. At the HF method the BSSE account for about two thirds of the interaction energy, while at both the MP2 and DFT methods the BSSEs account for about 71% and 91% of the interaction energy respectively.

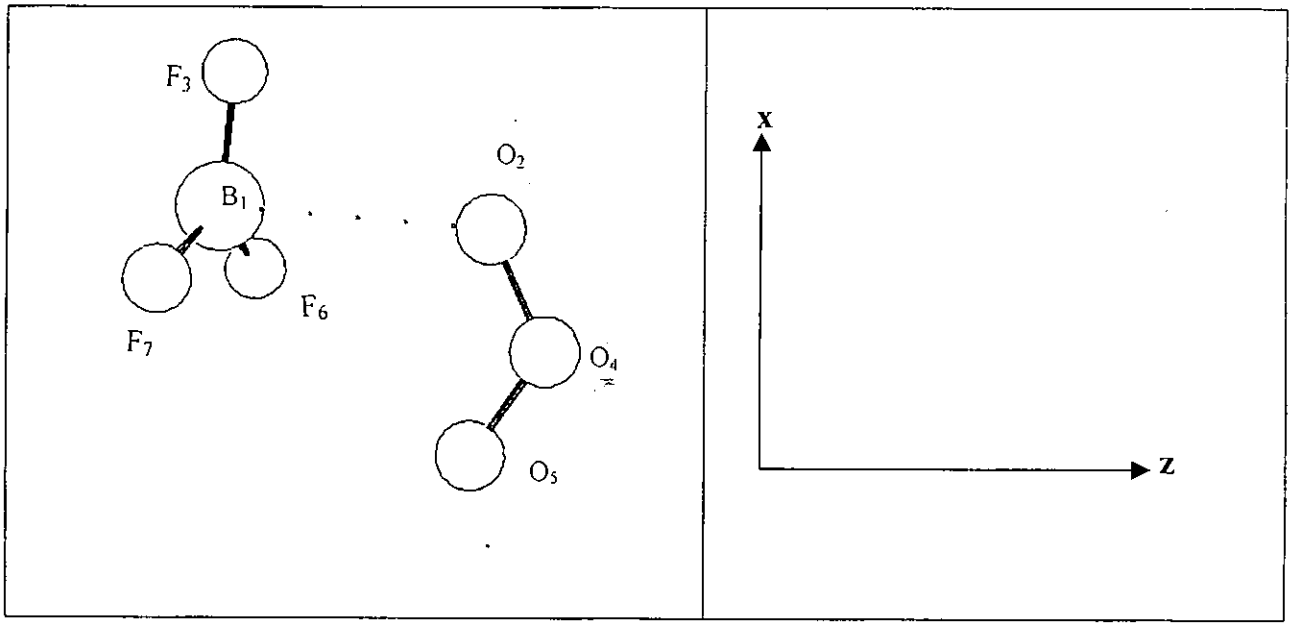

Figure 6.6 shows the optimized structure of the boron trifluoride-ozone complex together with the numbering of atoms and the orientation of the axis.

Table 6.5.1 The optimized geometrical parameters of the $BF_3.O_3$ complex calculated at the HF, MP2 and DFT levels of theory using the 6-31G(d, p) split-valence polarized basis set.

	Levels of theory		
Parameters	HF	MP2	DFT
r(B...O)/pm	271.0	259.0	251.4
$r(O_2O_4)$/pm	121.1	127.0	129.5
$r(O_4O_5)$/pm	119.7	125.0	130.6
$r(BF_4)$/pm	130.3	132.0	132.7
$B...\hat{O}_2O_4$/deg	119.4	116.3	115.8
$F_6\hat{B}...O_2 = F_7\hat{B}...O_2$/deg	92.7	93.8	93.6
$O_2\hat{O}_4O_5$/deg	119.0	118.0	116.4
$F_3\hat{B}...O_2$/deg	87.6	86.8	87.5
$F_6\hat{B}F_7$	120.0	120.0	120.0

Table 6.6.2 Interaction energy and basis set superposition error of the boron trifluoride-ozone complex calculated at the HF, MP2 and DFT using the 6-31G(d, p) split-valence polarized basis set.

	Levels of theory		
Energy/kJ mol^{-1}	HF	MP2	DFT
$\Delta E_{(uncorrected)}$	-12.00	-19.14	-16.16
BSSE	8.38	13.65	14.63
$\Delta E_{(corrected)}$	-3.62	-5.49	-4.53

6.6.3 The vibrational wavenumbers and the band intensities

The vibrational harmonic wavenumbers together with the approximate descriptions of the normal modes are shown in Table 6.6.3. Table 6.6.4 shows that the computed intensities of the intermolecular modes of the boron trifluoride-ozone complex calculated at all the three levels are negligible. The correspondence between each of the complex modes and its counterpart in the monomer are presented in Table 6.6.5, in which the monomer-complex wavenumber shifts are reported. This table indicates that all the shifts derived from the BF_3 monomer are considerably shifted on either direction. The theoretical prediction is that on complexation, the symmetric BF_3-stretching vibration mode correlating with the ν_4 mode of the complex and shifted to the opposite direction at all the levels of computation. All the complex modes correlating with bending ν_2 mode of the monomer are blue shifted. The antisymmetric BF_3 bending mode undergoes the smallest changes on complexation, splitting into a pair of bands (ν_7 and ν_{12}) shifted to the opposite direction, with the exception of ν_{12} mode of the complex at both the HF and DFT methods, which remain unperturbed. The antisymmetric BF_3-stretching vibration undergoes largest changes on complexation in either direction at all the levels of computation. All the shifts caused by the impact of the ozone monomer to the complex are red shifted with the exception of the ν_3 mode of the complex at the HF method.

The complex/monomer intensities ratios are shown in Table 6.6.5. This table shows that all the ratios are cluttered around the value of 2.0. The increases in intensity on complexation are consistent with the prediction of Friedrich and Person [78], while the modest values of the ratios testify to the weakness of the interaction as noted in Table 6.6.2.

Our calculations qualitatively predict that the spectrum of the $BF_3.O_3$ complex should yield two BF-stretching bands, two appearing close to the monomer antisymmetric BF-stretching band and the other one will be weakly observed near the symmetric BF_3-vibration. In the same manner they should be three BF-bending vibration for the B...O bonded species.

Table 6.6.3 The computed wavenumbers of the $BF_3.O_3$ complex calculated at the HF, MP2, and DFT using the 6-31G(d, p) basis set.

			Levels of theory		
Symmetry Species	Mode	Approximate description	HF $\tilde{\upsilon}/cm^{-1}$	MP2 $\tilde{\upsilon}/cm^{-1}$	DFT $\tilde{\upsilon}/cm^{-1}$
a′	ν_1	ν(BF)	1567	2404	1477
	ν_2	ν(OO)(nonbonded)	1540	1450	1276
	ν_3	ν(OO)(bonded)	1420	1169	1225
	ν_4	$\nu_s(BF_3)$	905	879	881
	ν_5	$\tau(BF_3)$	856	738	746
	ν_6	δ(OO)	929	658	647
	ν_7	$\delta_a(BF_3)$	504	479	477
	ν_8	R_x	100	117	97
	ν_9	T_z	89	111	92
	ν_{10}	R_y	59	80	65
a″	ν_{11}	$\nu a(BF_3)$	1493	1486	1480
	ν_{12}	$\delta a(BF_3)$	508	481	478
	ν_{13}	T_y	160	188	164
	ν_{14}	R_z	90	53	38
	ν_{15}	T_x	57	32	28

Table 6.6.4 The computed intensities of the BF_3. O_3 complex calculated at the HF, MP2, and DFT levels of theory using the 6-31G(d, p) split-valence polarized basis set

			Levels of theory		
Symmetry Species	Mode	Approximate description	HF A/km mol^{-1}	MP2 A/km mol^{-1}	DFT A/km mol^{-1}
a′	ν_1	ν(BF)	346	1473	337
	ν_2	ν(OO)(nobonded)	292	331	28
	ν_3	ν(OO)(bonded)	518	5	112

Table 6.6.4 Continued

			Levels of theory		
Symmetry Species	Mode	Approximate description	HF A/km mol^{-1}	MP2 A/km mol^{-1}	DFT A/km mol^{-1}
	ν_4	$\nu_s(BF_3)$	1	2	2
	ν_5	$T(BF_3)$	10	6	6
	ν_6	δ(OOO)	222	184	165
	ν_7	δ_a(B...O)	9	10	7
	ν_8	R_x	0.3	1	0.04
	ν_9	$T_z(BF_2)$	1	1	2
	ν_{10}	R_y	1	0.2	0.3
a"	ν_{11}	$\nu_a(BF_3)$	463	385	362
	ν_{12}	$\delta_a(BF_3)$	14	10	10
	ν_{13}	T_y	2	0.2	1
	ν_{14}	R_z	3	0.001	0.1
	ν_{15}	T_x	0.04	0.2	1

Table 6.6.5 Comparison of the predicted wavenumbers and intensities of the Boron trifluoride-ozone Complex and of those of the individual parent monomer at the HF, MP2 and DFT Levels of theory using the 6-31G (d, p) split-valence polarized basis set.

	$BF_3.O_3$			BF_3			O_3				
Levels of Theory	mode (symmetry species)	$\tilde{\upsilon}/cm^{-1}$	A/km mol^{-1}	mode (symmetry species)	$\tilde{\upsilon}/cm^{-1}$	A/km mol^{-1}	mode (symmetry species)	$\tilde{\upsilon}/cm^{-1}$	A/km mol^{-1}	$^{a}\Delta\tilde{\upsilon}/cm^{-1}$	$\frac{A_{complex}}{A_{monomer}}$
HF/6-31G(d, p)	$\nu_1(a')$	1567	346	$\nu_3(e')$	1575	485				-8	0.71
	$\nu_2(a')$	1546	392	$\nu_3(e')$	1575	485				-29	0.81
	$\nu_3(a')$	1420	518				$\nu_1(a)$	1256	849	164	0.61
	$\nu_4(a')$	905	1	$\nu_1(a'_1)$	943	-				-38	-
	$\nu_5(a')$	856	10				$\nu_3(b)$	849	9	7	1.11
	$\nu_6(a')$	729	222				$\nu_2(a_2)$			-54	1.49
	$\nu_7(a')$	504	9	$\nu_4(e')$	568	16				-4	0.56
	$\nu_{11}(a'')$	1493	463	$\nu_3(e')$	1575	485				82	0.95
	$\nu_{12}(a'')$	508	14	$\nu_4(e')$	508	16				0	0.88
MP2/6-31G(d, p)	$\nu_1(a')$	2404	1473				$\nu_3(b)$	2381	1489	23	0.99
	$\nu_2(a')$	1480	331	$\nu_3(e')$	1497	409				-17	0.81
	$\nu_3(a')$	1169	5				$\nu_1(a_1)$	1173	2	-4	2.50
	$\nu_4(a')$	879	2	$\nu_1(a'_1)$	889	-				-10	-
	$\nu_5(a')$	738	6				$\nu_2(a_2)$	727	8	11	0.75
	$\nu_6(a')$	658	184	$\nu_2(a''_2)$	699	101				-69	1.82
	$\nu_7(a')$	479	10	$\nu_4(e')$	481	13				-2	0.77

Table 6.6.7 Continued

	$BF_3.O_3$			BF_3			O_3				
Levels of Theory	mode (symmetry species)	$\tilde{\upsilon}/cm^{-1}$	A/km mol^{-1}	mode (symmetry species)	$\tilde{\upsilon}/cm^{-1}$	A/km mol^{-1}	mode (symmetry species)	$\tilde{\upsilon}/cm^{-1}$	A/km mol^{-1}	$^{a}\Delta\tilde{\upsilon}/cm^{-1}$	$\frac{A_{complex}}{A_{monomer}}$
	$\nu_{11}(a'')$	1456	385	$\nu_3(e')$	1497	409				-41	0.94
	$\nu_{12}(a'')$	481		$\nu_4(e')$	481					0	0.77
DFT/6-31G(d, p)	$\nu_1(a')$	1477	337	$\nu_3(e')$	1448	382				29	0.88
	$\nu_2(a')$	1276	28	$\nu_3(e')$	1448	382				-172	0.10
	$\nu_3(a')$	1225	112				$\nu_1(a_1)$	1266	166	-41	0.67
	$\nu_4(a')$	881	2	$\nu_1(a')$	889	-				-8	-
	$\nu_5(a')$	746	6	$\nu_2(a''_2)$	685	56				61	0.75
	$\nu_6(a')$	647	165				$\nu_2(a_2)$	735		-88	2.95
	$\nu_7(a')$	477	7	$\nu_4(e')$	479	11				-2	0.64
	$\nu_{11}(a'')$	1480	362	$\nu_3(e')$	1448	382				32	0.95
	$\nu_{12}(a'')$	478	10	$\nu_4(e')$	479	11				-1	0.91

$^{a}\Delta\tilde{\upsilon} = (\tilde{\upsilon}/cm^{-1})_{complex} - (\tilde{\upsilon}/cm^{-1})_{monomer}$

6.7 The boron trifluoride-sulphur dioxide complex

A number of sulphur dioxide complexes have been studied by high-resolution spectroscopic techniques. Many complexes can be classified into three categories depending upon whether the interaction partner is a nitrogen or oxygen Lewis donor base. The number of example involving interaction of SO_2 with a strong Lewis acid such as another SO_2 or CO_2 [130] is much smaller. The boron halides are among the prototype Lewis acid systems and the detailed structures of their complexes in the gas phase has recently been the subject of increasing attention. In this work we report the results of our ab initio studies on B...O bonded of the 1:1 $BF_3.SO_2$ complex. Then the ab initio results were compared with the experimental data available.

6.7.1 The optimized geometrical parameters of the complex

The optimized structural parameters of the boron trifluoride-sulphur dioxide molecular complex are presented in Table 6.7.1. The computed bond length and bond angles of both the boron trifluoride and sulphur dioxide monomers are collected in Table 4.1 (see chapter 4, page 22). The sulphur dioxide monomer bond length calculated at the HF, MP2 and DFT levels of theory is r(SO) equal to 141.4, 147.8 and 146.4 pm respectively. It is observed from Table 4.1 that the SO bond length of the SO_2 monomer is significantly changed on complexation. The boron trifluoride monomer bond angle $F\hat{B}F$ remain unchanged on complexation at all the levels of computation. The $O\hat{S}O$ bond angle of the monomer undergoes small changes in the complex in all the levels of theory, while the high value of interaction is observed at all the three levels of computation.

6.7.2 The energy of the complex

The binding energy of the complex studied here has been determined as uncorrected and corrected interaction energies, with the associated BSSEs and are shown in Table 6.7.2. This table shows that the BF_3. SO_2 complex is strongly interacting before and after correcting for the interaction energy, although it must be stressed that the interaction found in all the three levels of theory is weak.

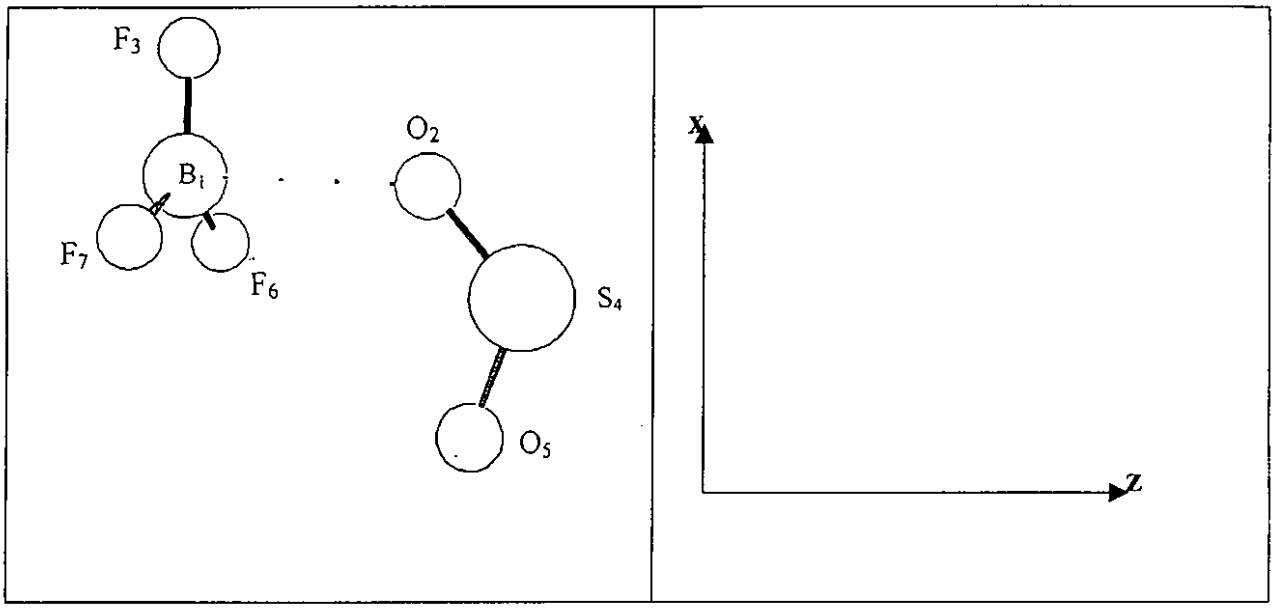

Figure 6.7 shows the optimized structure of the boron trifluoride-sulphur dioxide complex together with the numbering of atoms and the orientation of the axis.

Table 7.6.1 The optimized geometrical parameters of the $BF_3.SO_2$ complex calculated at the HF, MP2 and DFT levels of theory using the 6-31G(d, p) split-valence polarized basis set.

	Levels of theory		
Parameters	HF	MP2	DFT
$r(B_1...O_2)$/pm	257.7	259.0	251.4
$r(B_1F_3)$/pm	130.3	132.0	132.7
$r(B_1F_6) = r(B_1F_7)$/pm	130.4	132.0	132.7
$r(S_4O_2)$/pm	141.9	127.0	129.5
$r(S_4O_5)$/pm	141.1	125.0	130.6
$B_1...\hat{O}_2S_4$ /deg	134.6	116.3	115.8
$O_2\hat{S}_4O_5$/deg	118.4	118.0	116.4
$F_3\hat{B}_1...O_2\ F_3$/deg	92.0	86.8	87.5
$F_6\hat{B}_1F_7$ /deg	120.0	120.0	120.0

Table 7.6.2 Interaction energy and basis set superposition error of the boron trifluoride sulphur dioxide complex calculated at the HF, MP2 and DFT using the 6-31G(d, p) split-valence polarized basis set.

	Levels of theory		
Energy/kJ mol^{-1}	HF	MP2	DFT
$\Delta E_{(uncorrected)}$	-15.62	-23.84	-16.48
BSSE	4.31	9.70	4.63
$\Delta E_{(corrected)}$	-11.31	-14.14	-11.85

6.7.3 The vibrational wavenumbers and the band intensities

The HF, MP2 and DFT harmonic vibrational analysis for the boron trifluoride-sulphur dioxide, together with the approximate description of normal modes and the experimental wavenumbers, are given in Table 6.7.3. The boron trifluoride-sulphur dioxide molecular complex has C_s symmetry, and their normal modes transform as

$\Gamma_{vib}=10a'+5a''$

The computed intensity of the $BF_3.SO_2$ species is listed in Table 6.7.4, along with the approximate descriptions of the modes for all the levels of theory. This table shows that the intensities of the intermolecular modes are low. The calculated/experimental wavenumber ratios of the $BF_3.SO_2$ complex are shown in Table 6.7.5. This table shows that both the HF and DFT levels of computation overestimate the experimental wavenumbers by ca. 11 and ca. 1% on average respectively, while the MP2 method predict the correct values. Since the MP2 approach results are close to the experimental ones, we are going to base our predictions on this method. The corresponce between each of the molecular complex modes and its counterpart in the monomer at all the levels of theory are presented in Table 6.7.6, in which the monomer-complex wavenumber shifts are reported. Table 6.7.6 shows that, while the modes of the SO_2 moiety in the complex shows small wavenumber increases relative to the monomer, those of the BF_3 fragment show much larger wavenumber shifts in either direction. The symmetric BF_3-stretching mode of the monomer correlate with the ν_1 and ν_9 modes of the complex and experience a red shifts at both the modes. The symmetric SO_2-stretching mode of the complex (ν_2) is red shifted at this method (MP2). The symmetric BF_3-bending mode of the monomer goes over into ν_5 mode of the complex and is shifted to the opposite direction. The antisymmetric bending ν_7 mode show very small wavenumbers shifts in opposite direction while the antisymmetric bending ν_{12} modes remain unpertubed. All the components of the degeneracy symmetric SO-stretching and bending vibration (ν_3 and ν_7) modes are blue shifted.

The intensities of the boron trifluoride-sulphur dioxide are presented in Table 6.7.4 Since the infrared intensities in the spectrum of a given molecule typically span several orders of magnitude, a more approximate way of indicating changes in those intensities on complexation is by determining the ratios of the intensities rather than the differences. The complex/monomer intensities ratios are given in Table 6.7.6. This table indicates that, apart from the SO symmetric stretching mode, with very exceptions the ratio lie in the range from 0.8 to 1.5. The exception include the modes derived from the antisymmetric SO_2 at the HF method, which is 0.06 on complexation, and symmetric BF_3 stretching mode of the BF_3 which is virtually zero in the monomer at all the levels of computation. The modes of the complex which correlates with those of the monomer vibrations are all computed to be very weak.

The spectrum of the $BF_3.SO_2$ molecular complex should contain two antisymmetric BF_3-bending, one symmetric BF_3-stretching and another one from the bending BF_3 vibration.

Table 6.7.3 The computed and the experimental wavenumbers of the $BF_3.SO_2$ complex calculated at the HF, MP2, and DFT using the 6-31G(d, p) split-valence polarized basis set.

			Levels of theory			
Symmetry Species	Mode	Approximate description	HF $\tilde{\upsilon}/cm^{-1}$	MP2 $\tilde{\upsilon}/cm^{-1}$	DFT $\tilde{\upsilon}/cm^{-1}$	[a]Experimental $\tilde{\upsilon}/cm^{-1}$
a′	ν_1	ν(BF)	1570	1487	1482	1433
	ν_2	ν(SO)(nonbonded)	1557	1301	1331	1346
	ν_3	ν(SO)(bonded)	1358	1080	1140	1154
	ν_4	$\nu_s(BF_3)$	934	880	882	864
	ν_5	$\tau(BF_3)$	704	652	645	637
	ν_6	$\delta(SO_2)$	597	495	507	524
	ν_7	$\delta_a(BF_3)$	507	478	478	474
	ν_8	R_x	118	124	99	___[b]
	ν_9	T_z	88	106	79	___[b]
	ν_{10}	R_y	37	28	28	___[b]
a″	ν_{11}	$\nu_a(BF_3)$	1561	1482	1477	1421
	ν_{12}	$\delta_a(BF_3)$	508	481	479	474
	ν_{13}	T_y	142	149	128	___[b]
	ν_{14}	R_z	37	40	29	___[b]
	ν_{15}	T_x	21	13	8	___[b]

[a]Ref: 130, [b] band not observed in this region

Table 6.7.4 The computed band intensities of the BF_3. SO_2 complex calculated at the HF, MP2, and DFT levels of theory using the 6-31G(d, p) split-valence polarized basis set.

			Levels of theory		
Symmetry Species	Mode	Approximate description	HF A/km mol^{-1}	MP2 A/km mol^{-1}	DFT A/km mol^{-1}
a′	ν_1	ν(BF)	720	366	356
	ν_2	ν(SO)(nonbonded)	18	89	163
	ν_3	ν(SO)(bonded)	81	19	39

Table 6.7.4 continue

			Levels of theory		
Symmetry Species	Mode	Approximate description	HF A/km mol^{-1}	MP2 A/km mol^{-1}	DFT A/km mol^{-1}
	ν_4	$\nu_s(BF_3)$	4	4	3
	ν_5	$\tau(BF_3)$	229	219	185
	ν_6	$\delta(SO_2)$	91	41	49
	ν_7	$\delta_a(BF_3)$	13	14	9
	ν_8	R_x	1	1	1
	ν_9	T_z	1	1	1
	ν_{10}	R_y	1	1	1
	ν_{11}	$\nu_a(BF_3)$	454	382	358
a"	ν_{12}	$\delta_a(BF_3)$	16	12	10
	ν_{13}	T_y	6	4	5
	ν_{14}	R_z	14	7	7
	ν_{15}	T_x	0	0.001	0.2

Table 6.7.5 Ratios of the computed to the experimental wavenumbers observed in nitrogen matrices of the intramolecular modes of the boron trifluoride-sulphur dioxide complex.

	Levels of theory		
Mode	HF	MP2	DFT
ν_1	1.10	1.04	1.03
ν_2	1.16	0.97	0.99
ν_3	1.18	0.94	0.99
ν_4	1.08	1.02	1.02
ν_5	1.11	1.02	1.01
ν_6	1.14	0.94	1.01
ν_7	1.07	1.01	1.01
ν_{11}	1.10	1.04	1.04
ν_{12}	1.07	1.01	1.01
Mean Average	1.11	1.00	1.01

[a]Ratio=$\tilde{\upsilon}_{calc} / \tilde{\upsilon}_{expt}$

Ref. 130

Table 6.7.6 Comparison of the predicted wavenumbers and the band intensities of the boron trifluoride-sulphur dioxide Complex and of those of the individual parent monomer at the HF, MP2 and DFT Levels of theory using the 6-31G (d, p) split-valence basis set.

$BF_3.SO_2$				BF_3			SO_2				
Levels of Theory	mode (symmetry species)	$\tilde{\upsilon}/cm^{-1}$	A/km mol^{-1}	mode (symmetry species)	$\tilde{\upsilon}/cm^{-1}$	A/km mol^{-1}	mode (symmetry species)	$\tilde{\upsilon}/cm^{-1}$	A/km mol^{-1}	$^{a}\Delta\tilde{\upsilon}/cm^{-1}$	$\frac{A_{compex}}{A_{monomer}}$
HF/6-31G(d, p)	$\nu_1(a')$	1570	720	$\nu_3(e')$	1575	485				-5	1.48
	$\nu_2(a')$	1557	18				$\nu_3(a_2)$	1569	322	-8	0.06
	$\nu_3(a')$	1358	81				$\nu_1(a_1)$	1359	64	-1	1.23
	$\nu_4(a')$	934	4	$\nu_1(a''_1)$	943	-				-8	-
	$\nu_5(a')$	704	229	$\nu_2(a'_2)$	738	149				-34	1.54
	$\nu_6(a')$	597	91				$\nu_2(a_1)$	592	62	5	1.48
	$\nu_7(a')$	507	13	$\nu_4(e')$	508	16				-1	0.81
	$\nu_{11}(a'')$	1561	454	$\nu_3(e')$	1575	485				-14	0.94
	$\nu_{12}(a'')$	508	16	$\nu_4(e')$	508	16				0	1.00
MP2/6-31G(d, p)	$\nu_1(a')$	1487	366	$\nu_3(e')$	1497	409				-10	0.89
	$\nu_2(a')$	1301	89				$\nu_3(a_2)$	1305	79	-4	1.13
	$\nu_3(a')$	1080	19				$\nu_1(a_1)$	1077	13	3	1.46
	$\nu_4(a')$	880	4	$\nu_1(a'_1)$	889	-				-9	-
	$\nu_5(a')$	652	219	$\nu_2(a'_2)$	699	101				-47	2.17
	$\nu_6(a')$	495	41				$\nu_2(a_1)$	486	32	9	1.28

Table 6.7.6 continue

BF_3. SO_2				BF_3			SO_2				
Levels of Theory	mode (symmetry species)	$\tilde{\upsilon}/cm^{-1}$	A/km mol^{-1}	mode (symmetry species)	$\tilde{\upsilon}/cm^{-1}$	A/km mol^{-1}	mode (symmetry species)	$\tilde{\upsilon}/cm^{-1}$	A/km mol^{-1}	$^{a}\Delta\tilde{\upsilon}/cm^{-1}$	$\frac{A_{compex}}{A_{monomer}}$
MP2/6-31G(d, p)	$\nu_7(a')$	478	14	$\nu_4(e')$	481	13				-3	1.08
	$\nu_{11}(a'')$	1482	382	$\nu_3(e')$	1497	409				-15	0.93
	$\nu_{12}(a'')$	481	12	$\nu_4(e')$	481	13				0	0.92
DFT/6-31G(d, p)	$\nu_1(a')$	1482	356	$\nu_3(e')$	1448	382				34	0.93
	$\nu_2(a')$	1331	163				$\nu_3(a_2)$	1336	165	-5	0.99
	$\nu_3(a')$	1140	39				$\nu_1(a_1)$	1139	28	3	1.39
	$\nu_4(a')$	882	3	$\nu_1(a'_1)$	889	-				-7	-
	$\nu_5(a')$	645	185	$\nu_2(a'_2)$	685	56				-40	3.30
	$\nu_6(a')$	507	49				$\nu_2(a_1)$	502	34	7	1.44
	$\nu_7(a')$	478	9	$\nu_4(e')$	479	11				-1	0.81
	$\nu_{11}(a'')$	1482	358	$\nu_3(e')$	1448	382				29	0.94
	$\nu_{12}(a'')$	479	10	$\nu_4(e')$	479	11				0	0.91

$^{a}\Delta\tilde{\upsilon} = (\tilde{\upsilon}/cm^{-1})_{complex} - (\tilde{\upsilon}/cm^{-1})_{monomer}$

CHAPTER SEVEN

7. Summary

This chapter summarises the results obtained by (theoretically) ab initio molecular orbital calculations as compared with the results obtained experimentally from the literature. The good correlation that exists between the results obtained emphasises the strength of using the matrix isolation technique together with ab initio calculations for studying molecular interactions. The structures, interaction energies and the infrared spectra of both the dimeric isomers and the molecular complexes investigated in this work have been predicted by means of ab initio MO calculations at the HF, MP2 and DFT levels of theory with the standard 6-31G(d, p) split-valence polarized basis set. The computed infrared spectra obtained in this project have been analysed and used as guides in the assignment and interpretation of the matrix isolation infrared spectra obtained from the literature, where available. Table 7.1 shows the summary of the dimers and the complexes studied in this project where X represents the dimers and Z represents the complexes.

Table 7.1 The summary of the dimers and the complexes studied in this project.

	BF_3	CO	CO_2	H_2O	N_2O	O_2	O_3	SO_2
BF_3	X							
CO	Z	X						
CO_2	Z		X					
H_2O	Z			X				
N_2O	Z				X			
O_2	Z							
O_3	Z							
SO_2	Z							X

7.1.1 The monomers

Chapter four reports the results of the monomers calculated at the HF, MP2 and DFT levels of computation using the 6-31G(d, p) basis set. As it has been stated earlier in the previous chapters, the monomers have enjoyed a lot of investigations in the past years, and hence in this work they are not discussed in great detail. These results show that the geometrical parameters obtained by ab initio methods are substantially overestimated to those obtained by microwave, electron diffraction and infrared spectroscopic techniques at all the levels of theory, even though at some stage the HF method turns out to substantially overestimate the experimental results. The monomers values were used to correlate the wavenumber shifts of both the dimers and the complexes as well as for the changes in the geometrical parameters accompyanying complex formation.

7.1.2 The Homodimers

The results of the homodimers are reported in chapter five. The intermolecular modes of both the $(CO_2)_2$ of the T-shaped structure and $(SO_2)_2$ are calculated to have one negative eigenvalue at all the levels of computation; suprisingly, the water linear dimer is calculated to have a negative eigenvalue at the MP2 level. The results of the homodimers, particularly the CO_2 and N_2O dimers, showed some interesting features. As both the CO_2 and N_2O species are iso-electronic, their dimers happen to yield two types of isomers, namely; the T-shaped and the slipped parallel conformers. The T-shaped isomer for the N_2O species belongs to the C_s symmetry point group whereas for the CO_2 species it belongs to the C_{2v} point group. The slipped-parallel or edge-on parallel isomer for both the CO_2 and N_2O dimeric species belongs to the C_{2h} symmetry point group. The results obtained in this work confirm the earliest studies by Nxumalo and his co-workers [109, 130] that the C_{2h} structure is more stable than the T-shaped structure for both the CO_2 and N_2O dimers. Table 7.2 summarises the r(O...B) bond length, bond angles and corrected interaction energies for the homodimers where O stands for the oxygen donor ligand and BX represents electron acceptor . The H_2O dimer has much shorter O...B separation, probably resulting from the vibrational averaging effects of the dimer during the proton-donor acceptor interchange and also indicating the stregth of the interaction. The linearity of the AO...B bond angle, where A donates the fragment of the oxygen donor ligand is slightly affected with the exception of both the N_2O and CO_2 dimers. The r(O...B) bond length is increasing with the decreasing corrected interaction energies. The following trend in terms of the energies is followed:

$(H_2O)_2>(SO_2)_2>(BF_3)_2>(N_2O)_2>(CO_2)_2>(CO)_2$

Table 7.3 summarises the changes in the AO in-plane bending wavenumber shifts and the intensity ratio. This table shows that most of the bending modes are shifted to the blue and are also small. Table 7.4 summarises the changes in the AO bond length wavenumber shifts and the intensity ratios. The dimer with the greatest change in the AO bond distance also undergoes the largest wavenumber shifts, with the SO_2 dimer being the least. The high wavenumbers shifts also resulted to high A_d/A_m ratios but most of the intensities ratio lie within a factor of 2, which is in good accord with the Friedrich and Persons Theory [78]. Overall the interaction found in all the dimers studied in this work is very weak (van der Waals interaction and / or electron donor-acceptor type).

7.1.3 The Heterodimers

Chapter six reports the results of the molecular complexes (heterodimers). All of the seven complexes reported in this work feature the B...O electron donor-accepter interaction. The geometrical parameters obtained by the ab initio methods for the sub-unit of the monomer in the molecular complex are close to or the same as those calculated for the individual monomer. It has been observed that while the bond length increases, the bond angle decreases at the HF method, when compared with the other two methods. By correlating the calculated wavenumbers of the complex together with those of the parent monomers, we have established that the degree of the magnitudes of the in-plane bending mode and the antisymmetric stretching mode vibration wavenumber shifts of the electron acceptor moiety in the complex can be employed as dopes for determining the strength of the binding energy as well as the nature of the intermolecular interaction. The small wavenumber shifts expressed in terms of the in-plane bending and antisymmetric stretching modes of the electron acceptor (boron trifluoride in this case) signify very weak intermolecular interactions accompanied by a high intermolecular interaction distances and low interaction energies, after the latter has been corrected for basis set superposition error (BSSE).

Table 7.5 presents the summary of the bond lengths, bond angles and corrected interaction energies for the heterodimers. The $BF_3.H_2O$ complex has a much shorter

B...O separation, probably resulting from the vibrational averaging effects of the complex during the proton-donor acceptor interchange. The B...OA bond angle for the $BF_3.CO$, $BF_3.CO_2$ and $BF_3.N_2O$ are close to linearity, while other complexes showed diffent cases in terms of structural changes. The complex with the shorter intermolecular bond distance showed high interaction energy.

Table 7.6 shows the summary of the changes in the AO in-plane bending wavenumber shifts and intensity ratios. Table 7.7 shows the summary of the changes in the AO bond length, wavenumber shifts and intensity ratios. The complex with the greates change in the AO bond distance also undergoes the largest wavenumber shifts. The $BF_3.H_2O$ complex experiences a greater change in the AO bond length. Since intensity measurement is in reality a semi-quantitative parameter, we have established that the degree of the strength of the intensity is usually expressed in terms of the complex/monomer intensity ratio which is always either above or below a factor of 2 and weaker intensities are easily identified when the complex/monomer ratio is below a factor of 2. This trend was also observed for more complex 1:1 molecular species. The predicted wavenumbers on the other hand lie within approximately 11% deviation at the HF method with respect to the experimental results obtained from the literature in nitrogen matrices, while both the MP2 and DFT methods turn out to either overestimate or underestimate the experimental values by only small amounts. This corroborated the accuracy of both the MP2 and DFT methods since the two levels include electron correlation effects.

Table 7.2 The summary of the changes in the AO bond length, AO stretching wavenumber shifts and the dimer to monomer intensity ratios.

	HF/6-31G(d, p)			MP2/6-31G(d, p)			DFT/6-31G(d, p)		
Dimers	Δr^a(AO)	-Δν(AO)	A_d/A_m	Δr^a(AO)	-Δν(AO)	A_d/A_m	Δr^a(AO)	-Δν(AO)	A_d/A_m
$(BF_3)_2$	0	29	2.01	15.1	334	1.96	1.6	-7	2.25
$(CO)_2$	0	-3	1.06	0	-2	1.04	1.00	-2	0.0
$(CO_2)_2$	0.2	0	0.98	0.1	0	1.96	0.9	0	1.60
$(H_2O)_2$	0.4	-6	5.93	0.6	23	4.56	1.5	2	2.35
$(N_2O)_2$	0	3	2.13	0.2	7	1.89	0.4	-5	1.90
$(SO_2)_2$	0.1	10	0.98	0.1	1	1.00	0.1	5	0.97

[a]A is electron acceptor and O is oxygen donor ligand, $\Delta r = r_{complex} - r_{monomer}$, $\Delta \nu = \nu_{complex} - \nu_{monomer}$.

Table 7.3: The summary of the changes in the AO bending wavenumber shifts and the dimer to the monomer intensity ratios.

	HF/6-31G(d, p)		MP2/6-31G(d, p)		DFT/6-31G(d, p)	
Dimers	$-\Delta\delta^a$ (AO)	A_d/A_m	$-\Delta\delta^a$ (AO)	A_d/A_m	$-\Delta\delta^a$ (AO)	A_d/A_m
$(BF_3)_2$	1	0.95	0	1.00	0	2.07
$(CO)_2$	-24	1.91	-25	1.82	-66	2.81
$(CO_2)_2$	-4	1.94	-2	1.88	-2	2.23
$(H_2O)_2$	-42	1.36	-32	0.97	-32	1.03
$(N_2O)_2$	-10	1.47	-8	0.97	-8	1.15
$(SO_2)_2$	-2	1.95	0	1.80	0	1.89

[a]A is electron acceptor and O is oxygen donor ligand , $\Delta\delta=\delta_{complex}-\delta_{monomer,}$.

Table 7.4: The summary of the geometrical parameters and the corrected interaction energies for the homodimers.

	HF/6-31G(d, p)			MP2/6-31G(d, p)			DFT/6-31G(d, p)		
Dimers	r^a(A…B)	*AÔ...B*	ΔE/kJ mol^{-1}	r^a(A…B)	*AÔ...B*	ΔE/kJ mol^{-1}	r^a(A…B)	*AÔ...B*	ΔE/kJ mol^{-1}
$(BF_3)_2$	337.6	108.2	-4.20	230.4	117.9	-1.97	323.9	108.0	-6.25
$(CO)_2$	383.7	158.5	-0.10	263.4	158.4	-2.99	399.7	134.5	-2.34
$(CO_2)_2$	239.4	180.0	-2.56	347.2	180.0	-2.25	354.6	180.0	-2.33
$(H_2O)_2$	203.9	180.0	-23.34	196.6	165.5	-19.61	193.1	163.0	-24.39
$(N_2O)_2$	353.5	172.2	-3.93	297.7	180.0	-2.80	310.8	180.0	-4.23
$(SO_2)_2$	372.1	118.1	-9.49	344.6	119.1	-4.93	356.9	118.4	-3.64

[a]A is electron acceptor and B is electron donor

Table 7.5: The summary of the changes in the AO bond length, AO stretching wavenumber shifts and the dimer to monomer intensity ratios.

	HF/6-31G(d, p)			MP2/6-31G(d, p)			DFT/6-31G(d, p)		
Complexes	Δr^a(AO)	-Δν(AO)	A_c/A_m	Δr^a(AO)	-Δν(AO)	A_c/A_m	Δr^a(AO)	-Δν(AO)	A_c/A_m
BF_3. CO	0.1	4	0.96	0	3	0.96	1.1	-40	0.96
$BF_3.CO_2$	0.3	-2	0.96	0.4	26	0.96	0.3	-47	1.04
$BF_3.H_2O$	0.6	100	0.93	0.7	138	1.11	1.1	95	1.19
$BF_3.N_2O$	0.4	-2	0.96	0.4	-3	0.95	0.5	-45	0.96
$BF_3.O_2$	0.3	-47	0.97	2.8	18	0.97	0	-22	0.97
$BF_3.O_3$	0.3	-82	0.95	3.0	41	0.94	3.1	-32	0.95
$BF_3.SO_2$	0.5	14	0.94	20.0	15	0.93	16.9	-29	0.94

[a]A is electron acceptor and O is oxygen donor ligand, $\Delta r = r_{dimer} - r_{monomer}$, $\Delta\nu = \nu_{complex} - \nu_{monomer}$.

Table 7.6: The summary of the changes in the AO bending wavenumber shifts and the complex to the monomer intensity ratios.

	HF/6-31G(d, p)		MP2/6-31G(d, p)		DFT/6-31G(d, p)	
Complexes	$-\Delta\delta^a$(AO)	A_c/A_m	$-\Delta\delta^a$(AO)	A_c/A_m	$-\Delta\delta^a$(AO)	A_c/A_m
$BF_3.CO$	0	1.00	-1	0.92	0	0.91
$BF_3.CO_2$	0	0.94	0	0.92	-1	0.91
$BF_3.H_2O$	103	1.50	42	1.50	53	1.50
$BF_3.N_2O$	0	0.94	0	0.92	-1	0.91
$BF_3.O_2$	-2	0.94	0	0.85	2	0.82
$BF_3.O_3$	4	0.56	2	0.77	2	0.64
$BF_3.SO_2$	1	0.81	3	1.08	1	0.81

[a]A is electron acceptor and O is oxygen donor ligand, $\Delta\delta=\delta_{dimer}-\delta_{monomer}$.

Table 7.7: The summary of the geometrical parameters and the corrected interaction energies for the heterodimers.

	HF/6-31G(d, p)			MP2/6-31G(d, p)			DFT/6-31G(d, p)		
Complexes	r^a(A…B)	$A\hat{O}...B$	ΔE/kJ mol^{-1}	r^a(A…B)	$A\hat{O}...B$	ΔE/kJ mol^{-1}	r^a(A…B)	$A\hat{O}...B$	ΔE/kJ mol^{-1}
BF_3. CO	279.0	180.0	- 4.12	268.9	180.0	-2.71	274.2	180.0	-2.57
$BF_3.CO_2$	271.4	179.6	-6.61	262.3	179.5	-4.55	272.6	179.4	-3.95
$BF_3.H_2O$	193.4	108.4	-15.91	180.3	106.7	-15.90	184.2	106.8	-14.43
$BF_3.N_2O$	263.8	180.0	-7.30	261.9	180.0	-3.49	267.4	180.0	-4.16
$BF_3.O_2$	272.5	109.6	-5.01	250.2	103.4	-7.05	251.4	110.8	-5.42
$BF_3.O_3$	271.0	119.0	-3.62	259.0	118.0	-5.49	251.4	116.4	-4.53
$BF_3.SO_2$	257.7	118.4	-11.31	259.0	118.0	-14.14	251.4	116.4	-11.85

[a]A is electron acceptor and B is electron donor

CHAPTER EIGHT

Conclusion and recommendation

The quantum-mechanical methods of the conventional ab initio approach at the HF, MP2 and DFT levels of theory with the standard 6-31G(d, p) split-valence polarized basis set provide very useful information on the molecular parameters (structural geometries and energies) and in the interpretation of the infrared spectra. Since the DFT calculations are less time-consuming or require less time than the MP2 technique, the DFT is highly recommended for the prediction of the equilibrium structures and vibrational spectra of a variety of electron donor-acceptor molecular complexes and similar systems. The calculations of the infrared spectra carried out at the HF, MP2 and DFT levels of theory provide data for reliable interpretation of the absorption spectra of isolated molecular complexes studied under cryogenic conditions obtained from the literature, where available (nitrogen matrices).

Based on this work we may conclude that the infrared spectra obtained using the MP2 and the DFT methods reproduce the experimental spectra better than that obtained by the HF approach since the latter lacks electron correlation effects. Due to the harmonic approximation applied in the calculations, the spectra of the molecular modes are not reproduced precisely. Analysis of the DFT results for the predictions of the interaction energies shows that the DFT approach might not be a good tool for this purpose. 62 % of the calculated/experimental wavenumbers showed that the results of the MP2 method are substantially overestmated to the experimental when compared with the 32 % of the calculated/experimental wavenumbers of the DFT level. When comparing the two post Hartree-Fock methods the MP2 method is more reliable than the DFT approach in the prediction of the experimental results. The MP2 and DFT are both virtually always an improvement on Hartree-Fock method.

In the past chemistry has been tradditionally an experimental science, this implied that no molecule or complexes could be investigated unless is found in nature. That was all that was possible at the time and now has been eliminated by the advent of computers. As stated at the beginning, with the advancement of computer speeds and capabilities, this area of chemistry is changing very quickly. However, this new approach is not infallible and the continuous checking of the theoretical results against the experimental ones is usually required. Ab initio calculations offer

valuable insight into the physical properties of the molecules and as such are a very valuable tool in the chemical world of today. As a result of our investigations we found that in most cases MP2 calculations can be used for investigations in future research work as it is procedure superior than to the DFT method and it is also virtually always be an improvement on the Hartree-Fock.

References:

1. H.A Benasi and J.H. Hildebrand, J. Chem. Soc, **71**, 2703 (1949)

2. L.M. Nxumalo and T.A. Ford; Spectrochim. Acta, part A, **53**, 2511 (1997).

3. D.J. Wales, Mol, Phys., **74**, 1 (1991).

4. T.R. Dyke, B. Howard and W. Klemperer, J.Chem. Phys., **56**, 2442 (1972).

5. S.E. Novick, K.C. Janda, S.L. Holmgren, M. Waldman and W. Klemperer, J.Chem. Phys., **65**, 114 (1976).

6. A.J. Stone, Chem. Phys. Lett., **83**, 233 (1981).

7. A.D. Buckingham and P.W. Fowler, Can. J. Chem., **63**, 2018 (1985).

8. A.D. Buckingham, P.W. Fowler, and J.M. Hutson, Chem. Rev., **88**, 963, (1988).

9. A.D. Buckingham and P.W. Fowler, Can. J. Chem. Phys.,**79**, 6426 (1983).

10. A.C. Legon and D.J. Millen, Faraday Discuss. Chem. Soc., **73**, 71(1928).

11. A.C. Legon and D.J. Millen, Faraday Acc. Chem. Rev, **20**, 39 (1982).

12. V.Magnasco and R. McWeeny, ''Weak Interaction Between The Molecules and Their Physical Interaction,, Theoretical Models of Chemical Bonding, Part 4, Z.B. Maksic (editor), Springer-Verlag, Berlin, pp.134-169 (1991)

13. P.O. Lowdin, Rev. Mol. Phys., **36**, 966 (1964).

14. J.A. Pople and R.K. Nesbet, J. Chem. Phys., **22**, 571 (1954).

15. (a) C. C. J. Roothaan, Rev. Mod., Phys., **32**, 179 (1960).

(b) J.S. Binkley, J.A. Pople, and P.A.Dobosh, Mol. Phys.,**28**, 1423 (1974).

16. C. Møller and M.S Plesset, Phys, Rev., **46**, 618-622 (1934).

17. W. Kohn and L.J. Sham, Phys. Rev. A., 1133 (1965).

18. J.A. Pople, in Modern Chemistry (H.F. Schaeter,111,ed.) Vol 3, method of Electronic Structure Theory, Plenum, New Jork (1977).

19. Becke A.D., J. Phys. Chem., **98**, 5648 (1993).

20. (a) J.A. Pople, R. Seeger and R. Krishnan, Int.J. Quant. Chem. Symp., **11**, 149 (1977).
(b) R. Krishnan and J.A. Pople, Int. J. Quant.Chem., **14**, 91 (1978).

21. J.G.C.M. Van Duijenveldt-Van De Rijt and F,B. Van Duijenveldt, J. Mol. Struct., **35**, 263 (1976).

22. J.A. Pople, R. Krishnan, H.B. Schlegel and J.S. Binkley, Int.J. Quant. Chem. Symp. **13**, 225 (1979).

23. Goddard, N.C. Handy and H.F. Chaefer, III, J. Chem. Phys.,**71**, 1525 (1979).

24. S. Kato and K. Marokuma, Chem. Phys. Letters, **65**, 19 (1979).

25. H.B. Schlegel, J. Chem. Phys., **77**, 3676 (1982).

26. B. A. Murtaugh and R.W.H. Sargent, Comput. J., **13**, 185 (1982).

27. D. Poppinger, Chem, Phys. Letter, **34**, 332 (1975).

28. S.F. Boys and F.Bernadi, Mol, Phys., **19**, 553 (1970).

29. D.Hirst, ''A computational Approach to Chemistry`` Blackwell Scientific Publishers, Oxford, pp.10-20 (1990).

30. N.R. Kestner, M.D. Newton and E.L Mathers, Int.J. Quant. Chem. Quant. Symp., **17**, 431 (1983).

31. M.D. Newton, J. Chem. Phys., **87**, 4288 (1983).

32. M.A. Navena, B. Silvi and J. Capriani, J. Chem. Phys, **76**, 4573 (1983).

33. W. Kolos, Theor. Chim. Acta., **51**, 219 (1979).

34. C. K. Johnson, "ORTEP A Fortran Thermal-Ellipsoidal plot program for crystal structure illustration", Report No. ORNL-3794, Oak ridge National laboratory, Oak ridge, Tennessee, 1965

35. D.G. Evans, G.A. Yeo and T.A. Ford, Faraday Discuss. Chem. Soc., **86**, 55 (1988).

36. G.A. Yeo and T.A. Ford, Ford, S. Afr. J. Chem., **39**, 243, (1986).

37. G. A. Yeo and T. A. Ford, J. Mol. Structure., **200**, 507 (1989).

38. M.J Frisch, J.S. Binkley, H.B. Schlegel, K. Raghava Chari, C.F. Melius, R.L Martin, J.J. Stewart, F. W. Bromowicz, C.M. Rohling, L.R. Kahn, D.J. De Frees, R. Seeger, R.A. Whiteside, D.J. Fox, E.M. Fleuder and J.A. Pople, Gaussian-98, Gaussian Inc., Pittsburgh, P.A, 1988

39. (a) J.A. Paldus, J. Chem.Phys., **61**, 5321, (1974).
(b) J.A. Paldus, Int. J. Quant. Chem. Symp., **9**, 165, (1975).
(c) J.A. Paldus, Phys. Rev. A, **14**,1620 (1976).

40. C.C.J. Roothan, Rev. Mod. Phys., **23**, 69 (1951).

41. P.V. Harihan and J.A. Pople, Theor. Chim. Acta, **28**, 217 (1972).

42. M.M. Francl, W.J. Pretro, W.J. Hehre, J.S. Binkley, M.S. Gordon, D.J. De Frees and J.A. Pople, J. Chem. Phys., **77**, 3654 (1982).

43. K. Kuchitsu and S. Konaka, J. Chem. Phys., **45**, 4342 (1966).

44. D.F Wolfe and G.L..Humphrey, J. Mol. Struct.,**3**, 293 (1969).

45. T.A.Ford and W.J. Orville-Thomas, Spectrochim. Acta, **23A**, 579 (1967).

46. J. Aron and T.A. Ford, S. Afr. J. Chem., **35**, 129 (1982).

47. J. Aron and T.A. Ford, S. Afr. J. Chem., **39**, 33 (1982).

48. J. Aron, L.R. Hindler and T.A. Ford, S. Afr. J. Chem., **39**, 39 (1986).

49. D.C. McKean, J. Chem. Phys., **24**, 1002 (1956).

50. S. Chin, T.A. Ford and W.B. Person, J. Mol. Struct., **113**, 341 (1984).

51. S. Chin and T.A. Ford, J. Mol. Struct (Theochem), **113**, 193 (1985).

52. S. Chin and W.B. Person, J. Phys. Chem., **88**, 553 (1984).

53. K.C. Janda L.S. Bernstein, J.M. Steed, S.E. Novick and W. Klemperer, J. Am. Chem. Soc.,**100**, 8074 (1978).

54. D. G. Evans, G. A. Yeo and T. A. Ford, Faraday Discuss. Chem. Soc., **86**, 55 (1988).

55. F. M. M. O'neill, G. A. Yeo and T.A. Ford, J. Mol. Struct., **173**, 337 (1988).

56. K. R. Leopold, G. T. Fraser and W.A. Klemperer, J. Am. Chem. Soc., **106**, 897 (1984).

57. J. Gebicki and J. Liang, J. Mol. Struct., **117**, 283 (1984).

58. J. M. McIver, Acc. Chem. Res., **7**, 72 (1974).

59. F. Hirota, Y. Konyana and S. Shibata, J. Mol. Struct., **70**, 305 (1981).

60. R. L. Hunt and B.S. Ault, Spectrosc Int. J., **1**, 45 (1982).

61. W.J. Hehre, L. Radom, P.v.R. Schleyer and J.A. Pople, A*b Initio Molecular Orbital Theory*, Wiley-Interscience, pp.133-344 (1986).

62. D. Mokomela, I. Rencken, G.A. Yeo and T.A Ford, J. Mol. Struct., **343**, 13, (1995).

63. S. Chin and T.A Ford, J. Mol. Struct (Theochem), **152**, 363 (1987).

64. P. Hobza and R. Zahradnik, Weak Intermolecular Interactions in Chemistry and Biology, Elsevier, Amsterdam, (1980).

65. H. Ratajczak and W.J. Orville-Thomas (eds.), Intermolecular Interactions, Wiley, Chichester, Vols. 4, (1977).

66. P. Kollman, in Modern Theoretical Chemistry, (H.F. Schaefer, III, ed.), Plenum Press, New York, Vol. 4, (1977).

67. P. Schuster (ed.), Hydrogen bonds, Topics in current Chemistry, Vol. 120, Springer-Verlag, Berlin (1984).

68. A.C. Legon and D.J.Millen, Chem. Rev., **86**, 507 (1986).

69. F.G. Celli and K.S.Janda, Chem, Rev., **86**, 514 (1986).

70. W.B. Person and J.D.Rogers, Analytiktreffen 1980, Schwingungs-spektroskopie, Theorie and Anwenduge, Karl Marx Universitat, Leipzig, pp. 262-300 (1980).

71. T. Shimanouchi, J. Phys. Chem. Ref. Data., **6**, 993 (1977).

72. J.M. Bassler, P.L. Timms and J.L. Margrave, J. Chem. Phys., **45**, 2704 (1996).

73. I.W. Levin and Abramowitz, Chem. Phys. Letters, **9**, 247 (1971)

74. R.C. Lord and E. Nielsen, J. Chem. Phys., **19**, 1 (1951)

75. H. Gerding and E. Smit, Z. Physik, Chem., **B50**, 171 (1941)

76. L.M. Nxumalo and T.A. Ford J. Mol. Struct, **325-338**, 300 (1993)

77. S.F. Boys and F. Bernardi, Mol. Phys., **19**, 553 (1970)

78. H.B. Friedrich and W.B. Person, J. Chem. Phys., **44**, 2161 (1966)

79. M.J. Frisch, M. Head-Gordon, H.B. Schlegel, K. Raghavacheri, J.S. Binkley, C. Conzalez, D.J. Defree, D.J. Fox, R.A. Whiteside, R. Seeger, C.F. Melius, J. Barker, R. Martin, L.R. Hahn, J.J.P. Stewart, E.M. Fleuder, S. Topiol, J.A. Pople, GAUSSIAN-98 Gaussian, Inc., Pittsburgh, P.A. 15213, 1998

80. L.M. Nxumalo and T.A. Ford, J. Mol. Struct. (Theochem), **236**, 135 (1991)

81. L.M. Nxumalo and T.A. Ford, S. Afr. J. Chem., **48**, 230 (1995)

82. L.M Nxumalo, Ford, T.A. J. Mol. Struct., **436-437** , 69 (1997)

83. L.M. Nxumalo, G.A. Yeo and T.A. Ford. Theor. Chem. Acc., **96**, 157 (1997).

84. L.M. Nxumalo and T.A. Ford, in 9th international conference on Fourier Transform Spectroscopy, John E. Bertie and Hal Wieser, Editors, Proc. Spie, **200**, 2089 (1993).

85. L.M. Nxumalo., M. Andrzejak, and T.A. Ford, J. Chem. Info. Comput. Sci., **12**, 221 (1996).

86. L.M. Nxumalo., M. Andrzejak, and T.A. Ford, Vibr. Spectrosc., **12**, 221 (1996).

87. L.M. Nxumalo and T.A. Ford, Spectrochim. Acta, PartA, **53**, 2511 (1997).

88. L.M. Nxumalo, G.A. Yeo and T.A. Ford. S. Afi. J. Chem.,**51**, 25 (1998).

89. L.M. Nxumalo and T.A. Ford, Microchimica Acta, (Suppl.**14**), 383 (1997).

90. L.M. Nxumalo and T.A. Ford, J. Mol. Struct (Theochem), **115**, 369 (1996).

91. S.A Peebles, L. Sun, R.L. Kuczkowski, L.M. Nxumalo and T.A. Ford, J. Mol. Struct., **235**, 471 (1998).

92. H.E. Hallan, in Infrared Spectroscopy and Molecular Structures, (M. Davies, ed.), Elsevier, Chapter XII, pp.**405-432** (1963).

93. R. Guasti, V. Schettino and N. Brigot, Chem. Phys., **34**, 391 (1978)

94. M.J. Irvine and A.D.E. Pullin, Aust. J. Chem., **35**, 1961 (1982)

95. A.E. Borton, A. Chable and B.J. Howard, Chem. Phys Lett., **60**, 414 (1979)

96. K.W.Jucks, Z.S. Huang, D. Dayton, R.E. Miller and W.J. Lafferty, J. Chem. Phys., **86**, 4341 (1987).

97. M.A. Walsh, T.H. England, T.R. Dyke and B.J. Howard, Chem. Phys. Lett., **142**, 265 (1987).

98. K.W.Jucks, Z.S. Huang, R.E. Miller, G.T. Fraser, A.S. Pine and W.J. Lafferty, J. Chem. Phys., **88**, 2185 (1988).

99. A.S. Pine and G.T. Fraser, J. Chem. Phys., **89**, 100 (1988).

100. A. Koide and T. Kihara, Chem. Phys., **5**, 34 (1974).

101. N. Brigot, S. Odiot, S.H. Walmsey and J.L. Whitten, Chem. Phys. Lett., **49**, 157 (1977).

102. N. Brigot, S. Odiot and S.H. Walmsey, Chem. Phys. Lett., **88**, 543 (1982).

103. A.J. Illies, M.L. McKee and H.B. Schlegel, J. Chem. Phys., **91**, 3489 (1987).

104. R,G.A. Bone and N.C. Handy, Theor. Chim. Acta, **78**, 133 (1990)

105. R. Eggenberger, S. Gerber and H. Huber, Mol. Phys., **72**, 433 (1991).

106. J.S. Muenter, J. Chem. Phys., **94**, 2781 (1991).

107. K.B. Domanski, O. Kitao and K. Nakanishi, Chem. Phys, Lett., **199** 525 (1992).

108. Z. Slanina S.J. Kim and K. Fox, Vibr. Spectrosc., **4**, 251 (1983).

109. L.M. Nxumalo, T.A. Ford and A.J. Cox, J. Mol. Struct. (Theochem), **307** 153 (1994).

110. K. Hiraoka, T. Shoda, K. Morise, S. Yamabe, E. Kawai and K. Hirao, J. Chem. Phys., **84**, 2091 (1986).

111. R.L. De Leon, A. Yokozeki and J.S. Muenter, J. Chem. Phys., **73**, 2044 (1980).

112. T.B. MaCrury, W.A. Steele and B.J. Berne, J. Chem. Phys., **64**, 1288 (1976).

113. R.M. Bentwood, A.J. Barnes and W.J. Orville-Thomas, J. Mol. Spect., **84**, 391 (1980).

114. M. Van Thiel, E.D. Becker and G.C. Pimentel, J. Chem. Phys., **27**, 486 (1957).

115. G.P. Ayers and A.D.E. Pullin, Spectrochim. Acta, **32A**, 1629 (1976).

116. M.J. Frisch, J.E. Del Bene, J.S. Binkley and H.F. Schaefer III, J. Chem. Phys., **84**, 2279 (1986).

117. D.M. Bishop, J. Pipin and Kirtman, J. Chem. Phys., **102**, 6778 (1995).

118. W.C. Topp and L.C. Allen, J. Am. Chem. Soc., **96**, 2591 (1974).

119. M.J. Frisch, J.A. Pople and J. Del Bene, J. Phys. Chem., **89**, 3664 (1985).

120. K. Kim and K.D. Jordan, J. Phys. Chem., **98**, 10089 (1984).

121. J.E. Del Bene, W.B. Person and K. Szczepanick, J. Phys. Chem., **99**, 10705 (1995).

122. J.E. Del Bene, J. Phys. Chem., **92**,2874 (1988).

123. B. van Hensbergen, R. Block and L. Jensen, J. Chem. Phys., **76**, 3161 (1982).

124. L. Fredin, B. Nelander and G. Rebbegerd, J. Chem. Phys., **66**, 4065 (1977).

125. J.P. Ayers and A.D.E. Pullin, Spectrochim. Acta, **32A**, 1695 (1976).

126. P. Kollman, J. Mckelvey, A. Johansson and S. Rothenberg, J. Am. Chem. Soc., **97**, 955 (1975).

127. K. Morokuma and H. Umeyama, J. Am. Chem. Soc., **99**, 1316 (1977).

128. C.J. Marsden, B.J. Smith, J.A. Pople, H.F. Schaefer III and L. Randon, J. Chem. Phys., **95**, 1825 (1991).

129. F.F. Marguet, G.W. Robinsen and M.P. Basset, Muguel, Int. J. Quant. Chem., **39**, 449 (1991).

130. L.M. Nxumalo, PhD Thesis, University of the Witwatersrand, Johannesburg, 1993.

131. G.A. Yeo and T.A. Ford, Struct. Chem., **2**, 3 (1992).

132. G.C. Pimentel and A.L. McClellan, The Hydrogen Bond, Freeman, San Francisco, pp. 71-90 (1960)

133. T. E. Gough, R.E. Miller and G. Scholes, J. Chem. Phys., **69**, 1588 (1978).

134. R.E. Miller and R.O. Watts and A. Ding, Chem. Phys., **83**, 155 (1984).

135. R.E. Miller and R.O. Watts, Chem. Phys. Lett., **105**, 409 (1984).

136. B.J. Howard, Paper WA2, Presented at the 42nd Symposium on Molecular Spectroscopy, Ohio State University, Columbus, Ohio, 1987

137. Z.S. Huang and R.E. Miller, J. Chem. Phys., **89**, 5408 (1988).

138. M. Takami, Y. Ohshima, S. Yamamoto and Y. Matsumoto, Faraday Discuss. Chem. Soc., **86**, 1 (1988).

139. Y. Ohshima, S. Yamamoto, M. Takami and K. Kuchitsu, Chem. Phys. Lett., **152**, 294 (1988).

140. R.B. Bernstein and C.E. Kolbe, J. Chem. Phys., **71**, 2818 (1979).

141. J.R. Sodeau and R. Withmal, J. Phys. Chem., **89**, 4484 (1985).

142. D.A. Morales and G.E. Ewing, Phys. Chem., **53**, 141 (1980).

143. J.A. Beswick and J. Jortnet, Chem. Phys., **74**, 6725 (1981).

144. J. Sadlej and M. Sicinski, J. Mol. Struct. (Theochem), **204**, 1 (1990).

145. K. Mogi, T. Komine and K. Hirao, J. Chem. Phys., **95**, 8999 (1991)

146. R.S. Mulliken and W.B. Person, Molecular Complexes, Wiley-Interscience, New York (1969).

147. Z.S. Huang and R.E. Miller, J. Chem. Phys., **89**, 5408 (1988).

148. H.E. Hallam, in *Infrared Spectroscopy and Molecular Structure*, (M. Davie, ed.), Elsevier, Chapter XII, pp. 405-432 (1963).

149. P.L. Hanst and S.T. Hanst, in M.W. Sigrist (ed.), Air Monotoring by Spectroscopic Techniques, Willey, New York, pp. 335-470 (1994).

150. J.W. Hastie, R. Hauge and J.L. Margrave, J. Inorg. Nucl. Chem., **31**, 281 (1969).

151. M. Allarena, R. Rysnik, D. White, V. Ealder and D.E. Mann, J. Chem. Phys., **50**, 3399 (1969).

152. M. Fredin, Chem. Scr., **4**, 97 (1973).

153. D. Maillard, M. Allavena and J. P. Perchard, Specrochim. Acta, **31A**, 1523 (1975).

154. L.Nord, J. Mol. Struct, **96**, 19 (1982).

155. D. Nelson, Jr., G.T. Fraser and W. Klemperer, J. Chem. Phys., **83**, 945 (1985).

156. K. Matrumura, F.J. Lovas and R.D. Suenram, J. Chem. Phys., **91**, 5887 (1989).

157. A. Taleb-Bendiab, K.W. Hilling II and R.L. Kuczkowski, J. Chem. Phys., **94**, 6956 (1991).

158. L.H. Coudert and J.T. Hougen, J. Mol. Spectrosc., **130**, 86 (1988).

159. L.M. Nxumalo and T.A. Ford, J. Mol. Struct., **347**, 13 (1995).

160. B.A. Wofford, J.W. Bevan, W.B. Olson and W.J. Lafferty, J. Chem. Phys., **83**, 6188 (1985).

161. J. Hodge, G.D. Hayman, T.R. Dyke and B.J. Howard, J. Chem. Soc., Faraday Trans. 2, **82**, 1137 (1986).

162. B.A. Watford, J.W. Bevan, W.B. Olson and W.J. Lafferty, Chem. Phys. Lett., **124**, 579 (1986).

163. B.A. Wofford, M.W. Jackson, J.W. Bevan, W.B. Olson and W.J. Lafferty, J. Chem. Phys., **84**, 6115 (1986).

164. B.A. Wofford, J.W. Bevan, W.B. Olson and W.J. Lafferty, J. Chem. Phys., **85**, 105 (1986).

165. S. Geller and J.L. Hoard, Acta Crystallogr., **3**, 121 (1950).

166. J.L. Hoard, T.B. Owen, A. Buzzell and O.L. Salmon, Acta Crystallogr., **3**, 130 (1950).

167. J.L. Hoard, S. Geller and W.M. Cashin, Acta Crystallogr.,**4**, 396 (1951).

168. R.L. Amster and R.C. Taylor, Spectrochim. Acta, **20**, 1487 (1964).

169. R.C. Taylor, H.S. Gabelnick, K. Aida and R.L. Amster, Inorg. Chem., **8**, 605 (1969).

170. B. Swanson and D.F. Shriver,. Inorg. Chem., **9**, 1405 (1970).

171. S.E. Novick, P.B. Davies, T.R. Duke and W. Klemperer, J. Am. Chem. Soc., **95**, 8547 (1973).

172. K.C. Janda, L.S. Bernstein, J.M. Steed, S.E. Novick and W. Klemperer, J. Am. Chem. Soc., **100**, 8074 (1978).

173. T. Pradeep, S.C. Sreekanth and C.N.R. Rao, J. Chem. Phys., **90**, 4704 (1989).

174. M.C. Durrant, M.S. Hegde and C.N.R. Rao, J. Chem. Phys., **85**, 6356 (1986).

175. K.R. Leopold, G.T. Fraser and W. Klemperer, J. Am. Chem. Soc., **106**, 897, (1984).

176. T. Pradeep and C.N.R. Rao, J. Mol. Struct (Theochem), **200**, 339 (1989).

177. T. Pradeep, C.S. Sreekanth, M.S. Hegde and C.N.R. Rao, J. Am. Chem. Soc., **111**, 5058 (1989).

178. D.G Evans, G.A Yeo and T. A. Ford, Faraday Discuss. Chem. Soc., **86**, 377 (1996).

179. L.M. Nxumalo and T.A. Ford, J. Mol. Struct. (Theochem), **369**, 115 (1996).

180. L.M. Nxumalo, M. Andrzejak and T.A. Ford, J. Chem. Inf. Comput Sci., **36**, 377 (1996).

181. L.M. Nxumalo, M. Andrzejak and T.A. Ford, Vib Spectrosc., Science., **12**, 221 (1996).

182. L.M. Nxumalo T.A. Ford, S Afr J. Chem., **48**, 30 (1996).

183. A.C. Legon and D.J. Millen, Acc. Chem. Res., **20**, 39 (1987).

184. D.R. Lloyd and N. Lynaugh, J. Chem. Soc. Faraday Trans. II, **68**, 947 (1972).

185. A.H. Cowley, R.A. Kemp, M. Lattman and M.L. McKee, Inorg. Chem., **21**, 85 (1982).

186. T. Pradeep, C.S. Sreekanth, M.S. Hegde and C.N.R. Rao, J. Mol. Struct., **194**, 163 (1989).

187. T. Pradeep, M.S. Hegde and C.N.R. Rao, J. Phys. Chem, **90**, 4704 (1989).

188. P.V. Pamath, M.S. Hegde and C.N.R. Rao, J. Phys. Chem, **90**, 1990 (1986).

189. M.C. Durrant, M.S. Hegde and C.N.R. Rao, J. Phys. Chem, **90**, 4704 (1989).

190. P.V. Harihan and J.A. Polple, Theor. Chim. Acta, **28**, 213 (1973).

191. T. Shimanouchi, J. Phys. Chem. Ref. Data, **6**, 993 (1977).

192. L.M. Nxumalo and T.A. Ford, J. Mol. Structure., **436-437**, 69 (1996).

193. P.S. Bryan and R.L. Kuczkowski, Inorg. Chem., **10**, 200 (1971).

194. W. Gordy and H. Ring, Phys. Rev., **78**, 512 (1950).

195. E.W. Hughes, J. Am. Chem. Soc., **78**, 502 (1956).

196. N.N. Greenwood, Q. Rev. Chem. Soc., **8**, 1 (1954).

197. F.J. Lovas and D.R. Johnson, J. Chem. Phys., **55**, 41 (1971).

198. P.A. Freedman and W.J. Johnson, J. Mol. Spectrosc., **54**, 182 (1975).

199. W.M. Huo, J. Chem. Phys., **43**, 624 (1956).

200. G. Das and A.C. Wahl, J. Chem. Phys., **44**, 87 (1975).

201. H.C. Brown and R.R. Holmes, J. Am. Chem. Soc., **78**, 2173 (1956).

202. F.A. Cotton and J.R. Leto, J. Chem. Phys., **30**, 993 (1959)

203. T.R. Dyke, K.M. Mack and J.S. Muenter, J. Chem. Phys., **66**, 498 (1977).